Volume 4, No 2. April 2016

Transactions on Networks and Communications

ISSN: 2054-7420

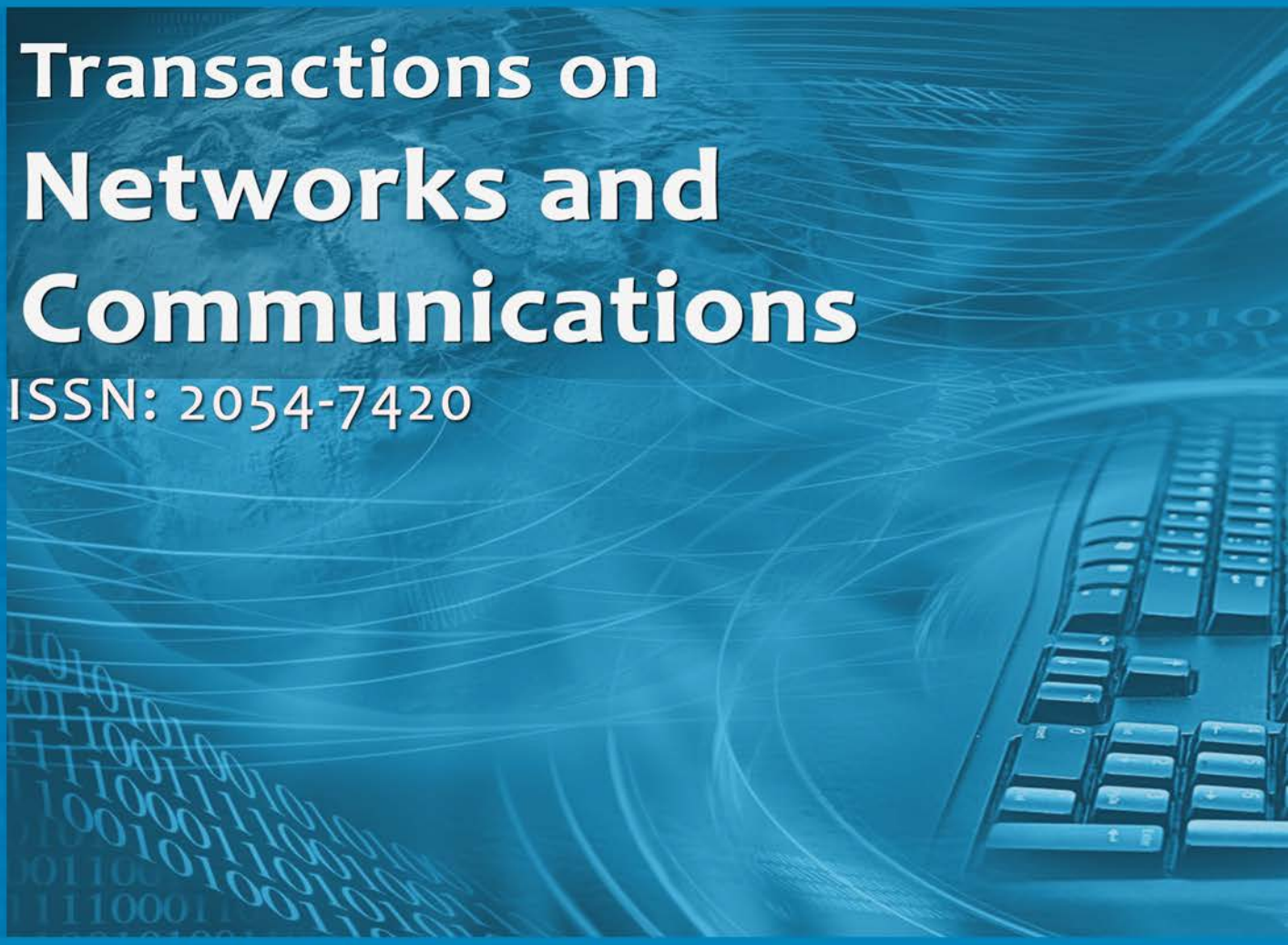

Society for Sciences and Education - United Kingdom

TABLE OF CONTENTS

EDITORIAL ADVISORY BOARD

DISCLAIMER

All the contributions are published in good faith and intentions to promote and encourage research activities around the globe. The contributions are property of their respective authors/owners and the journal is not responsible for any content that hurts someone's views or feelings etc.

SOCIETY FOR SCIENCE AND EDUCATION
UNITED KINGDOM

TNC TRANSACTIONS ON NETWORKS AND COMMUNICATIONS

VOLUME 4, ISSUE 2
ISSN: 2054 -7420

Magnetron High Voltage System Eight Cavity Stability Analysis under Parameters Variation

Ofer Aluf
Netanya, Israel
oferaluf@bezeqint.net

***Abstract*—A magnetron is a high power microwave oscillator in which the potential energy of an electron cloud near the cathode is converted into RF energy in a series of cavity resonators. As depicted by the low frequency analog, the rear wall of the structure may be considered the inductive portion, and the vane tip region the capacitor portion of the equivalent resonant circuit. The resonance frequency of a microwave cavity is thereby determined by the physical dimension of the resonator together with the reactive effect of any perturbations to the inductive or capacitive portion of the equivalent circuit. In order to sustain oscillations in a resonant circuit, it is necessary to continuously input energy in the correct phase. An eight cavity magnetron is the typical magnetron we analyze with discussion of stability. For an eight-resonator magnetron, the important modes are $n = 1, 2, 3, 4$. In general $n = 1, 2, 3...N/2$ where N is the number of resonators or cavity. The equivalent circuit of a chain of LC elements may be considered in a planar circuit using split-ring resonators to realize each LC. The open space between the magnetron's cathode and anode is called interaction space, where E and B fields interact with electrons—these are accelerated and emit radiation at a frequency determined by the cavity dimensions. The eight cavity magnetron equivalent circuit can be analyzed for stability behavior under different parameter variations. There is a practical guideline that combines graphical information with analytical work to effectively study the local stability of models. The stability of a given steady state is determined by phase space plot of a number of magnetron parameters.**

***Index Terms*—Magnetron, Cavity resonators, Slot, Hole and slot, Efficiency, stability, fixed point, oscillations.**

I. INTRODUCTION

BASICALLY, we can characterize the magnetron as a electronic diode in an environment of strong magnetic field. The natural path of electron in a magnetron is a movement from the cathode to anode and surrounding by magnetic field. The magnetic field is at right angels reference to the electron motion direction. The electrons are under influence of another force at right angles concern the direction of motion and the magnetic field. The curve path is the way which the electrons move along. We can see similarity to DC motor rotation. When we use configuration of coaxial cavity, the frequency range of operation is between 200 kHz to 10 MHz. The structure is a enclosure of a glass envelope regarding the cathode. Sealing is the key issue. It is when ferromagnetic material create the covering member when the ends are close and open and all related to cylinder. Parts in the comparison are outer cylinder (made of ferromagnetic material) and a cover (outer cylinder). Anode cylinder surrounding by outer cylinder. The curve path of electrons is from cathode to anode by influence of a strong magnetic field. It is perpendicular to the electric field. Good practical behavior is magnetron with 12 cm cavity which oscillate at 2.5 GHz. The history of magnetron engineering implementation is very interesting. Start from pulsed radar transmitter (~10 kW to 3 MW peak power, frequency range between ~600 MHz to 47 GHz), then microwave ovens (Continue Wave type, 2.45 GHz frequency, output power between 65–1200 W and efficiency ~65%). The applications for microwave oven are industrial. Military radars magnetron are in the S band and the power is around 50 kW. We drive the military radars magnetron by a pulse of 30 kV 1.0 μs pulse. We get ~30% efficiency results and (WW2) ~65%. Other characteristic can be 167 kW input peak power and peak current 5.6 A, 1000 repetition. The average input power is 167 W. Magnetron interaction space is the active area. It is where electric and magnetic fields (E and H) interact and we get microwaves in cavities. In the particular case of magnetron with eight cavity anodes, all cavities are induced by microwave energy. We get an output of microwave energy. In our analysis we concentrate on the equivalent circuit of magnetron and specialy cavity with cylindrical hole. It is a copper anode and slot which the interaction and cavity are connected. We represent in our analysis the hole and slot equivalent circuit as a capacitor (C) in parallel to circular inductor. Magnetron's slot has parallel sides which can be consider as a plates of capacitor. The walls of the hole are considered as an inductor. We can characterize the magnetron hole and slot as a resonant LC circuit with high quality factor (Q). Magnetron anode is constructed from number of cavities. The cavity LC tanks are in series (no strapping). In the case of strapping, cavities are connected in parallel [1] [2] [3].

*Corresponding author. Tel.: +972 9 8320206.
E-mail address: oferaluf@bezeqint.net (O. Aluf).

II. MAGNETRON OPERATION AND PARAMETERS

A magnetron is a high power microwave oscillator in which the potential energy of an electron cloud near the cathode is converted into RF energy in a series of cavity resonators. As depicted by the low frequency analog, the rear wall of the structure may be considered the inductive portion, and the vane tip region the capacitor portion of the equivalent resonant circuit. The resonant frequency of a microwave cavity is thereby determined by the physical dimension of the resonator together with the reactive effect of any perturbations to the inductive or capacitive portion of the equivalent circuit. In order to sustain oscillations in a resonant circuit, it is necessary to continuously input energy in the correct phase. If the instantaneous RF field, due to steady state oscillations in the

DOI: 10.14738/tnc.42.1933
Publication Date: 25th March 2016
URL: http://dx.doi.org/10.14738/tnc.42.1933

resonator, is in the direction, and, an electron with velocity was to travel through the RF field such that the RF field retarded the electron velocity by an amount, the decrease in electron energy will be exactly offset by an increase in the RF field strength. In a magnetron, the source of electrons is a heated cathode located on the axis of an anode structure containing a number of microwave resonators. Electrons leave the cathode and are accelerated toward the anode, due to the DC field established by the voltage source E.

A. Magnetron magnetic field and electron

The presence of a strong magnetic field B in the region between cathode and anode produces a force on each electron which is mutually perpendicular to the dc field and the electron velocity vectors, thereby causing the electrons to spiral away from the cathode in paths of varying curvature, depending upon the initial electron velocity at the time it leaves the cathode. As this cloud of electrons approaches the anode, it falls under the influence of the RF fields at the vane tips, and electrons will either be retarded in velocity, if they happen to face an opposing RF field, or accelerated if they are in the vicinity of an aiding RF field. Since the force on an electron due to the magnetic field B is proportional to the electron velocity through the field, the retarded velocity electrons will experience less *curling force* and will therefore drift toward the anode, while the accelerated velocity electrons will curl back away from the anode. The result is an automatic collection of electron *spokes* as the cloud nears the anode, with each spoke located at a resonator having an opposing RF field. On the next half cycle of RF oscillation, the RF field pattern will have reversed polarity and the spoke pattern will rotate to maintain its presence in an opposing field. The "automatic" synchronism between the electrons spoke pattern and the RF field polarity in a crossed field device allows a magnetron to maintain relatively stable operation over a wide range of applied input parameters. For example, a magnetron designed for an output power of 200 kW peak will operate quite well at 100 kW peak output by simply reducing the modulator drive level.

B. Magnetron important parameters

There are typical magnetron important parameters. Thermal Drift**:** At the time high voltage is first applied to a magnetron, the thermal equilibrium of the device is suddenly altered. The anode vanes being to heat at the tips due to electron bombardment and the entire anode/cathode structure undergoes a transient change in thermal profile. During the time required for each part of the magnetron to stabilize at its normal operating temperature, the output frequency of the magnetron will drift. The curve of output frequency vs. time during the period following initial turn on is called the *thermal Drift* curve [9] [10]. Temperature Coefficient: After the thermal drift period has expired and a stable operating frequency has been achieved, changes to ambient conditions which cause a corresponding change in the magnetron temperature will produce a change in the output frequency.

C. Magnetron frequency and temperature behavior

In this content ambient changes include cooling air temperature or pressure in air cooled magnetrons; mounting plate temperature in heat sink cooled magnetrons; and flow rate or temperature in liquid cooled magnetrons. The change in magnetron output frequency for each degree change in body temperature, as measured at a specified point on the outside surface of the magnetron body, is defined as the Temperature Coefficient for the magnetron and is usually expressed in MHz/°C. For most magnetrons the temperature coefficient is a negative (frequency decreases as temperature increases) and is essentially constant over the operating range of the magnetron. Pushing Figure: The pushing figure of a magnetron is defined as the change in magnetron frequency due to a change in the peak cathode current. The resonant frequency of a vane resonator is determined by its mechanical dimensions plus the reactive effect of any perturbation. The presence of electrons in the vicinity of the vane tips affects the equivalent capacitance of the resonator by an amount proportional to the density of the electrons and, since electron density is similarly related to peak pulse current, changes in pulse current level will produce changes in output frequency. The pushing figure expressed in MHz/Amp is represented by the slope of a frequency vs. peak current curve plotted for a particular magnetron type [16].

III. Different Types of Magnetron

The early types of magnetron are non-oscillation diode with magnetic field. The early types of magnetron are Hull original diode, Split anode, Split anode with internal resonator, improved split anode and four-segment anode. In the crossed electric and magnetic fields which exist between the cathode and anode an electron that is emitted by the cathode moves under the influence of a force $F_e = Ee$ and a force $F_m = \frac{e}{c}(\mathbf{V} \times \mathbf{B})$ where E *is* the electric field, B the magnetic field, c the velocity of light, V the velocity of the electron, and e is its charge. The solution of the resulting equations of motion, which neglect space-charge effects, shows that the path of the electron is a Quasi-cyclonical orbit with a frequency given approximately by$f_T = eB/mc$. When this orbit touches the anode, a condition of cutoff is said to exist, and the following equation holds: $\frac{V}{B^2} = \frac{er_a^2}{8mc^2}[1 - (\frac{r_c}{r_a})^2]^2$. Where V *is* the potential difference between the anode and the cathode And r_a and r_c are their radii. The relation is an important one from the standpoint of magnetron operation. It implies that for V/B^2 less than the right side of the equation, no currents flows and, as V/B^2 is increased through the cutoff condition, a rapid increase in current takes place. The first type of Hull original diode can be made to oscillate at very high frequencies if the cathode and anode are made part of a resonant circuit with reasonably high impedance and low losses. Conditions for oscillation are that V/B^2 must be adjusted close to the cutoff condition and that the frequency of the resonant current be close to the transit frequency of the electrons. Split-anode magnetrons will also oscillate when the frequency of the resonant circuit (now connected to the two segments) is close to the transit frequency of the electrons and the anode voltage adjusted close to cutoff conditions [18].

A. Magnetron important modifications

An important modification in the design of split-anode magnetrons was made when the resonant circuit was placed entirely within the vacuum system. This step was the result of efforts to increase, I, both the frequency and power output. This type of tube has produced power outputs of 100–400 W at 50 cm and 80 W at 20 cm. A particularly important feature of this design is that for a given B and r_a. The four-segment magnetron can be made to oscillate at twice the frequency of a two-segment one. Posthumus' developed a theory for oscillation of this type, which although space-charge effects are neglected, gives a reasonable explanation of the observed characteristics. This explanation can be made conveniently in terms of the four-segment tube. For oscillations to occur the angular velocity of the electrons must approximate that of one of the rotating waves so that the electrons retain for an appreciable length of time their phase relationship with the RF field. Posthumus showed that this condition exists when $f = \frac{4\pi n V_a}{r_a^2 B}$. When f is the frequency, V_a and r_a the anode potential and radius, B the magnetic field, n the number of pairs of segments. The theory also shows-that electrons which are retarded by the RF field and thus contribute energy to it spiral outward and eventually strike the anode. Equation $f = \frac{4\pi n V_a}{r_a^2 B}$ is consistent with the characteristics of these oscillations as observed by Posthumus. The upper-frequency limit for a given tube is inversely proportional to B, and for $n = 2$ this limiting frequency is twice that for $n = 1$. The theory is also consistent with such facts, that the anode voltage is proportional to r^2. and that for oscillations to occur the ratio *V/B* must remain constant. Of the three types of oscillations—cyclotron frequency, negative resistance, and traveling wave—the last has proved the most effective in magnetrons that are used as practical sources of microwaves. Some advantages of the traveling-wave type of oscillations are good efficiencies at high frequencies, moderate magnetic field requirements, and stability of operation over a wide range of input and output conditions. Other type is a British cavity magnetron. Perfected a traveling-wave type magnetron with internal resonators that when pulsed produced microwave radiation with peak powers several orders of magnitude greater than had been obtained before by any means. It is a very high pulsed-power output at wavelengths of 10 cm.

B. Microwave magnetron description

Microwave magnetron is another type. This system is composed of a number of coupled resonators surrounding a relatively large cylindrical cathode. These magnetrons are self-excited oscillators, the purpose of which is to convert the DC input power into RF output power. This conversion takes place in the interaction *space I* which is between the cylindrical *cathode C* and the *anode block A*. A constant and nearly uniform magnetic field is maintained in this interaction space in a direction parallel to the axis of the tube. In operation, the cathode is maintained at a negative potential, while the anode block is usually at ground potential. The anode block is pierced in a direction parallel to the axis by a number of *resonators R* which open into the interaction space so that the anode surface consists of alternate segments and gaps. The ends of the resonating cavities open into chambers that are called "end spaces" through which the lines of flux extending from one resonator to the next pass. The coupling between the resonators is increased by conducing bars called straps S which connect alternate segments.

C. Microwave magnetron operation

Power is extracted from one resonator, one method being a coupling *loop L* which forms a part of the *output circuit.* The combination of resonant cavities, end spaces, straps, and output circuit is called the *resonant system.* In this design, the cathode C is oxide-coated and heated indirectly by an internal heating coil of tungsten or molybdenum. It is attached mechanically to two cathode stems supported by glass to provide anode to-cathode insulation. Coaxial line chokes K are frequently placed on these stems to prevent the escape of any stray radiation that may be picked up by the cathode structure. At each end of the cathode there is an end shield H whose purpose is to prevent electrons from leaving the cathode structure in a direction parallel to the axis of the magnetron. These end shields must be kept at a temperature too low to cause the emission of electrons. The radial dimensions of the interaction space depend upon the wavelength and voltage at which the magnetron is to operate and for any given type are proportional to the wavelength and to the square root of the anode voltage. For efficient operation, the ratio of cathode diameter to anode diameter must remain within narrow limits set by the number of resonators. In a 12-resonator magnetron, this ratio is about $1/2$ the anode; for fewer oscillators, it is somewhat smaller, and for more than 12 oscillators, somewhat larger. The combination of the anode block, output circuit, end spaces, and other parts that contribute to the RF properties of the tube is defined as the resonant system. It is a most important part of the magnetron, for it determines the frequency and also plays a most important role in the electronic processes. This integration of the entire oscillating system into one tube complicates the problems of design and limits the versatility of single magnetrons as compared with low-frequency oscillators where the oscillator tube is distinct from the associated resonant circuits.

D. Magnetron resonant system

The function of the resonant system is to present to the space charge an RF field of the desired frequency and with the proper configuration and magnitude to effect an efficient generation of radio frequency and further to transmit this power to an external load. The resonant system accomplishes this by storing a quantity of the energy to produce the RF fields, at the same time releasing a portion to the external load. There is a hole-and-slot anode block, will be used as a specific magnetron. When operating in the desired manner, oscillations result in a disposition of charge and electric field [19]. One-quarter of a period later the electric field and charges have disappeared and currents are flowing around the inside of the cavities, producing a magnetic field along the hole portion of the cavities. Oscillations of this character are called π-mode

oscillations from the fact that the phase difference between adjacent resonators is π. Other modes are possible, however, and each is characterized by varying phase differences among the eight coupled resonators that comprise this particular resonant system. The number of possible modes is reduced by the fact that the resonator system is a closed one and the total phase shift around the resonator system must be a multiple n of 2π, where n is called the mode number. For an eight-resonator magnetron, the important modes are $n = 1, 2, 3, 4$. In general $n = 1, 2, 3...N/2$ where N is the number of resonators. The phase differences between the resonators in the example chosen for $n = 1, 2, 3, 4$ are $\pi/4$, $\pi/2$, $3\pi/4$, and π. In principle, one would also expect modes corresponding to $n > N/2$ in which the phase difference between resonators is some multiple of m corresponding to harmonics of the individual resonators. These modes apparently are unimportant to the operation of magnetrons and have only rarely been observed.

E. Types of magnetron cavities

The explanation of the effect of strapping can be made in several ways. The simplest is to conceive of the strap as maintaining m-mode oscillations by tying together points that for this type of oscillation remain at the same potential. A more sophisticated explanation arises from a consideration of the effective capacitance and inductance of the straps for the various modes. For π-mode operation the concentration of charge on the strap is a maximum and the effective capacitance of the strap is relatively large. For any other mode the potential difference between adjacent segments will be less, resulting in less charge on the strap and thus decreasing the effective capacitance that it contributes to the resonant system. Other modes, currents will flow along the entire strap, decreasing the effective inductance of the resonant cavity. Thus the straps present both a reduced capacitance and a reduced inductance for all non-π modes, and the frequency of these modes is increased with respect to the π-mode. The uses to which a magnetron is put are usually such that it is desirable to attain both high efficiency and high-frequency stability against changes in load and changes in input conditions. These objectives are not consistent, and most magnetrons represent a compromise between efficiency and stability that depends on the particular application. The problem is a most important one in magnetron design. For any given frequency, a variety of oscillator configurations is possible corresponding to different oscillator impedances of *L/C* ratios, and the efficiency and frequency stability desired determine the proper oscillator impedance to use. There are three forms of oscillators arranged in order of increasing impedance. The three common types of magnetron cavities: slot, hole and slot, and vane. The efficiency η with which a magnetron converts the input power into RF power at the output (cathode power is excluded) is given by $\eta = \frac{\text{Power input} - \text{Losses}}{\text{Power input}}$. The losses arise from the bombardment of the anode by the electrons and from the circulating RF currents producing I^2R losses in the copper and other materials. To distinguish these two sources of energy loss it is customary to express the over-all efficiency η of a magnetron as the product of the electronic efficiency η_e, and circuit efficiency η_c, or $\eta = \eta_e\eta_c$. The electronic efficiency is defined as the fraction of the input power that is converted into RF power within the anode block, and the circuit efficiency is the fraction of this RF power which is transmitted to the load. The problem of high efficiency may then be restarted as one of making the product $\eta_e\eta_c$ a maximum. Both η_c and η_e are affected by the impedance of the oscillators, but in a different ways [23].

IV. Magnetron DC voltage magnetic field relashionship

There is a simple expression relating the operating voltage V, the magnetic field B, the wavelength λ, and the anode and cathode radii, respectively r_a and r_c. For efficient operation of the magnetron V and B must be such that the angular velocity of the electron keeps pace with the changes in phase of the resonators. Thus an electron must move from a point opposite any segment to a point opposite the next in one-half a period. Assuming that the electron is intermediate between the cathode and anode then the electron radius is this distance is $\frac{r_a+r_c}{2}$ then the circle circumference is $2\pi(\frac{r_a+r_c}{2})$ and for one magnetron segment (N segments) $\frac{2\pi}{N}(\frac{r_a+r_c}{2})$ when N is the number of resonators. The velocity must then be $v = \frac{\text{distance}=\frac{\pi}{N}(r_a+r_c)}{\text{time}=2T|_{T=1/f}=2/f} = \frac{\pi}{N}(r_a+r_c)\frac{f}{2} = \frac{\pi(r_a+r_c)}{N\frac{2}{f}}$ where f is the frequency of the magnetron. The mode number $n = \frac{N}{2}$; $\lambda_0 = \frac{c}{f}$; $f = \frac{c}{\lambda_0}$; $v = \frac{\pi(r_a+r_c)}{N\frac{2}{f}} = \frac{c\pi(r_a+r_c)}{n\lambda_0}$

An electron moves through crossed, uniform electric and magnetic fields with a velocity v that is normal to E and B. The force equation under these conditions is $\frac{Bev}{c} = eE + \frac{1}{R}mv^2$ where R is the radius of the orbit of the electrons and we consider that R is positive for orbits curving down. Where the path of the electrons is a straight line, the condition is obtained by letting $R \to \infty$. In the case of infinite radius of the orbit of electrons $\lim_{R\to\infty} \frac{1}{R}mv^2 = 0$ then $\frac{Bev}{c} = eE \Rightarrow v = \frac{cE}{B}$. For $v < \frac{cE}{B}$ the electromagnetic force will be reduced and the electrons will be deflected in the direction of the electric force [25]. For $v > \frac{cE}{B}$, the deflection will be in the direction of the magnetic force. The deflection that an electron suffers in this example when speeded up or slowed down thus corresponds to what happens in a magnetron, and it is significant that the operating conditions are ones for which$v \approx \frac{cE}{B}$. The velocity of the electron is given by $v = Ec/B \Rightarrow E = \frac{vB}{c}$ and the field E,

$$\frac{V_e}{B(r_a - r_c)} = \frac{c\pi(r_a + r_c)}{n\lambda_0} \tag{1}$$

We get the expression for magnetron voltage vs other parameters,

$$V = \frac{c\pi(r_a + r_c)}{n\lambda_0}B(r_a - r_c) \approx \frac{\pi}{n\lambda_0}(r_a^2 - r_c^2)B \tag{2}$$

By rigorously solution we get

$$V = \frac{\pi}{n\lambda_0}(r_a^2 - r_c^2)(B - \frac{2\pi mc}{en\lambda_0}r_a^2) \tag{3}$$

Integration with the previous equations and we get the reduce equation: $V[\text{volt}] = \frac{300\pi}{n_0}(r_a^2 - r_c^2)(B - \frac{10.6}{n_0})$.

The voltage which is a linear function of B is known as the Hartree voltage [26]. The voltage is that at which oscillations should start provided at the same that B is sufficiently large so that the undistorted space charge does not extend to the anode.

V. Magnetron Electron Velocity and Acceleration Physical Verification

A magnetron physical verification is done by checking parameter ranges. We plot electron velocity and acceleration, this makes physical reality check. If an electron gets into a range where the acceleration or velocity is unrealistic or impossible then it is a physical limit of a magnetron. Magnetron are magnetized plasma devices that are widely used as sputtering sources for thin film deposition. There are several geometrical configurations, including cylindrical magnetrons, planar magnetron, and sputter guns. The cathode is bombarded by ions to produce the desired sputtering flux. Magnetrons are characterized by nonuniform electric and magnetic fields E and B that are configured to provide confinement of electrons in the vicinity of the cathode. The electric field is established by the electric sheath between the plasma and the cathode. The magnetic field is provided externally by a set of permanent magnets or electromagnets located behind the cathode. The electrons are confined in a closed circuit in which they move in the ExB direction. As a result of confining the electrons near the cathode, it is possible to operate the discharge at a neural pressure and a lower discharge voltage than would be required without confinement. Other possibility, that turbulence is responsible for electron transport. Low frequency turbulence is characterized by random electric fields that result in random ExB velocities, which perturb an electron out of its stable orbit. There are two categories of electrons, fast and bulk, according to their origin. Fast electron originate at the cathode or in the sheath, while the bulk electrons are created in the main discharge region. There are energetic electrons, which refers to those electrons that have enough energy to ionize neutrals. Another discussion is on ExB drift, magnetron, is electrical discharge device used for sputter deposition of thin films. Modern magnetrons use crossed ExB fields that cause a Hall current (Hall drift), directed across both field vectors. Uncontrolled Hall current will lead to electrons escape from the discharge. Electron losses can be limited by closing the drift current. The use of closed drift configurations ensured a significant increase in the plasma density and discharge efficiency. There are magnetron layouts, the planar one and cylindrical one. In planar devices, the closed drift current flows between the anode and cathode, while cylindrical, or axial magnetrons the drift current circulates around the electrode (cathode). Electrons are trapped in the region of a high magnetic field and rotate around cylindrical cathode due to Hall effect, thus creating Hall current. In addition electrons diffuse across the magnetic field due to collisions thus sustaining the main discharge current [12].

We already the electron movement through crossed, uniform electric and magnetic fields with a velocity v that is normal to E and B. V is the magnetron operation voltage (potential difference between the magnetron anode and cathode) and it is a function of other magnetron parameters.

$$V = \frac{\pi}{n\lambda_0}(r_a^2 - r_c^2)(B - \frac{2\pi mc}{en\lambda_0 r_a^2}); \lambda_0 = \frac{c}{f}; f = \frac{c}{\lambda_0} \quad (4)$$

$$B = \frac{Vn\lambda_0}{\pi(r_a^2 - r_c^2)} + \frac{2\pi mc}{en\lambda_0}r_a^2 \quad (5)$$

The velocity of electron is given by $v = \frac{Ec}{B}$.

$$v = \frac{Ec}{(\frac{Vn\lambda_0}{\pi(r_a^2 - r_c^2)} + \frac{2\pi mc}{en\lambda_0}r_a^2)} \quad (6)$$

$$v = \frac{Ec}{(\frac{Vne}{\pi(r_a^2 - r_c^2)f} + \frac{2\pi me}{en\lambda_0}r_a^2)}$$
$$v = \frac{E}{(\frac{Vn}{\pi(r_a^2 - r_c^2)f} + \frac{2\pi m}{en\lambda_0}r_a^2)} \quad (7)$$

$$v = \frac{E\pi(r_a^2 - r_c^2)fen\lambda_0}{Vn^2e\lambda_0 + 2\pi^2mr_a^2(r_a^2 - r_c^2)f}; E = \frac{V}{(r_a - r_c)} \quad (8)$$

If $r_a = r_c$ then the velocity of electron is zero ($v = 0$).

$$v = \frac{V}{(r_a - r_c)}(\frac{\pi(r_a^2 - r_c^2)fen\lambda_0}{Vn^2e\lambda_0 + 2\pi^2mr_a^2(r_a^2 - r_c^2)f}) \quad (9)$$

$$v = \frac{V}{(r_a - r_c)}(\frac{\pi(r_a + r_c)(r_a - r_c)fen\lambda_0}{Vn^2e\lambda_0 + 2\pi^2mr_a^2(r_a^2 - r_c^2)f}) \quad (10)$$

$$v = \frac{V\pi(r_a + r_c)fen\lambda_0}{Vn^2e\lambda_0 + 2\pi^2mr_a^2(r_a^2 - r_c^2)f} \quad (11)$$

$$v = \frac{V\pi(r_a + r_c)enc}{Vn^2e\frac{c}{f} + 2\pi^2mr_a^2(r_a^2 - r_c^2)f} \quad (12)$$

We check the physical limit when the electron velocity is infinite ($v \to \infty$).

$$Vn^2e\frac{c}{f} + 2\pi^2mr_a^2(r_a^2 - r_c^2)f = 0; r_a > r_c \quad (13)$$

$$V = \frac{-2\pi^2mr_a^2(r_a^2 - r_c^2)f^2}{n^2ec} \quad (14)$$

We plot the electron velocity functions. $N = 4, 8, 12$ then Mode number $n = 2, 4, 6$. Three functions: $v = \Upsilon_1(V)$ $v = \Upsilon_2(r_a)$, $v = \Upsilon_3(f)$. $v = \Upsilon_1(V)$ for $f = 1$THz; $r_a = 0.004$m ; $r_c = 0.0015$m ; V : 15kV to 30kV. $v = \Upsilon_2(r_a)$ for $f = 1$THz ; $V = 25$kV,$r_c = 0.0015$m r_a : 0.003m to 0.009m. $v = \Upsilon_3(f)$ for $V = 25$kV $r_a = 0.004$m ; $r_c = 0.0015$m ; f : 0.1THz 10THz.

Decreasing magnetron number of cavity (lower magnetron mode number n) and increasing magnetron frequency or anode radius result on higher electron velocity value. Increasing magnetron filament voltage has no significant effect on electron velocity as can be seen in Figs. 1–3.

The magnetron radial DC electric field E perpendicular to the cathode is applied between cathode and anode. The electric field and the axial magnetic field (parallel and coaxial with the cathode) introduced by pole pieces at either end of the cathode provide the required crossed field configuration. The electron

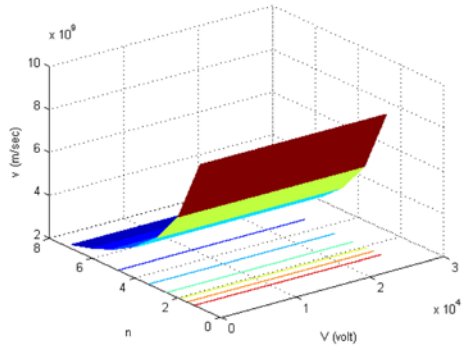

Fig. 1. A 3D plot of magnetron electron velocity, $v_{\text{magnetron}}$, versus filament voltage, V, and mode number, n. This is for frequency, $f = 1$THz, anode radius, $r_a = 0.004$m, cathode radius, $r_c = 0.0015$m, and magnetron voltage between $V = 15$ kV to $V = 30$ kV. Decreasing magnetron number of cavity (lower magnetron mode number n) result on higher electron velocity value. Increasing magnetron filament voltage has no significant effect on electron velocity as can be seen.

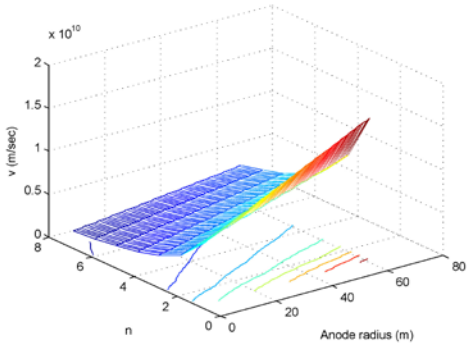

Fig. 2. A 3D plot of magnetron electron velocity, $v_{\text{magnetron}}$, versus anode radius r_a, and mode number, n. This is for frequency, $f = 1$THz, cathode radius, $r_c = 0.0015$m, and magnetron filament voltage, $V = 25$ kV and anode radius between $r_a = 0.003$m to $r_a = 0.009$. Decreasing magnetron number of cavity (lower magnetron mode number n) result on higher electron velocity value. Increasing magnetron anode radius result on higher electron velocity value as can be seen.

moving in the space between the cathode and anode block of a multi-resonator magnetron are acted upon by three fields. A constant electric field, a constant magnetic field, and a SHF electric field (from the resonator system).

The trajectory of an electron starting from rest at the cathode of a planar magnetron with static, spatially E and B fields is governed by the relation of the time rate of change of the particle's momentum to the forces caused by the applied

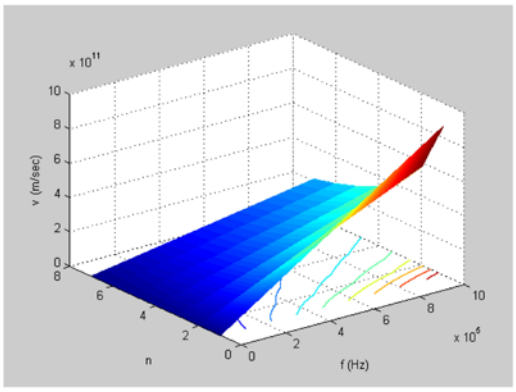

Fig. 3. A 3D plot of magnetron electron velocity, $v_{\text{magnetron}}$, versus frequency, f, and mode number, n. This is for frequency between $f = 0.1$THz to $f = 10$THz, anode radius, $r_a = 0.004$m, cathode radius, $r_c = 0.0015$m, and magnetron filament voltage $V = 25$ kV. Decreasing magnetron number of cavity (lower magnetron mode number n) result on higher electron velocity value. Increasing magnetron frequency result on higher electron velocity value as can be seen.

fields.

$$\frac{\partial p}{\partial t} = e(E + \frac{1}{c}(v \times B)) \tag{15}$$

Assuming constant particle mass and neglecting relativistic effects gives an equation for particle acceleration.

$$\frac{\partial^2 x}{\partial t^2} = \frac{e}{m}(E + \frac{1}{c}(v \times B)) \tag{16}$$

The second order differential equation can be recast as a system of first order equations $\frac{\partial X}{\partial t} = Y$ where X is the vector of position and velocity components and Y is the vector of velocity and acceleration components.

$$X = \begin{pmatrix} x \\ y \\ z \\ v_x \\ v_y \\ v_z \end{pmatrix}; Y = \begin{pmatrix} v_x \\ v_y \\ v_z \\ \frac{e}{m}(E_x + \frac{1}{c}(v \times B)_x) \\ \frac{e}{m}(E_y + \frac{1}{c}(v \times B)_y) \\ \frac{e}{m}(E_z + \frac{1}{c}(v \times B)_z) \end{pmatrix} \tag{17}$$

Lorentz force is define as $\overrightarrow{F} = e(\overrightarrow{E} + \overrightarrow{v} \times \overrightarrow{B})$.

$$\begin{array}{l} \frac{dv_x}{dt} = \frac{e}{m}(E_x + v_y B_z - v_z B_y) \\ \frac{dv_y}{dt} = \frac{e}{m}(E_y + v_z B_x - v_x B_z) \\ \frac{dv_z}{dt} = \frac{e}{m}(E_z + v_x B_y - v_y B_x) \end{array} \tag{18}$$

If we define operator $D = \frac{d}{dt}$ then we can write our magnetron velocity differential equations as

$$\overrightarrow{v} = \begin{pmatrix} v_x \\ v_y \\ v_z \end{pmatrix}; \overrightarrow{E} = \begin{pmatrix} \overrightarrow{E_x} \\ \overrightarrow{E_y} \\ \overrightarrow{E_z} \end{pmatrix} \tag{19}$$

$$\begin{pmatrix} D & -\frac{e}{m}B_z & \frac{e}{m}B_y \\ \frac{e}{m}B_z & D & -\frac{e}{m}B_x \\ -\frac{e}{m}B_y & \frac{e}{m}B_x & D \end{pmatrix} \overrightarrow{v} = \frac{e}{m}\overrightarrow{E} \tag{20}$$

The orthonormal vectors of the Cartesian based is $\{e_x, e_y, e_z\}$. $E = E_x e_x + E_y e_y + E_z e_z; B_z = B e_z$ then $\frac{dv_x}{dt} = \frac{e}{m}(E_x + v_y B); \frac{dv_y}{dt} = \frac{e}{m}(E_y - v_x B)$ $\frac{dv_z}{dt} = \frac{e}{m}E_z$(constant acceleration along z axis). If we an electron in E and B fields the Lorenz force on a point charge is $F = e(E + v \times B)$. $E[\frac{V}{m}]$ and B in T (or gauss, 10000 gauss=1T). We can consider two subcases:
(1) E is constant and uniform $E_x = Ee_x$and there is a constant acceleration along the x axis
$\frac{dv_x}{dt} = \frac{e}{m}E; \frac{dv_y}{dt} = 0; \frac{dv_z}{dt} = 0.$
(2) B is constant and uniform $B_z = Be_z$ then

$$\frac{dv_x}{dt} = \frac{e}{m}v_y B; \frac{dv_y}{dt} = -\frac{e}{m}v_x B; \frac{dv_z}{dt} = 0 \\ \frac{d}{dt}\{\frac{dv_x}{dt} = \frac{e}{m}v_y B\}; \frac{d^2 v_x}{dt^2} = \frac{e}{m}\frac{dv_y}{dt}B \quad (21)$$

$$\frac{d^2 v_x}{dt^2} = \frac{e}{m}(-\frac{e}{m}v_x B)B; a_x = \frac{dv_x}{dt} \\ \frac{d^2 v_x}{dt^2} = -\frac{e^2}{m^2}v_x B^2; \frac{da_x}{dt} = -\frac{e^2}{m^2}v_x B^2 \quad (22)$$

The electron motion under the influence of an electromagnetic field in the absence of collisions is governed by the Lorentz differential equation: $\frac{dv}{dt} = \frac{e}{m}(E + v \times B)$with $v = v_r e_r + v_\phi e_\phi + v_z e_z$ the electron velocity vector field, t is the time, e is the electron charge, m the electron mass and E as well as B are the electric and magnetic vector fields, respectively [39]. The components of the electron velocity field in the r, φ, and z directions are denoted by $v_r, v_\phi$and v_z, respectively. Note that the parametric representation of the electron trajectories is described by $r = r(t); \phi = \phi(t)$as well as z=z(t) and a cylindrical polar coordinate system is adapted here with the r-axis an the cathode target and the z-axis pointing vertically upwards. The Cartesian and cylindrical polar coordinates are related by the equations $x = r\cos(\phi); y = r\sin(\phi)$and $z = z$. The orthonormal vectors of the cylindrical and Cartesian base $\{e_r, e_\phi, e_z\}$and $\{e_x, e_y, e_z\}$, respectively, are related by the following equations:

$$\{e_r, e_\phi, e_z\} \to \{e_x, e_y, e_z\}: \\ e_x = \cos(\phi)e_r - \sin(\phi)e_\phi \\ e_y = \sin(\phi)e_r + \cos(\phi)e_\phi; e_z = e_z \quad (23)$$

$$\{e_x, e_y, e_z\} \to \{e_r, e_\phi, e_z\}: \\ e_r = \cos(\phi)e_x + \sin(\phi)e_y \\ e_\phi = -\sin(\phi)e_x + \cos(\phi)e_y; e_z = e_z \quad (24)$$

The electron velocity in cylindrical polar coordinates is given by $v = \frac{dr}{dt}e_r + r\frac{d\phi}{dt}e_\phi + \frac{dz}{dt}e_z$. The magnetic field has the form $B = B_r e_r + B_z e_z$for symmetry reasons. The constant electric field is given by $E = E_z e_z$. Using these forms for the electric and magnetic fields, and other equation, the Lorentz differential equations can be written as follows: $B_r = B\cos(\theta); B_z = B\sin(\theta)$.

$$E_z = v_z(\frac{Vn}{\pi(r_a^2 - r_c^2)f} + \frac{2\pi m}{e n\lambda_0}r_a^2) \\ E_z = \frac{dz}{dt}(\frac{Vn}{\pi(r_a^2 - r_c^2)f} + \frac{2\pi m}{e n\lambda_0}r_a^2) \quad (25)$$

$$B = \frac{Vn\lambda_0}{\pi(r_a^2 - r_c^2)} + \frac{2\pi mc}{e n\lambda_0}r_a^2 \\ v_z = \frac{dz}{dt}; v_x = \frac{dx}{dt}, v_y = \frac{dy}{dt} \quad (26)$$

$$\frac{d^2 r}{dt^2} - r(\frac{d\phi}{dt})^2 = \frac{e}{m}r\frac{d\phi}{dt}B_z \\ r\frac{d^2\phi}{dt^2} + 2\frac{dr}{dt}\frac{d\phi}{dt} = \frac{e}{m}(B_r\frac{dz}{dt} - B_z\frac{dr}{dt}) \quad (27)$$

$$\frac{d^2 z}{dt^2} = \frac{e}{m}(E_z - r\frac{d\phi}{dt}B_r) \quad (28)$$

We can write our magnetron set of differential equations in cylindrical polar coordinate:

$$\frac{d^2 r}{dt^2} - r(\frac{d\phi}{dt})^2 = \frac{e}{m}r\frac{d\phi}{dt}(\frac{Vn\lambda_0}{\pi(r_a^2 - r_c^2)} + \frac{2\pi mc}{e n\lambda_0}r_a^2)\sin(\theta) \quad (29)$$

$$r\frac{d^2\phi}{dt^2} + 2\frac{dr}{dt}\frac{d\phi}{dt} \\ = \frac{e(\frac{Vn\lambda_0}{\pi(r_a^2 - r_c^2)} + \frac{2\pi mc}{e n\lambda_0}r_a^2)}{m}(\cos(\theta)\frac{dz}{dt} - \sin(\theta)\frac{dr}{dt}) \quad (30)$$

$$\frac{d^2 z}{dt^2} = \frac{e}{m}(\frac{dz}{dt}(\frac{Vn}{\pi(r_a^2 - r_c^2)f} + \frac{2\pi m}{e n\lambda_0}r_a^2) \\ -r\frac{d\phi}{dt}(\frac{Vn\lambda_0}{\pi(r_a^2 - r_c^2)} + \frac{2\pi mc}{e n\lambda_0}r_a^2)\cos(\theta)) \quad (31)$$

We define new variables: $X_1 = \frac{d\phi}{dt}; X_2 = \frac{dr}{dt}; X_3 = \frac{dz}{dt}$ and we get the following differential equations: $\frac{dX_2}{dt} = rX_1^2 + \frac{e}{m}rX_1(\frac{Vn\lambda_0}{\pi(r_a^2 - r_c^2)} + \frac{2\pi mc}{e n\lambda_0}r_a^2)\sin(\theta)$

$$\frac{dX_1}{dt} = \frac{e(\frac{Vn\lambda_0}{\pi(r_a^2 - r_c^2)} + \frac{2\pi mc}{e n\lambda_0}r_a^2)}{rm}(\cos(\theta)X_3 - \sin(\theta)X_2) \\ -2X_2X_1\frac{1}{r} \quad (32)$$

$$\frac{dX_3}{dt} = \frac{e}{m}(X_3(\frac{Vn}{\pi(r_a^2 - r_c^2)f} + \frac{2\pi m}{e n\lambda_0}r_a^2) \\ -rX_1(\frac{Vn\lambda_0}{\pi(r_a^2 - r_c^2)} + \frac{2\pi mc}{e n\lambda_0}r_a^2)\cos(\theta)) \quad (33)$$

We find our magnetron system fixed points (equilibrium points) by setting:

$$\frac{d\phi}{dt} = 0; \frac{dr}{dt} = 0; \frac{dz}{dt} = 0; \frac{dX_1}{dt} = 0; \frac{dX_2}{dt} = 0; \frac{dX_3}{dt} = 0 \quad (34)$$

Our magnetron system fixed points:
$E^*(r^*, \phi^*, z^*, X_1^* = 0, X_2^* = 0, X_3^* = 0)$
Stability analysis: The standard local stability analysis about any one of the equilibrium points of the magnetron system consists in adding to coordinate $[r, \phi, z, X_1, X_2, X_3]$arbitrarily small increments of exponential form $[r, \phi, z, x_1, x_2, x_3]e^{\lambda t}$and retaining the first order terms in $[r, \phi, z, X_1, X_2, X_3]$. The magnetron system of six homogeneous equations leads to a polynomial characteristic equation in the eigenvalues. The polynomial characteristic equations accept by set the below variables with respect to time into magnetron system equations. Magnetron system fixed values with arbitrarily small increaments of exponential form $[r, \phi, z, x_1, x_2, x_3]e^{\lambda t}$are: j=0 (first fixed point), j=1 (second fixed point), j=2 (third fixed point), etc.

$$\phi(t) = \phi^{(j)} + \phi e^{\lambda t}; r(t) = r^{(j)} + re^{\lambda t} \\ z(t) = z^{(j)} + ze^{\lambda t}; X_1(t) = X_1^{(j)} + x_1 e^{\lambda t} \quad (35)$$

$X_2(t) = X_2^{(j)} + x_2 e^{\lambda t}; X_3(t) = X_3^{(j)} + x_3 e^{\lambda t}$. We choose these expressions for ourselves $r(t), \phi(t), z(t) X_1(t), X_2(t), X_3(t)$as a small displacement $[r, \phi, z, x_1, x_2, x_3]$from the magnetron system fixed points in time t=0.

$$\phi(t = 0) = \phi^{(j)} + \phi; r(t = 0) = r^{(j)} + r \\ z(t = 0) = z^{(j)} + z; X_1(t = 0) = X_1^{(j)} + x_1 \quad (36)$$

$X_2(t=0) = X_2^{(j)} + x_2; X_3(t=0) = X_3^{(j)} + x_3$. For $\lambda < 0, t > 0$, the selected fixed point is stable otherwise $\lambda > 0, t > 0$ is unstable. Our magnetron system tends to the selected fixed point exponentially for $\lambda < 0, t > 0$ otherwise go away from the selected fixed point exponentially. λ is the eigenvalue parameter which is established if the fixed point is stable or unstable; additionally, his absolute value ($|\lambda|$) establishes the speed of flow toward or away from the selected fixed point (Yuri, 1995; Jack and Huseyin, 1991). The speeds of flow toward or away from the selected fixed point for magnetron system variables with respect to time are $\frac{d\phi(t)}{dt} = \lambda\phi e^{\lambda t}; \frac{dr(t)}{dt} = \lambda r e^{\lambda t}; \frac{dz(t)}{dt} = \lambda z e^{\lambda t}; \frac{dX_1(t)}{dt} = \lambda x_1 e^{\lambda t}; \frac{dX_2(t)}{dt} = \lambda x_2 e^{\lambda t}; \frac{dX_3(t)}{dt} = \lambda x_3 e^{\lambda t}$. First, we take magnetron variables $r, \phi, z, X_1, X_2, X_3$ differential equations and adding to coordinate $[r, \phi, z, X_1, X_2, X_3]$ arbitrarily small increments of exponential terms $[r, \phi, z, x_1, x_2, x_3]e^{\lambda t}$and retaining the first order terms in $r, \phi, z, x_1, x_2, x_3$ then

$$E^*(r^*, \phi^*, z^*, X_1^*, X_2^*, X_3^*) = (r^*, \phi^*, z^*, 0, 0, 0) \quad r^{(j=0)} = r^*, \phi^{(j=0)} = \phi^*; z^{(j=0)} = z^* \tag{37}$$

$$X_1^{(j=0)} = X_1^*, X_2^{(j=0)} = X_2^*, X_3^{(j=0)} = X_3^* \tag{38}$$

$$\lambda r e^{\lambda t} = (X_2^* = 0) + x_2 e^{\lambda t} \Rightarrow -\lambda r + x_2 = 0 \quad \lambda z e^{\lambda t} = (X_3^* = 0) + x_3 e^{\lambda t} \Rightarrow -\lambda z + x_3 = 0 \tag{39}$$

$$\lambda\phi e^{\lambda t} = (X_1^* = 0) + x_1 e^{\lambda t} \Rightarrow -\lambda\phi + x_1 = 0 \tag{40}$$

$$\frac{dX_1}{dt} = \frac{e(\frac{V n\lambda_0}{\pi(r_a^2 - r_c^2)} + \frac{2\pi m_e}{e n\lambda_0} r_a^2)}{rm}(\cos(\theta)X_3 - \sin(\theta)X_2) \quad -2X_2X_1\tfrac{1}{r} \tag{41}$$

$$\lambda x_1 e^{\lambda t} = \frac{e(\frac{V n\lambda_0}{\pi(r_a^2 - r_c^2)} + \frac{2\pi m_e}{e n\lambda_0} r_a^2)}{(r^{(j)} + re^{\lambda t})m}(\cos(\theta)(X_3^{(j)} + x_3 e^{\lambda t}) \quad -\sin(\theta)(X_2^{(j)} + x_2 e^{\lambda t})) \quad -2(X_2^{(j)} + x_2 e^{\lambda t})(X_1^{(j)} + x_1 e^{\lambda t}) \cdot \tfrac{1}{(r^{(j)} + re^{\lambda t})} \tag{42}$$

$$\lambda x_1 e^{\lambda t} = \frac{e(\frac{V n\lambda_0}{\pi(r_a^2 - r_c^2)} + \frac{2\pi m_e}{e n\lambda_0} r_a^2)}{(r^{(j)} + re^{\lambda t})m}(X_3^{(j)}\cos(\theta) \quad +x_3\cos(\theta)e^{\lambda t} - X_2^{(j)}\sin(\theta) - x_2\sin(\theta)e^{\lambda t}) \quad -\frac{2(X_2^{(j)}X_1^{(j)} + X_2^{(j)}x_1 e^{\lambda t} + X_1^{(j)}x_2 e^{\lambda t} + x_2 x_1 e^{2\lambda t})}{(r^{(j)} + re^{\lambda t})} \quad x_2 x_1 \approx 0 \Rightarrow x_2 x_1 e^{2\lambda t} \approx 0 \tag{43}$$

$$\lambda x_1 e^{\lambda t} = \frac{e(\frac{V n\lambda_0}{\pi(r_a^2 - r_c^2)} + \frac{2\pi m_e}{e n\lambda_0} r_a^2)(r^{(j)} - re^{\lambda t})}{(r^{(j)} + re^{\lambda t})(r^{(j)} - re^{\lambda t})m}(X_3^{(j)}\cos(\theta) \quad +x_3\cos(\theta)e^{\lambda t} - X_2^{(j)}\sin(\theta) - x_2\sin(\theta)e^{\lambda t}) \quad -\frac{2(X_2^{(j)}X_1^{(j)} + X_2^{(j)}x_1 e^{\lambda t} + X_1^{(j)}x_2 e^{\lambda t})(r^{(j)} - re^{\lambda t})}{(r^{(j)} + re^{\lambda t})(r^{(j)} - re^{\lambda t})} \tag{44}$$

$$\lambda x_1 e^{\lambda t} = \frac{e(\frac{V n\lambda_0}{\pi(r_a^2 - r_c^2)} + \frac{2\pi m_e}{e n\lambda_0} r_a^2)(r^{(j)} - re^{\lambda t})}{([r^{(j)}]^2 + r^2 e^{2\lambda t})m}(X_3^{(j)}\cos(\theta) + x_3\cos(\theta)e^{\lambda t} - X_2^{(j)}\sin(\theta) \quad -x_2\sin(\theta)e^{\lambda t}) - \frac{2(X_2^{(j)}X_1^{(j)} + X_2^{(j)}x_1 e^{\lambda t} + X_1^{(j)}x_2 e^{\lambda t})(r^{(j)} - re^{\lambda t})}{([r^{(j)}]^2 + r^2 e^{2\lambda t})} \quad r^2 \approx 0 \Rightarrow r^2 e^{2\lambda t} \approx 0 \tag{45}$$

$$\lambda x_1 e^{\lambda t} = \frac{e(\frac{V n\lambda_0}{\pi(r_a^2 - r_c^2)} + \frac{2\pi m_e}{e n\lambda_0} r_a^2)(\frac{1}{r^{(j)}} - \frac{1}{[r^{(j)}]^2} r e^{\lambda t})}{m}(X_3^{(j)}\cos(\theta) + x_3\cos(\theta)e^{\lambda t} - X_2^{(j)}\sin(\theta) \quad -x_2\sin(\theta)e^{\lambda t}) - 2(X_2^{(j)}X_1^{(j)} + X_2^{(j)}x_1 e^{\lambda t} \quad +X_1^{(j)}x_2 e^{\lambda t})(\tfrac{1}{r^{(j)}} - \tfrac{1}{[r^{(j)}]^2} r e^{\lambda t}) \tag{46}$$

$$\lambda x_1 e^{\lambda t} = \frac{e(\frac{V n\lambda_0}{\pi(r_a^2 - r_c^2)} + \frac{2\pi m_e}{e n\lambda_0} r_a^2)}{m}(\tfrac{1}{r^{(j)}}X_3^{(j)}\cos(\theta) \quad +\tfrac{1}{r^{(j)}}x_3\cos(\theta)e^{\lambda t} - \tfrac{1}{r^{(j)}}X_2^{(j)}\sin(\theta) - \tfrac{1}{r^{(j)}}x_2\sin(\theta)e^{\lambda t} \quad -X_3^{(j)}\cos(\theta)\tfrac{1}{[r^{(j)}]^2} r e^{\lambda t} - r x_3\cos(\theta)e^{2\lambda t}\tfrac{1}{[r^{(j)}]^2} \quad +X_2^{(j)}\sin(\theta)\tfrac{1}{[r^{(j)}]^2} r e^{\lambda t} + r x_2\sin(\theta)e^{2\lambda t}\tfrac{1}{[r^{(j)}]^2}) \quad -2(X_2^{(j)}X_1^{(j)}\tfrac{1}{r^{(j)}} + X_2^{(j)}x_1 e^{\lambda t}\tfrac{1}{r^{(j)}} + X_1^{(j)}x_2 e^{\lambda t}\tfrac{1}{r^{(j)}} \quad -X_2^{(j)}X_1^{(j)}\tfrac{1}{[r^{(j)}]^2} r e^{\lambda t} - X_2^{(j)}x_1 r e^{2\lambda t}\tfrac{1}{[r^{(j)}]^2} \quad -X_1^{(j)}r x_2 e^{2\lambda t}\tfrac{1}{[r^{(j)}]^2}) \tag{47}$$

$$r x_3 \approx 0 \Rightarrow r x_3\cos(\theta)e^{2\lambda t}\tfrac{1}{[r^{(j)}]^2} \approx 0; r x_2 \approx 0 \quad r x_2\sin(\theta)e^{2\lambda t}\tfrac{1}{[r^{(j)}]^2} \approx 0 \tag{48}$$

$$x_1 r \approx 0 \Rightarrow X_2^{(j)}x_1 r e^{2\lambda t}\tfrac{1}{[r^{(j)}]^2} \approx 0; r x_2 \approx 0 \quad X_1^{(j)}r x_2 e^{2\lambda t}\tfrac{1}{[r^{(j)}]^2} \approx 0 \tag{49}$$

$$\lambda x_1 e^{\lambda t} = \frac{e(\frac{V n\lambda_0}{\pi(r_a^2 - r_c^2)} + \frac{2\pi m_e}{e n\lambda_0} r_a^2)}{m}(\tfrac{1}{r^{(j)}}X_3^{(j)}\cos(\theta) \quad +\tfrac{1}{r^{(j)}}x_3\cos(\theta)e^{\lambda t} - \tfrac{1}{r^{(j)}}X_2^{(j)}\sin(\theta) \quad -\tfrac{1}{r^{(j)}}x_2\sin(\theta)e^{\lambda t} - X_3^{(j)}\cos(\theta)\tfrac{1}{[r^{(j)}]^2} r e^{\lambda t} \quad +X_2^{(j)}\sin(\theta)\tfrac{1}{[r^{(j)}]^2} r e^{\lambda t}) - 2(X_2^{(j)}X_1^{(j)}\tfrac{1}{r^{(j)}} \quad +X_2^{(j)}x_1 e^{\lambda t}\tfrac{1}{r^{(j)}} + X_1^{(j)}x_2 e^{\lambda t}\tfrac{1}{r^{(j)}} \quad -X_2^{(j)}X_1^{(j)}\tfrac{1}{[r^{(j)}]^2} r e^{\lambda t}) \tag{50}$$

$$\lambda x_1 e^{\lambda t} = \frac{e(\frac{V n\lambda_0}{\pi(r_a^2 - r_c^2)} + \frac{2\pi m_e}{e n\lambda_0} r_a^2)}{m r^{(j)}}(X_3^{(j)}\cos(\theta) \quad -X_2^{(j)}\sin(\theta)) - 2X_2^{(j)}X_1^{(j)}\tfrac{1}{r^{(j)}} \quad \tfrac{e(\frac{V n\lambda_0}{\pi(r_a^2 - r_c^2)} + \frac{2\pi m_e}{e n\lambda_0} r_a^2)}{m}(\tfrac{1}{r^{(j)}}x_3\cos(\theta)e^{\lambda t} \quad -\tfrac{1}{r^{(j)}}x_2\sin(\theta)e^{\lambda t} - X_3^{(j)}\cos(\theta)\tfrac{1}{[r^{(j)}]^2} r e^{\lambda t} \quad +X_2^{(j)}\sin(\theta)\tfrac{1}{[r^{(j)}]^2} r e^{\lambda t}) - 2(X_2^{(j)}x_1 e^{\lambda t}\tfrac{1}{r^{(j)}} \quad +X_1^{(j)}x_2 e^{\lambda t}\tfrac{1}{r^{(j)}} - X_2^{(j)}X_1^{(j)}\tfrac{1}{[r^{(j)}]^2} r e^{\lambda t}) \tag{51}$$

At fixed points (equilibrium points):
$X_1^{(j)} = X_1^* = 0, X_2^{(j)} = X_2^* = 0, X_3^{(j)} = X_3^* = 0$

$$\frac{e(\frac{V n\lambda_0}{\pi(r_a^2 - r_c^2)} + \frac{2\pi m_e}{e n\lambda_0} r_a^2)}{m r^{(j)}}(X_3^{(j)}\cos(\theta) - X_2^{(j)}\sin(\theta)) \quad -2X_2^{(j)}X_1^{(j)}\tfrac{1}{r^{(j)}} = 0 \tag{52}$$

$$\lambda x_1 e^{\lambda t} = \frac{e(\frac{V n\lambda_0}{\pi(r_a^2 - r_c^2)} + \frac{2\pi m_e}{e n\lambda_0} r_a^2)}{m}(\tfrac{1}{r^{(j)}}x_3\cos(\theta)e^{\lambda t} \quad -\tfrac{1}{r^{(j)}}x_2\sin(\theta)e^{\lambda t}) \tag{53}$$

Dividing the two side of the above equation by $e^{\lambda t}$ term

$$\lambda x_1 = \frac{e(\frac{Vn\lambda_0}{\pi(r_a^2-r_c^2)}+\frac{2\pi mc}{en\lambda_0}r_a^2)}{m}(\frac{1}{r^{(j)}}x_3\cos(\theta) - \frac{1}{r^{(j)}}x_2\sin(\theta)) \quad (54)$$

$$-\lambda x_1 + \frac{e(\frac{Vn\lambda_0}{\pi(r_a^2-r_c^2)}+\frac{2\pi mc}{en\lambda_0}r_a^2)}{m}(\frac{1}{r^{(j)}}x_3\cos(\theta) - \frac{1}{r^{(j)}}x_2\sin(\theta)) = 0 \quad (55)$$

$$\Gamma_1 = \frac{e(\frac{Vn\lambda_0}{\pi(r_a^2-r_c^2)}+\frac{2\pi mc}{en\lambda_0}r_a^2)}{mr^{(j)}} \quad -\lambda x_1 + \Gamma_1 x_3\cos(\theta) - \Gamma_1 x_2\sin(\theta) = 0 \quad (56)$$

$$\frac{dX_2}{dt} = rX_1^2 + \frac{e}{m}rX_1(\frac{Vn\lambda_0}{\pi(r_a^2-r_c^2)}+\frac{2\pi mc}{en\lambda_0}r_a^2)\sin(\theta) \quad (57)$$

$$\lambda x_2 e^{\lambda t} = r(X_1^{(j)} + x_1e^{\lambda t})^2 + \frac{e}{m}(r^{(j)} + re^{\lambda t}) (X_1^{(j)} + x_1e^{\lambda t})(\frac{Vn\lambda_0}{\pi(r_a^2-r_c^2)}+\frac{2\pi mc}{en\lambda_0}r_a^2)\sin(\theta) \quad (58)$$

$$\lambda x_2 e^{\lambda t} = r([X_1^{(j)}]^2 + x_1^2e^{2\lambda t} + 2X_1^{(j)}x_1e^{\lambda t}) + \frac{e}{m}(r^{(j)} + re^{\lambda t})(X_1^{(j)} + x_1e^{\lambda t})(\frac{Vn\lambda_0}{\pi(r_a^2-r_c^2)} + \frac{2\pi mc}{en\lambda_0}r_a^2)\sin(\theta) \quad (59)$$

$$\lambda x_2 e^{\lambda t} = r([X_1^{(j)}]^2 + x_1^2e^{2\lambda t} + 2X_1^{(j)}x_1e^{\lambda t}) + \frac{e}{m}(X_1^{(j)}r^{(j)} + x_1e^{\lambda t}r^{(j)} + X_1^{(j)}re^{\lambda t} + x_1re^{2\lambda t}) (\frac{Vn\lambda_0}{\pi(r_a^2-r_c^2)} + \frac{2\pi mc}{en\lambda_0}r_a^2)\sin(\theta) \quad (60)$$

$$x_1^2 \approx 0 \Rightarrow x_1^2e^{2\lambda t} \approx 0; x_1r \approx 0 \Rightarrow x_1re^{2\lambda t} \approx 0 \quad (61)$$

$$\lambda x_2 e^{\lambda t} = r([X_1^{(j)}]^2 + 2X_1^{(j)}x_1e^{\lambda t}) + \frac{e}{m}(X_1^{(j)}r^{(j)} + x_1e^{\lambda t}r^{(j)} + X_1^{(j)}re^{\lambda t})(\frac{Vn\lambda_0}{\pi(r_a^2-r_c^2)} + \frac{2\pi mc}{en\lambda_0}r_a^2)\sin(\theta) \quad (62)$$

$$\lambda x_2 e^{\lambda t} = r[X_1^{(j)}]^2 + \frac{e}{m}X_1^{(j)}r^{(j)}(\frac{Vn\lambda_0}{\pi(r_a^2-r_c^2)} + \frac{2\pi mc}{en\lambda_0}r_a^2)\sin(\theta) + 2rX_1^{(j)}x_1e^{\lambda t}) + \frac{e}{m}(x_1e^{\lambda t}r^{(j)} + X_1^{(j)}re^{\lambda t})(\frac{Vn\lambda_0}{\pi(r_a^2-r_c^2)} + \frac{2\pi mc}{en\lambda_0}r_a^2)\sin(\theta) \quad (63)$$

At fixed points (equilibrium points): $X_1^{(j)} = 0$

$$r[X_1^{(j)}]^2 + \frac{e}{m}X_1^{(j)}r^{(j)}(\frac{Vn\lambda_0}{\pi(r_a^2-r_c^2)} + \frac{2\pi mc}{en\lambda_0}r_a^2)\sin(\theta) = 0 \quad (64)$$

$$\lambda x_2 e^{\lambda t} = \frac{e}{m}x_1e^{\lambda t}r^{(j)}(\frac{Vn\lambda_0}{\pi(r_a^2-r_c^2)}+\frac{2\pi mc}{en\lambda_0}r_a^2)\sin(\theta) \quad (65)$$

Dividing the two sides of the above equation by $e^{\lambda t}$

$$\lambda x_2 = \frac{e}{m}x_1r^{(j)}(\frac{Vn\lambda_0}{\pi(r_a^2-r_c^2)}+\frac{2\pi mc}{en\lambda_0}r_a^2)\sin(\theta) \quad (66)$$

$$-\lambda x_2 + \frac{e}{m}x_1r^{(j)}(\frac{Vn\lambda_0}{\pi(r_a^2-r_c^2)}+\frac{2\pi mc}{en\lambda_0}r_a^2)\sin(\theta) = 0 \quad (67)$$

$$\Gamma_2 = r^{(j)}(\frac{Vn\lambda_0}{\pi(r_a^2-r_c^2)} + \frac{2\pi mc}{en\lambda_0}r_a^2)\frac{e}{m} \quad -\lambda x_2 + \Gamma_2 x_1\sin(\theta) = 0 \quad (68)$$

$$\frac{dX_3}{dt} = \frac{e}{m}(X_3(\frac{Vn}{\pi(r_a^2-r_c^2)f} + \frac{2\pi m}{en\lambda_0}r_a^2) - rX_1(\frac{Vn\lambda_0}{\pi(r_a^2-r_c^2)} + \frac{2\pi mc}{en\lambda_0}r_a^2)\cos(\theta)) \quad (69)$$

$$\lambda x_3 e^{\lambda t} = \frac{e}{m}((X_3^{(j)} + x_3e^{\lambda t})(\frac{Vn}{\pi(r_a^2-r_c^2)f} + \frac{2\pi m}{en\lambda_0}r_a^2) - (r^{(j)} + re^{\lambda t})(X_1^{(j)} + x_1e^{\lambda t})(\frac{Vn\lambda_0}{\pi(r_a^2-r_c^2)} + \frac{2\pi mc}{en\lambda_0}r_a^2)\cos(\theta)) \quad (70)$$

$$\lambda x_3 e^{\lambda t} = \frac{e}{m}(X_3^{(j)}(\frac{Vn}{\pi(r_a^2-r_c^2)f} + \frac{2\pi m}{en\lambda_0}r_a^2) + x_3e^{\lambda t}(\frac{Vn}{\pi(r_a^2-r_c^2)f} + \frac{2\pi m}{en\lambda_0}r_a^2) - (r^{(j)}X_1^{(j)} + r^{(j)}x_1e^{\lambda t} + X_1^{(j)}re^{\lambda t} + rx_1e^{2\lambda t}) (\frac{Vn\lambda_0}{\pi(r_a^2-r_c^2)} + \frac{2\pi mc}{en\lambda_0}r_a^2)\cos(\theta)) \quad (71)$$

$$rx_1 \approx 0 \Rightarrow rx_1e^{2\lambda t} \approx 0 \quad (72)$$

$$\lambda x_3 e^{\lambda t} = \frac{e}{m}(x_3e^{\lambda t}(\frac{Vn}{\pi(r_a^2-r_c^2)f} + \frac{2\pi m}{en\lambda_0}r_a^2) - r^{(j)}x_1e^{\lambda t}(\frac{Vn\lambda_0}{\pi(r_a^2-r_c^2)} + \frac{2\pi mc}{en\lambda_0}r_a^2)\cos(\theta)) \quad (73)$$

Dividing the two side of the above equation by $e^{\lambda t}$

$$\lambda x_3 = \frac{e}{m}(x_3(\frac{Vn}{\pi(r_a^2-r_c^2)f} + \frac{2\pi m}{en\lambda_0}r_a^2) - r^{(j)}x_1(\frac{Vn\lambda_0}{\pi(r_a^2-r_c^2)} + \frac{2\pi mc}{en\lambda_0}r_a^2)\cos(\theta)) \quad (74)$$

$$-\lambda x_3 + \frac{e}{m}(x_3(\frac{Vn}{\pi(r_a^2-r_c^2)f} + \frac{2\pi m}{en\lambda_0}r_a^2) - r^{(j)}x_1(\frac{Vn\lambda_0}{\pi(r_a^2-r_c^2)} + \frac{2\pi mc}{en\lambda_0}r_a^2)\cos(\theta)) = 0 \quad (75)$$

$$\Gamma_3 = \frac{e}{m}(\frac{Vn}{\pi(r_a^2-r_c^2)f} + \frac{2\pi m}{en\lambda_0}r_a^2) \quad -\lambda x_3 + \Gamma_3 x_3 - \Gamma_2 x_1\cos(\theta) = 0 \quad (76)$$

We can summery our magnetron system arbitrarily small increments equations:

$$-\lambda r + x_2 = 0; -\lambda z + x_3 = 0; -\lambda\phi + x_1 = 0 \quad -\lambda x_1 + \Gamma_1 x_3\cos(\theta) - \Gamma_1 x_2\sin(\theta) = 0 \quad -\lambda x_2 + \Gamma_2 x_1\sin(\theta) = 0 \quad -\lambda x_3 + \Gamma_3 x_3 - \Gamma_2 x_1\cos(\theta) = 0 \quad (77)$$

$$\begin{pmatrix} \Upsilon_{11} & \dots & \Upsilon_{16} \\ \vdots & \ddots & \vdots \\ \Upsilon_{61} & \dots & \Upsilon_{66} \end{pmatrix} \begin{pmatrix} r \\ \phi \\ z \\ x_1 \\ x_2 \\ x_3 \end{pmatrix} = 0; \Upsilon_{11} = -\lambda \quad (78)$$

$$\Upsilon_{12} = \Upsilon_{13} = \Upsilon_{14} = 0; \Upsilon_{15} = 1; \Upsilon_{16} = 0$$

$$\Upsilon_{21} = 0; \Upsilon_{22} = -\lambda; \Upsilon_{23} = 0; \Upsilon_{24} = 1 \quad \Upsilon_{25} = \Upsilon_{26} = 0; \Upsilon_{31} = \Upsilon_{32} = 0; \Upsilon_{33} = -\lambda \quad \Upsilon_{34} = \Upsilon_{35} = 0; \Upsilon_{36} = 1; \Upsilon_{41} = \Upsilon_{42} = \Upsilon_{43} = 0 \quad (79)$$

$$\Upsilon_{44} = -\lambda; \Upsilon_{45} = -\Gamma_1\sin(\theta); \Upsilon_{46} = \Gamma_1\cos(\theta) \quad \Upsilon_{51} = \Upsilon_{52} = \Upsilon_{53} = 0; \Upsilon_{54} = \Gamma_2\sin(\theta); \Upsilon_{55} = -\lambda \quad \Upsilon_{56} = 0; \Upsilon_{61} = \Upsilon_{62} = \Upsilon_{63} = 0; \Upsilon_{64} = -\Gamma_2\cos(\theta) \quad \Upsilon_{65} = 0; \Upsilon_{66} = -\lambda + \Gamma_3 \quad (80)$$

$$A-\lambda I=\begin{pmatrix}\Upsilon_{11} & \cdots & \Upsilon_{16}\\ \vdots & \ddots & \vdots\\ \Upsilon_{61} & \cdots & \Upsilon_{66}\end{pmatrix};\det(A-\lambda I)=0 \quad (81)$$

We get for our magnetron system's eigenvalues equation:

$$\lambda^3[\lambda^3-\lambda^2\Gamma_3+\lambda\Gamma_1\Gamma_2-(\prod_{k=1}^{3}\Gamma_k)\sin^2(\theta)]=0 \quad (82)$$

We got for our magnetron system's electron motion investigation six eigenvalues. Three eigenvalues are equal to zero ($\lambda_1=\lambda_2=\lambda_3=0$). If all other eigenvalues are negative real number ($\lambda_4<0;\lambda_5<0;\lambda_6<0$) then our magnetron system's electron motion fixed points are attraction line. If all other eigenvalues are positive real number ($\lambda_4>0;\lambda_5>0;\lambda_6>0$) then our magnetron system's electron motion fixed points are repelling line. If at least one of eigenvalues $\lambda_4,\lambda_5,\lambda_6$ is positive and others are negative real numbers then our magnetron system's electron motion fixed points are saddle line. Other complicate magnetron system's fixed points classification is presented in the below table.

Eigenvalues	Fixed points classification
$\mathrm{Re}(\lambda_4)>0;\lambda_5=\lambda_4^*;\lambda_6>0$	Unstable spiral node line
$\mathrm{Re}(\lambda_4)>0;\lambda_5=\lambda_4^*;\lambda_6<0$	Unstable spiral saddle line
$\mathrm{Re}(\lambda_4)<0;\lambda_5=\lambda_4^*;\lambda_6>0$	Unstable spiral saddle line
$\mathrm{Re}(\lambda_4)<0;\lambda_5=\lambda_4^*;\lambda_6<0$	Stable spiral node line

Table 1. Magnetron system's electron motion fixed points classification.

VI. Magnetron Operating Frequency Versus Various Design Parameters

We plot graphs of magnetron operating frequency versus various important design parameters: $f=f_{\mathrm{magnetron}}=\psi(V,r_a,r_c,n,B)$ or by some functions:

$$\begin{aligned}&f_{\mathrm{magnetron}}=\psi_1(r_a,r_c);f_{\mathrm{magnetron}}=\psi_2(V)\\&f_{\mathrm{magnetron}}=\psi_3(n);f_{\mathrm{magnetron}}=\psi_4(B)\end{aligned} \quad (83)$$

$$V[\mathrm{volt}]=\frac{\pi}{n\lambda_0}(r_a^2-r_c^2)(B-\frac{2\pi mc}{en\lambda_0}r_a^2). \quad (84)$$

V voltage is a linear function of B (Hartree voltage). The voltage (V) is that at which oscillations should start provided at the same time that B is sufficiently large so that the undistorted space charge does not extend to the anode.

f – Magnetron frequency.
B – Magnetron magnetic field.
n – Numbers of pairs of segment.
e – Electron charge (1.6×10^{-19} C).
r_a – Magnetron anode radius.
r_c – Magnetron cathode radius.
c – Speed of light 3×10^8 m/s.
$n=N/2$; N – number of resonators. $N=8\gg n=4$.
m – Electron mass (9.1×10^{-31} kg).

$$\begin{aligned}&V[\mathrm{volt}]=\tfrac{\pi}{n\lambda_0}(r_a^2-r_c^2)(B-\tfrac{2\pi mc}{en\lambda_0}r_a^2)\\&\lambda_0=\tfrac{c}{f}\Rightarrow f=f_{\mathrm{magnetron}}=\tfrac{c}{\lambda_0}\\&V[\mathrm{volt}]=\tfrac{\pi}{n\frac{c}{f}}(r_a^2-r_c^2)(B-\tfrac{2\pi mc}{en\frac{c}{f}}r_a^2)\\&=\tfrac{\pi f}{nc}(r_a^2-r_c^2)(B-\tfrac{2\pi mf}{en}r_a^2)\end{aligned} \quad (85)$$

$$\begin{aligned}&V[\mathrm{volt}]=\tfrac{\pi}{nc}(r_a^2-r_c^2)(fB-\tfrac{2\pi mf^2}{en}r_a^2)\\&\Rightarrow V+\tfrac{\pi}{nc}(r_a^2-r_c^2)(\tfrac{2\pi mf^2}{en}r_a^2-fB)=0\end{aligned} \quad (86)$$

$$\frac{\pi}{nc}(r_a^2-r_c^2)\frac{2\pi m}{en}r_a^2f^2-f\frac{\pi}{nc}(r_a^2-r_c^2)B+V=0 \quad (87)$$

$$f_{\mathrm{magnetron}}=\frac{\frac{\pi}{nc}(r_a^2-r_c^2)B\pm\sqrt{\{\frac{\pi^2}{n^2c^2}(r_a^2-r_c^2)^2B^2-4\frac{\pi}{nc}(r_a^2-r_c^2)\frac{2\pi m}{en}r_a^2V\}}}{2\frac{\pi}{nc}(r_a^2-r_c^2)\frac{2\pi m}{en}r_a^2} \quad (88)$$

We define discriminant as Δ

$$\Delta=\frac{\pi^2}{n^2c^2}(r_a^2-r_c^2)^2B^2-4\frac{\pi}{nc}(r_a^2-r_c^2)\frac{2\pi m}{en}r_a^2V \quad (89)$$

Our $f_{\mathrm{magnetron}}>0$ and real number then $\Delta\geq0$ and we have two subcases: Case I: $\Delta=0$, Case II: $\Delta>0$.

Case I: $\Delta=0$

$$\begin{aligned}&\Delta=\tfrac{\pi^2}{n^2c^2}(r_a^2-r_c^2)^2B^2\\&-4\tfrac{\pi}{nc}(r_a^2-r_c^2)\tfrac{2\pi m}{en}r_a^2V=0\end{aligned} \quad (90)$$

$$\frac{(r_a^2-r_c^2)\pi^2}{n^2c}[\frac{1}{c}(r_a^2-r_c^2)B^2-\frac{8m}{e}r_a^2V]=0. \quad (91)$$

Case I-1: $\frac{(r_a^2-r_c^2)\pi^2}{n^2c}=0$ then
$r_a^2-r_c^2=0\Rightarrow r_a=r_c$ or $r_a=-r_c$ cannot exist since $r_a>r_c$.

Case I-2:

$$\begin{aligned}&\tfrac{1}{c}(r_a^2-r_c^2)B^2-\tfrac{8m}{e}r_a^2V=0\Rightarrow\\&\tfrac{1}{c}(r_a^2-r_c^2)B^2=\tfrac{8m}{e}r_a^2V\end{aligned} \quad (92)$$

$$\begin{aligned}&f_{\mathrm{magnetron}}=\tfrac{\frac{\pi}{nc}(r_a^2-r_c^2)B}{2\frac{\pi}{nc}(r_a^2-r_c^2)\frac{2\pi m}{en}r_a^2}=\tfrac{Ben}{4\pi mr_a^2}\\&\Rightarrow f_{\mathrm{magnetron}}=\tfrac{Ben}{4\pi mr_a^2}\end{aligned} \quad (93)$$

When orbit touches the anode, a condition of cutoff is said to exist. The V is the potential difference between magnetron's anode and cathode. r_a and r_c their radii. $\frac{V}{B^2}=\frac{er_a^2}{8mc^2}[1-(\frac{r_c}{r_a})^2]$.

No current flow when $\frac{V}{B^2}<\frac{er_a^2}{8mc^2}[1-(\frac{r_c}{r_a})^2]$.

The value of $\frac{V}{B^2}$ grows up then there is a rapid increase in the current. The condition of no cutoff must fulfil in our case then $\frac{V}{B^2}\geq\frac{er_a^2}{8mc^2}[1-(\frac{r_c}{r_a})^2]$.

In that subcase we have the following results:

$$\begin{aligned}&\Delta=0\Rightarrow\tfrac{1}{c}(r_a^2-r_c^2)B^2=\tfrac{8m}{e}r_a^2V\\&\Rightarrow\tfrac{V}{B^2}=\tfrac{\frac{1}{c}(r_a^2-r_c^2)}{\frac{8m}{e}r_a^2}\Rightarrow\tfrac{V}{B^2}=\tfrac{e}{8cm}(1-\tfrac{r_c^2}{r_a^2})\end{aligned} \quad (94)$$

No cutoff region: $\frac{V}{B^2}\geq\frac{er_a^2}{8mc^2}[1-(\frac{r_c}{r_a})^2]$

$$\{\frac{V}{B^2}=\frac{e}{8mc}(1-\frac{r_c^2}{r_a^2}\}\cup\{\frac{V}{B^2}\geq\frac{r_a^2}{c}\frac{e}{8mc}[1-(\frac{r_c}{r_a})^2]\}\\ \Rightarrow\frac{r_a^2}{c}<1\Rightarrow r_a^2<c \quad (95)$$

Which exist and then $f_{\text{magnetron}}=\frac{Ben}{4\pi mr_a^2}$.

The magnetron frequency is independent on the voltage V but V must fulfil two conditions.

Case II: $\Delta>0$

$$\Delta=\frac{\pi^2}{n^2c^2}(r_a^2-r_c^2)^2B^2-4\frac{\pi}{nc}(r_a^2-r_c^2)\frac{2\pi m}{en}r_a^2V>0 \quad (96)$$

$$\frac{(r_a^2-r_c^2)\pi^2}{n^2c}[\frac{1}{c}(r_a^2-r_c^2)B^2-\frac{8m}{e}r_a^2V]>0\\ r_a>r_c\Rightarrow\frac{(r_a^2-r_c^2)\pi^2}{n^2c}>0 \quad (97)$$

$$\frac{1}{c}(r_a^2-r_c^2)B^2-\frac{8m}{e}r_a^2V>0\Rightarrow\\ \frac{1}{c}(r_a^2-r_c^2)B^2>\frac{8m}{e}r_a^2V \quad (98)$$

$$\frac{e}{8m}(1-\frac{r_c^2}{r_a^2})>\frac{V}{B^2}. \quad (99)$$

No cutoff region: $\frac{V}{B^2}\geq\frac{er_a^2}{8mc^2}[1-(\frac{r_c}{r_a})^2]$

$$\{\frac{e}{8mc}(1-\frac{r_c^2}{r_a^2})>\frac{V}{B^2}\}\cap\{\frac{V}{B^2}\geq\frac{er_a^2}{8mc^2}[1-(\frac{r_c}{r_a})^2]\} \quad (100)$$

$$\frac{e}{8mc}(1-\frac{r_c^2}{r_a^2})>\frac{V}{B^2}\geq\frac{r_a^2}{c}\frac{e}{8mc}[1-(\frac{r_c}{r_a})^2]\;;\;\frac{r_a^2}{c}<1 \quad (101)$$

In that case:

$$f_{\text{magnetron}}=\frac{\frac{\pi}{nc}(r_a^2-r_c^2)B\pm\sqrt{\{\frac{\pi^2}{n^2c^2}(r_a^2-r_c^2)^2B^2-4\frac{\pi}{nc}(r_a^2-r_c^2)\frac{2\pi m}{en}r_a^2V\}}}{2\frac{\pi}{nc}(r_a^2-r_c^2)\frac{2\pi m}{en}r_a^2} \quad (102)$$

$$f_{\text{magnetron}}=\frac{\frac{\pi}{nc}(r_a^2-r_c^2)B\pm\sqrt{\frac{(r_a^2-r_c^2)\pi^2}{n^2c}[\frac{1}{c}(r_a^2-r_c^2)B^2-\frac{8m}{e}r_a^2V]}}{2\frac{\pi}{nc}(r_a^2-r_c^2)\frac{2\pi m}{en}r_a^2} \quad (103)$$

$$f_{\text{magnetron}}=\frac{\frac{\pi}{nc}(r_a^2-r_c^2)B\pm\frac{\pi}{n}\{\sqrt{\frac{(r_a^2-r_c^2)}{c}}\}\\ \{\sqrt{\frac{1}{c}(r_a^2-r_c^2)B^2-\frac{8m}{e}r_a^2V}\}}{2\frac{\pi}{nc}(r_a^2-r_c^2)\frac{2\pi m}{en}r_a^2} \quad (104)$$

We have two possible solutions and take only those which give $f_{\text{magnetron}}>0$

$$f\text{magnetron}_1=\frac{\frac{\pi}{nc}(r_a^2-r_c^2)B+\frac{\pi}{n}\{\sqrt{\frac{(r_a^2-r_c^2)}{c}}\}\\ \{\sqrt{\frac{1}{c}(r_a^2-r_c^2)B^2-\frac{8m}{e}r_a^2V}\}}{2\frac{\pi}{nc}(r_a^2-r_c^2)\frac{2\pi m}{en}r_a^2} \quad (105)$$

$$f\text{magnetron}_2=\frac{\frac{\pi}{nc}(r_a^2-r_c^2)B-\frac{\pi}{n}\{\sqrt{\frac{(r_a^2-r_c^2)}{c}}\}\\ \{\sqrt{\frac{1}{c}(r_a^2-r_c^2)B^2-\frac{8m}{e}r_a^2V}\}}{2\frac{\pi}{nc}(r_a^2-r_c^2)\frac{2\pi m}{en}r_a^2} \quad (106)$$

$f_{\text{magnetron}}>0$ And all other negative results are mathematics and not realistic. We plot graphs which are related to Case II: $\Delta>0$;8 cavity magnetron: $n=N/2$; N – number of resonators. If $N=8$ then the mode number is four $n=4$ and we choose $B=0.24$ T $V=25$ kV.

$$\frac{e}{c8m}=\frac{1.6\cdot10^{-19}}{8\cdot9.1\cdot10^{-31}\cdot3\cdot10^8}=7.326\\ \frac{V}{B^2}=\frac{25000}{2400^2}=0.0043 \quad (107)$$

$$7.326\cdot(1-\frac{r_c^2}{r_a^2})>0.0043\geq\frac{r_a^2}{3\cdot10^8}\cdot7.326\cdot[1-(\frac{r_c}{r_a})^2]\\ \frac{r_a^2}{3\cdot10^8}<1\Rightarrow r_a<17320\ m \quad (108)$$

$$7.326\cdot(1-\frac{r_c^2}{r_a^2})>0.0043\Rightarrow1-\frac{r_c^2}{r_a^2}>5.8695\cdot10^{-4}\\ \Rightarrow\frac{r_c^2}{r_a^2}<0.9994 \quad (109)$$

$$\frac{r_c^2}{r_a^2}<0.9994\Rightarrow0.9994-[\frac{r_c}{r_a}]^2>0\Rightarrow\\ (0.9997-\frac{r_c}{r_a})\cdot(0.9997+\frac{r_c}{r_a})>0 \quad (110)$$

$$\frac{r_c}{r_a}<0.9997\;\&\;\frac{r_c}{r_a}>-0.9997\;;r_c>0\;;r_a>0\\ \Rightarrow0<\frac{r_c}{r_a}<0.9997 \quad (111)$$

In magnetron $r_a>r_c\Rightarrow1>\frac{r_c}{r_a}$ which fulfil our case.

Overview on typical magnetron cathode and anode diameters: there are many magnetron types and we sort then by cathode and anode diameters and radius. $d_a=2\cdot r_a$; $d_c=2\cdot r_c$. LL3 is an eight oscillator tube with anode dimension identical with those of 2J39(LVS), $r_a=0.4$ cm, $r_c=0.15$ cm. LCW magnetron dimension in meter, $d_a=0.034$ m, $d_c=0.021$ m. CM16B magnetron dimension in meter, $d_a=0.0058$ m, $d_c=0.0034$ m. 2J38 and 2J39 magnetron dimension in meter, $d_a=0.008$ m, $d_c=0.003$ m. 2J32 magnetron dimension in meter, $d_a=0.016$ m, $d_c=0.005$ m. 4J70 and 4J77 magnetron dimension in meter, $d_a=0.02$ m, $d_c=0.011$ m. HP10V magnetron dimension in meter, $d_a=0.029$ m, $d_c=0.015$ m. BM50 magnetron in meter, $d_a=0.0025$ m, $d_c=0.0016$ m. 2J41 magnetron dimension in meter, $d_a=0.0024$ m, $d_c=0.001$ m. 2J42 magnetron in meter, $d_a=0.0039$ m, $d_c=0.0021$ m. 4J50 (4J52, 4J78) high power 3 cm magnetron dimension in meters for 4J50 and 4J52 type, $d_a=0.0081$ m, $d_c=0.0053$ m. AX9 magnetron dimension in meter, $d_a=0.019$ m, $d_c=0.0065$ m. Tube dimension in meters of 3J31 magnetron, $d_a=0.004$ m, $d_c=0.0024$ m. Dimensions in meters for 725 A magnetron anode dimensions, Hole and Slot or Vane type, $d_a=0.0051$ m, $d_c=0.0025$ m. First we analyze the graphs $f_{\text{magnetron}}=\psi_1(r_a,r_c)$.

$$\frac{\pi}{nc}(r_a^2-r_c^2)\frac{2\pi m}{en}r_a^2f^2-f\frac{\pi}{nc}(r_a^2-r_c^2)B+V=0\\ \Rightarrow af^2+bf+c_x=0 \quad (112)$$

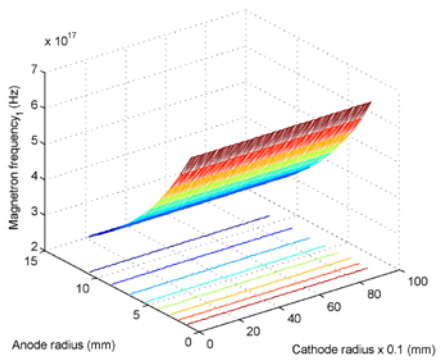

Fig. 4. A 3D plot of magnetron frequency, $f_{\text{magnetron}}$, versus anode radius, r_a, and cathode radius, r_c. This is for mode number, $n = 4$, magnetic field, $B = 0.24$ T, and magnetron voltage, $V = 25$ kV. Increasing magnetron anode radius decreases magnetron frequency. Increasing magnetron cathode radius has no significant effect on. First solution.

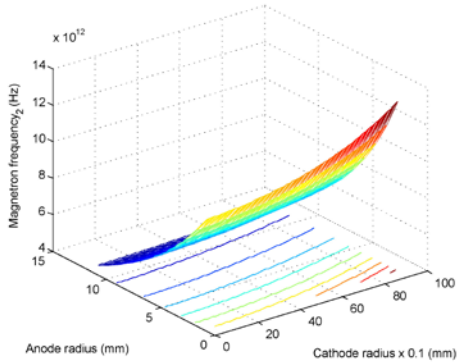

Fig. 5. A 3D plot of magnetron frequency, $f_{\text{magnetron}}$, versus anode radius, r_a, and cathode radius, r_c. This is for mode number, $n = 4$, magnetic field, $B = 0.24$ T, and magnetron voltage, $V = 25$ kV. Increasing magnetron anode radius decreases magnetron frequency. Increasing magnetron cathode radius has no significant effect on. Second solution.

$$a = \frac{\pi}{nc}(r_a^2 - r_c^2)\frac{2\pi m}{en}r_a^2 = 2.3365 \times 10^{-20}(r_a^2 - r_c^2)r_a^2 \quad (113)$$

$$b = -\frac{\pi}{nc}(r_a^2 - r_c^2)B = -(6.28 \times 10^{-6})(r_a^2 - r_c^2)$$
$$c_x = V\ ;\ f = f_{\text{magnetron}} \quad (114)$$

$$f\text{magnetron}_1 = \frac{-b + \sqrt{b^2 - 4ac_x}}{2a} \quad (115)$$

$$f\text{magnetron}_2 = \frac{-b - \sqrt{b^2 - 4ac_x}}{2a} \quad (116)$$

Increasing magnetron anode radius decreases magnetron frequency. Increasing magnetron cathode radius has no significant effect on as can be seen in Figs. 4–7.

Case A:
r_c: 0.001 m→ 0.01 m in steps of 0.0001 m.
r_a: 0.02 m→ 0.03 m in steps of 0.001 m, for $r_a > r_c$

Case B:
r_c: 0.1 m→ 1 m in steps of 0.01 m.
r_a: 2 m→ 3 m in steps of 0.1 m, for $r_a > r_c$

Conclusion: when we increase the dimension of our magnetron by higher values of r_a, r_c our magnetron frequency decrease. Only one graph describes the actual magnetron behavior. The other graph is a mathematic solution.

$f_{\text{magnetron}} = \psi_2(V)$, we choose $r_a = 0.4$ cm $= 0.004$ m, $r_c = 0.15$ cm $= 0.0015$ m

$r_a^2 = 0.000016$ $r_c^2 = 0.0000025$ $r_a^2 - r_c^2 = 0.00001375$. $n = 4$, $B = 0.24$ T, $V = 15$ kV to 30 kV.

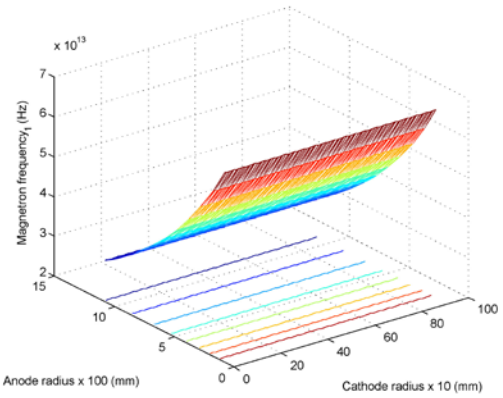

Fig. 6. The 3D plot of magnetron frequency is the same as Fig. 4, except the r_a and r_c ranges and steps. Increasing magnetron anode radius decreases magnetron frequency. Increasing magnetron cathode radius has no significant effect on. First solution.

Two different solutions for 2D plot of magnetron frequency, $f_{\text{magnetron}}$, versus magnetron voltage V. as can be seen in Figs. 8–9.

Results: We get two different behaviors for $f_{\text{magnetron}} = \psi_2(V)$, one solution is mathematic while the other is the actual magnetron behavior. $f_{\text{magnetron}} = \psi_3(n)$, we choose $r_a = 0.4$ cm $= 0.004$ m, $r_c = 0.15$ cm $= 0.0015$ m

$r_a^2 = 0.000016$; $r_c^2 = 0.0000025$; $r_a^2 - r_c^2 = 0.00001375$. $B = 0.24$ $T, V = 25$ kV. For an eight resonator magnetron, the important modes are $n = 1, 2, 3, \ldots, N/2$ where N is the number of resonators. The phase differences between the resonators is for $n = 1, 2, 3, 4$ are $\pi/4$, $\pi/2$, $3\pi/4$, and π. We change mode number n in the range $n = 1$ to $n = 4$

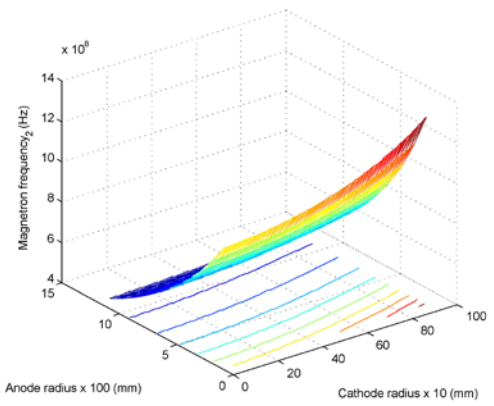

Fig. 7. The 3D plot of magnetron frequency is the same as Fig. 5, except the r_a and r_c ranges and steps. Increasing magnetron anode radius decreases magnetron frequency. Increasing magnetron cathode radius has no significant effect on. Second solution.

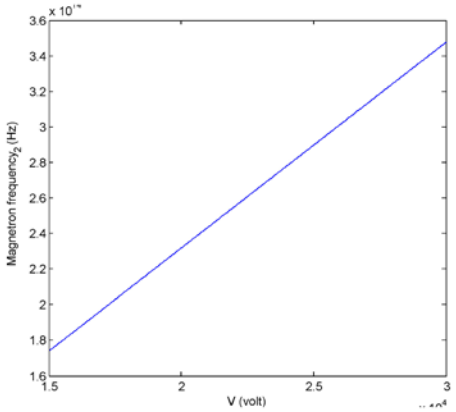

Fig. 9. A 2D plot of magnetron frequency, $f_{\text{magnetron}}$, versus magnetron voltage V. This is for mode number, $n = 4$, magnetic field, $B = 0.24$ T, anode radius, $r_a = 0.4$ cm, cathode radius, $r_c = 0.15$ cm and we change magnetron voltage between $V = 15$ kV to $V = 30$ kV. Increasing magnetron voltage causes increasing magnetron frequency. Second solution.

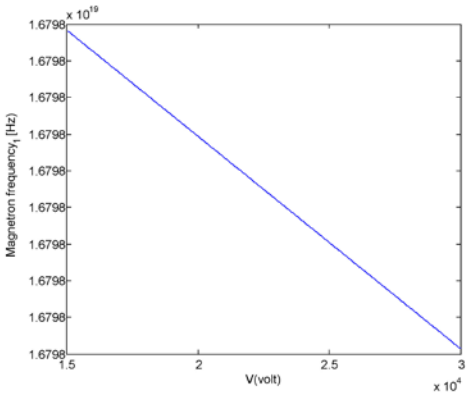

Fig. 8. A 2D plot of magnetron frequency, $f_{\text{magnetron}}$, versus magnetron voltage V. This is for mode number, $n = 4$, magnetic field, $B = 0.24$ T, anode radius, $r_a = 0.4$ cm, cathode radius, $r_c = 0.15$ cm and we change magnetron voltage between $V = 15$ kV to $V = 30$ kV. Increasing magnetron voltage causes decreasing magnetron frequency. First solution.

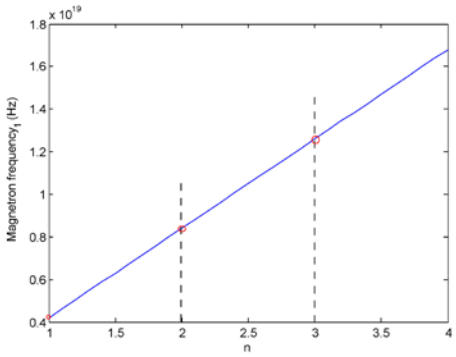

Fig. 10. A 2D plot of magnetron frequency, $f_{\text{magnetron}}$, versus magnetron mode number n. This is for magnetic field, $B = 0.24$ T, anode radius, $r_a = 0.4$ cm, cathode radius, $r_c = 0.15$ cm, magnetron voltage , $V = 25$ kV, and we change magnetron mode number between $n = 1$ to $n = 4$. Increasing magnetron mode number causes increasing magnetron frequency. First solution.

and get the values for a, b, c_x ; $a = \frac{8.2245\times10^{-29}}{n^2}$; $b = -\frac{3.454\times10^{-10}}{n}$; $c_x = 25000$

Two solutions for 2D plot of magnetron frequency, $f_{\text{magnetron}}$, versus magnetron mode number n as can be seen in Figs. 10–11.

Results: magnetron higher mode gives higher frequency. we get two behaviors, one is mathematic while the other is the actual behavior of magnetron.

$f_{\text{magnetron}} = \psi_4(B)$, we choose $r_a = 0.4$ cm $= 0.004$ m, r_c=0.15 cm=0.0015 m and

$r_a^2 = 0.000016$ $r_c^2 = 0.0000025$ $r_a^2 - r_c^2 = 0.00001375$. $V = 25$ kV, $n = 4$, $B = 0.2$ T to 0.3 T.

$a = (2.3365 \times 10^{-20}) \times 0.00001375 \times 0.000016$, $b = -\frac{3.14}{4\times3\times10^8} \times 0.00001375 \times B$

Two solutions for 2D plot of magnetron frequency, $f_{\text{magnetron}}$, versus magnetron magnetic field B as can be seen in Figs. 12–13.

Results: We have two different behaviors for $f_{\text{magnetron}} = \psi_4(B)$, one is a mathematic solution while the other is an actual magnetron behavior.

VII. Magnetron Design Weaknesses and Why It Might Not Work - Solution

We already plot our magnetron frequency versus magnetron voltage V and got two graphical solutions. The first graph shows the result that increasing magnetron voltage causes

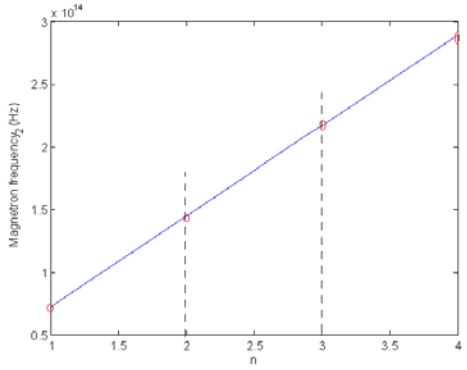

Fig. 11. A 2D plot of magnetron frequency, $f_{magnetron}$, versus magnetron mode number n. This is for magnetic field, $B = 0.24$ T, anode radius, $r_a = 0.4$ cm, cathode radius, $r_c = 0.15$ cm, magnetron voltage , $V = 25$ kV, and we change magnetron mode number between $n = 1$ to $n = 4$. Increasing magnetron mode number causes increasing magnetron frequency. Second solution.

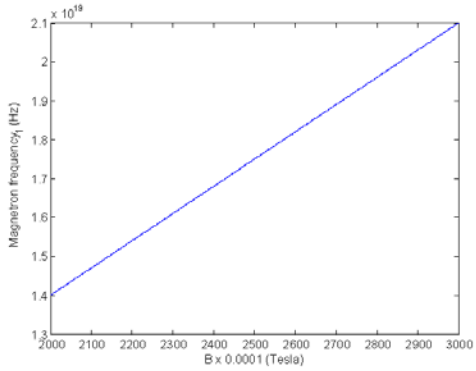

Fig. 12. A 2D plot of magnetron frequency, $f_{magnetron}$, versus magnetron magnetic field B. This is for mode number, $n = 4$, anode radius, $r_a = 0.4$ cm, cathode radius, $r_c = 0.15$ cm, magnetron voltage, $V = 25$ kV, and we change magnetron magnetic field between $B = 0.2$ T to $B = 0.3$ T. Increasing magnetron magnetic field causes increasing magnetron frequency. First solution.

decreasing magnetron frequency while the other shows that increasing magnetron voltage causes increasing magnetron frequency. One solution is only mathematical while the other is the real behavior of our magnetron. The function graphs magnetron frequency versus mode number n give two results. Both show the behavior that increasing magnetron mode number causes increasing magnetron frequency. The results show that the mode number n must be bigger than one. The function graphs magnetron frequency versus magnetron magnetic field B give two solutions. The first solution shows that increasing magnetron magnetic field causes increasing magnetron frequency while the other graph shows that increasing magnetron magnetic field causes decreasing magnetron

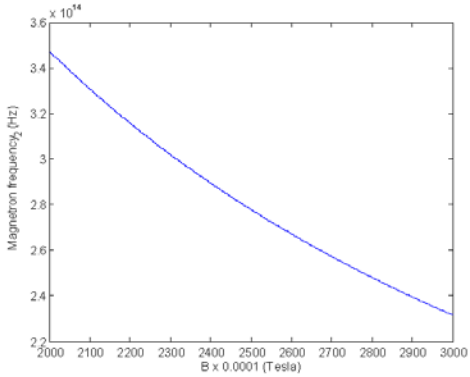

Fig. 13. A 2D plot of magnetron frequency, $f_{magnetron}$, versus magnetron magnetic field B. This is for mode number, $n = 4$, anode radius, $r_a = 0.4$ cm, cathode radius, $r_c = 0.15$ cm, magnetron voltage, $V = 25$ kV, and we change magnetron magnetic field between $B = 0.2$ T to $B = 0.3$ T. Increasing magnetron magnetic field causes decreasing magnetron frequency. First solution.

frequency. One solution is only mathematical while the other is the real behavior of our magnetron. The magnetic field B and mode number n can not be negative or complex numbers. We got two mathematical function solutions for magnetron frequency ($f_{magnetron1}$, $f_{magnetron2}$). The frequency must be a real number (not negative or complex).

$$\begin{aligned} f_{magnetron1} &= \frac{-b+\sqrt{b^2-4ac_x}}{2a} \\ f_{magnetron2} &= \frac{-b-\sqrt{b^2-4ac_x}}{2a} \end{aligned} \tag{117}$$

$$a = \frac{\pi}{nc}(r_a^2 - r_c^2)\frac{2\pi m}{en}r_a^2; b = -\frac{\pi}{nc}(r_a^2 - r_c^2)B; c_x = V \tag{118}$$

$$\begin{aligned} &Case I: b^2 - 4ac_x = 0 \Rightarrow b^2 = 4ac_x \Rightarrow \\ &\frac{\pi^2}{n^2c^2}(r_a^2 - r_c^2)^2B^2 = 4\frac{\pi}{nc}(r_a^2 - r_c^2)\frac{2\pi m}{en}r_a^2V \end{aligned} \tag{119}$$

$$\frac{\pi^2}{n^2c^2}(r_a^2 - r_c^2)^2B^2 - 8\frac{\pi}{nc}(r_a^2 - r_c^2)\frac{\pi m}{en}r_a^2V = 0 \tag{120}$$

$$\begin{aligned} &\frac{\pi^2}{n^2c}(r_a^2 - r_c^2)(\frac{1}{c}(r_a^2 - r_c^2)B^2 - 8\frac{m}{e}r_a^2V) = 0 \Rightarrow \\ &B = \sqrt{8\frac{m}{e}r_a^2V\frac{c}{(r_a^2 - r_c^2)}} \end{aligned} \tag{121}$$

Since $r_a \neq r_c; r_a > r_c$ then must fulfill
$\frac{1}{c}(r_a^2 - r_c^2)B^2 = 8\frac{m}{e}r_a^2V$

$$\begin{aligned} &f_{magnetron1} = f_{magnetron2} = \frac{-b}{2a} > 0 \\ &f_{magnetron1} = f_{magnetron2} = \frac{-b}{2a} \\ &= \frac{\frac{\pi}{nc}(r_a^2 - r_c^2)B}{2\frac{\pi}{nc}(r_a^2 - r_c^2)\frac{2\pi m}{en}r_a^2} \end{aligned} \tag{122}$$

$$f_{magnetron} = f_{magnetron1} = f_{magnetron2} = \frac{Ben}{4\pi m r_a^2} \tag{123}$$

1)

$$\frac{1}{c}(r_a^2-r_c^2)B^2=8\frac{m}{e}r_a^2V \\ B=\sqrt{8\frac{m}{e}r_a^2V\frac{c}{(r_a^2-r_c^2)}} \tag{124}$$

2)

$$f_{magnetron}=\frac{Ben}{4\pi mr_a^2} \\ B=\frac{4\pi mr_a^2}{en}f_{magnetron} \tag{125}$$

$$(1)=(2)\rightarrow \frac{4\pi mr_a^2}{en}f_{magnetron}=\sqrt{8\frac{m}{e}r_a^2V\frac{c}{(r_a^2-r_c^2)}} \\ f_{magnetron}=\frac{n}{2\pi r_a}\sqrt{\frac{2Vce}{(r_a^2-r_c^2)m}} \tag{126}$$

$1THz=10^{12}(Hz)$our magnetron $f_{magnetron}\in[0.1THz-10THz]$then $0.1THz\leq f_{magnetron}\leq 10THz$. Since $f_{magnetron}=f_{magnetron1}=f_{magnetron2}=\frac{Ben}{4\pi mr_a^2}$
The magnetron magnetic field is very important and we want to find the gap.

$$0.1THz\leq\frac{Ben}{4\pi mr_a^2}\leq 10THz\Rightarrow \\ \frac{4\pi mr_a^2}{en}10^{11}Hz\leq B\leq\frac{4\pi mr_a^2}{en}10^{13}Hz \tag{127}$$

$$n=4;\pi=314;m=9.1\times10^{-31}kg \\ e=1.6\times10^{-19}C;r_a=0.003m\rightarrow 0.009m \tag{128}$$

$$B_{\max}=\frac{4\pi mr_a^2}{en}10^{13}Hz;B_{\min}=\frac{4\pi mr_a^2}{en}10^{11}Hz \\ B_{\max(r_a=0.003m)}=0.0016T \\ B_{\max(r_a=0.009m)}=0.0048T \tag{129}$$

$$B_{\min(r_a=0.003m)}=1.6073\text{e}-005\text{T} \\ B_{\min(r_a=0.009m)}=4.8219\text{e}-005\text{T} \tag{130}$$

$$CaseII: b^2-4ac_x>0\Rightarrow b^2>4ac_x \\ \frac{\pi^2}{n^2c^2}(r_a^2-r_c^2)^2B^2>4\frac{\pi}{nc}(r_a^2-r_c^2)\frac{2\pi m}{en}r_a^2V \tag{131}$$

$$\frac{\pi^2}{n^2c^2}(r_a^2-r_c^2)^2B^2-8\frac{\pi}{nc}(r_a^2-r_c^2)\frac{\pi m}{en}r_a^2V>0 \tag{132}$$

$$\frac{\pi^2}{n^2c}(r_a^2-r_c^2)(\frac{1}{c}(r_a^2-r_c^2)B^2-8\frac{m}{e}r_a^2V)>0 \\ \frac{\pi^2}{n^2c}(r_a^2-r_c^2)>0;r_a>r_c;r_a\neq r_c \tag{133}$$

Since $r_a\neq r_c;r_a>r_c$ then must fulfill

$$\frac{1}{c}(r_a^2-r_c^2)B^2>8\frac{m}{e}r_a^2V \\ \frac{1}{c}(r_a^2-r_c^2)B^2-8\frac{m}{e}r_a^2V>0 \tag{134}$$

$$\frac{1}{c}(r_a^2-r_c^2)B^2-8\frac{m}{e}r_a^2V=(B\sqrt{\frac{(r_a^2-r_c^2)}{c}} \\ +r_a2\sqrt{\frac{2mV}{e}})(B\sqrt{\frac{(r_a^2-r_c^2)}{c}}-r_a2\sqrt{\frac{2mV}{e}}) \tag{135}$$

$(B\sqrt{\frac{(r_a^2-r_c^2)}{c}}+r_a2\sqrt{\frac{2mV}{e}})>0$ for all magnetron parameters values then
$B\sqrt{\frac{(r_a^2-r_c^2)}{c}}-r_a2\sqrt{\frac{2mV}{e}}>0$ must be fulfill.

$$B\sqrt{\frac{(r_a^2-r_c^2)}{c}}-r_a2\sqrt{\frac{2mV}{e}}>0 \\ \Rightarrow B\sqrt{\frac{(r_a^2-r_c^2)}{c}}>r_a2\sqrt{\frac{2mV}{e}} \\ \Rightarrow B>r_a2\sqrt{\frac{2mVc}{e(r_a^2-r_c^2)}} \tag{136}$$

$$B>r_a2\sqrt{\frac{2mVc}{e(r_a^2-r_c^2)}}. \tag{137}$$

$$f_{magnetron1}=\frac{-b+\sqrt{b^2-4ac_x}}{2a} \\ b<0\Rightarrow -b>0;a=\frac{\pi}{nc}(r_a^2-r_c^2)\frac{2\pi m}{en}r_a^2>0 \\ f_{magnetron1}>0 \tag{138}$$

$f_{magnetron2}=\frac{-b-\sqrt{b^2-4ac_x}}{2a}$. We need to find our magnetron parameters restriction for getting real and positive frequency ($f_{magnetron2}>0$).

$$-b-\sqrt{b^2-4ac_x}>0\Rightarrow -b>\sqrt{b^2-4ac_x} \tag{139}$$

$$\frac{\pi}{nc}(r_a^2-r_c^2)B> \\ \sqrt{\frac{\pi^2}{n^2c^2}(r_a^2-r_c^2)^2B^2-4\frac{\pi}{nc}(r_a^2-r_c^2)\frac{2\pi m}{en}r_a^2V} \tag{140}$$

$$\frac{\pi}{nc}(r_a^2-r_c^2)B> \\ \sqrt{(r_a^2-r_c^2)\frac{\pi^2}{n^2c}(\frac{1}{c}(r_a^2-r_c^2)B^2-\frac{8m}{e}r_a^2V)} \tag{141}$$

$$\frac{\pi}{nc}(r_a^2-r_c^2)B> \\ \frac{\pi}{n\sqrt{c}}\sqrt{(r_a^2-r_c^2)}\sqrt{(\frac{1}{c}(r_a^2-r_c^2)B^2-\frac{8m}{e}r_a^2V)} \tag{142}$$

$$\frac{\pi}{nc}(r_a^2-r_c^2)B \\ -\frac{\pi}{n\sqrt{c}}\sqrt{(r_a^2-r_c^2)}\sqrt{(\frac{1}{c}(r_a^2-r_c^2)B^2-\frac{8m}{e}r_a^2V)}>0 \tag{143}$$

$$\frac{\pi}{n\sqrt{c}}\sqrt{(r_a^2-r_c^2)}(B\sqrt{\frac{(r_a^2-r_c^2)}{c}} \\ -\sqrt{(\frac{1}{c}(r_a^2-r_c^2)B^2-\frac{8m}{e}r_a^2V))}>0 \tag{144}$$

$$\frac{\pi}{n\sqrt{c}}\sqrt{(r_a^2-r_c^2)}>0 then \\ B\sqrt{\frac{(r_a^2-r_c^2)}{c}}-\sqrt{(\frac{1}{c}(r_a^2-r_c^2)B^2-\frac{8m}{e}r_a^2V)}>0 \tag{145}$$

$$B>\sqrt{\frac{c}{(r_a^2-r_c^2)}}\sqrt{(\frac{1}{c}(r_a^2-r_c^2)B^2-\frac{8m}{e}r_a^2V)} \\ \Rightarrow B>\sqrt{(B^2-\frac{8m}{e}r_a^2V\frac{c}{(r_a^2-r_c^2)})} \tag{146}$$

$$B\sqrt{\frac{(r_a^2-r_c^2)}{c}}-B\sqrt{(\frac{1}{c}(r_a^2-r_c^2)-\frac{8m}{eB^2}r_a^2V)}>0 \tag{147}$$

$$B(\sqrt{\frac{(r_a^2-r_c^2)}{c}}-\sqrt{(\frac{1}{c}(r_a^2-r_c^2)-\frac{8m}{eB^2}r_a^2V)})>0 \\ B>0 \tag{148}$$

then

$$B\sqrt{\frac{(r_a^2-r_c^2)}{c}}(1-\sqrt{(1-\frac{8mc}{(r_a^2-r_c^2)eB^2}r_a^2V)})>0 \\ 1-\sqrt{(1-\frac{8mc}{(r_a^2-r_c^2)eB^2}r_a^2V)}>0 \tag{149}$$

$$\sqrt{(1-\frac{8m}{eB^2}\frac{c}{(r_a^2-r_c^2)}r_a^2V)}<1 \\ \Rightarrow 0\leq 1-\frac{8m}{eB^2}\frac{c}{(r_a^2-r_c^2)}r_a^2V<1 \tag{150}$$

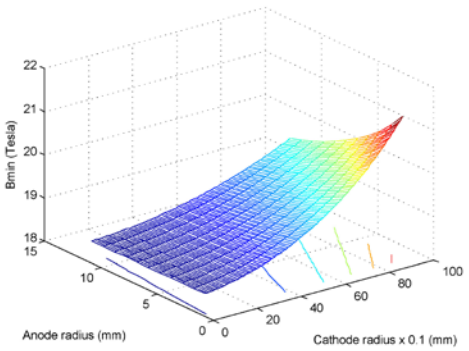

Fig. 14. The 3D plot of magnetron minimum magnetic field as a function of r_a and r_c ranges and steps. Increasing magnetron anode radius decreases magnetron minimum magnetic field value. Increasing magnetron cathode radius increases minimum magnetic field value.

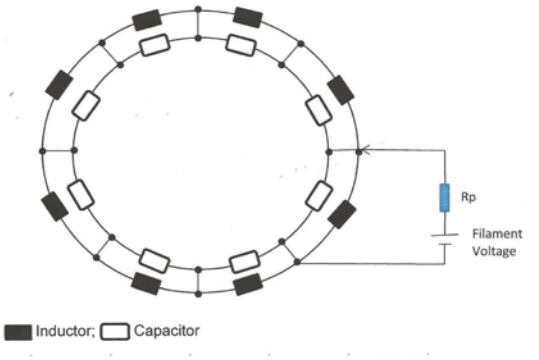

Fig. 15. Schematic of magnetron eight cavity anode equivalent circuit. One cavity equivalent circuit is represented as a parallel capacitor and inductor resonant circuit. We have eight magnetron cavities in loop series and one magnetron filament voltage source which is connected in parallel to one magnetron cavity element. Magnetron filament voltage source has parasitic resistance r_p.

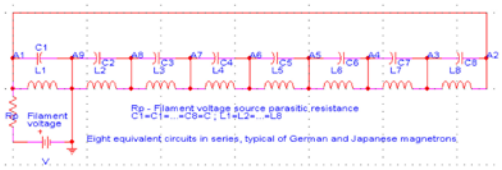

Fig. 16. Schematic of magnetron eight cavity anode equivalent circuit. One cavity equivalent circuit is represented as a parallel capacitor and inductor resonant circuit. We have eight magnetron cavities in loop series and one magnetron filament voltage source which is connected in parallel to one magnetron cavity element. It is typical German and Japanese magnetron. Magnetron filament voltage source has parasitic resistance r_p

$$0 \le 1 - \frac{8m}{eB^2}\frac{c}{(r_a^2-r_c^2)}r_a^2V < 1$$
$$\{\frac{8m}{eB^2}\frac{c}{(r_a^2-r_c^2)}r_a^2V > 0\} \cap \{\frac{8m}{eB^2}\frac{c}{(r_a^2-r_c^2)}r_a^2V \le 1\} \quad (151)$$

$$\frac{8m}{e}\frac{c}{(r_a^2-r_c^2)}r_a^2V \le B^2$$
$$\Rightarrow B^2 - \frac{8m}{e}\frac{c}{(r_a^2-r_c^2)}r_a^2V \ge 0 \quad (152)$$
$$(B + r_a\sqrt{\frac{8mcV}{e(r_a^2-r_c^2)}})(B - r_a\sqrt{\frac{8mcV}{e(r_a^2-r_c^2)}}) > 0$$

$B + r_a\sqrt{\frac{8mcV}{e(r_a^2-r_c^2)}} > 0$ always, then $B - r_a\sqrt{\frac{8mcV}{e(r_a^2-r_c^2)}}$ must fulfil.

$$B - r_a\sqrt{\frac{8mcV}{e(r_a^2-r_c^2)}} > 0 \Rightarrow B > r_a\sqrt{\frac{8mcV}{e(r_a^2-r_c^2)}} \quad (153)$$
$$(2) B > r_a\sqrt{\frac{8mcV}{e(r_a^2-r_c^2)}}$$

$$(1) \cap (2) = \{B > r_a 2\sqrt{\frac{2mVc}{e(r_a^2-r_c^2)}}\} \quad (154)$$
$$\cap \{B > r_a\sqrt{\frac{8mcV}{e(r_a^2-r_c^2)}}\} = B > r_a 2\sqrt{\frac{2mVc}{e(r_a^2-r_c^2)}}$$

$$B > B_{\min}; B_{\min} = r_a 2\sqrt{\frac{2mVc}{e(r_a^2-r_c^2)}} \quad (155)$$

We need to plot B_{min} function vs two magnetron variables r_a, r_c.

VIII. Magnetron Eight Cavity Anode Equivalent Circuit Stability Analysis

Magnetron eight cavity anode equivalent circuit is describe in figures Figs. 15–16. The elements C and L are magnetron one cavity capacitance and inductance equivalent circuit. The letters A_i for $i = 1, .., 9$ are relate to magnetron equivalent circuit nodes.

$$I_{R_P} = I_{C1} + I_{L1} + I_{C8} + I_{L8}\ ;\ I_{C8} + I_{L8} = I_{C7} + I_{L7}$$
$$I_{C7} + I_{L7} = I_{C6} + I_{L6}\ ;\ I_{C6} + I_{L6} = I_{C5} + I_{L5} \quad (156)$$

$$I_{C5} + I_{L5} = I_{C4} + I_{L4}\ ;\ I_{C4} + I_{L4} = I_{C3} + I_{L3}$$
$$I_{C3} + I_{L3} = I_{C2} + I_{L2}\ ;\ V = V_{R_P} + V_{L1} = V_{R_P} + V_{C1} \quad (157)$$

$$V_{A1} - V_{A9} = V_{C1} = V_{L1}\ ;\ V_{A2} - V_{A3} = V_{C8} = V_{L8}$$
$$V_{A3} - V_{A4} = V_{C7} = V_{L7}\ ;\ V_{A4} - V_{A5} = V_{C6} = V_{L6} \quad (158)$$

$$V_{A5} - V_{A6} = V_{C5} = V_{L5}\ ;\ V_{A6} - V_{A7} = V_{C4} = V_{L4}$$
$$V_{A7} - V_{A8} = V_{C3} = V_{L3}\ ;\ V_{A8} - V_{A9} = V_{C2} = V_{L2} \quad (159)$$

$$V_{A9} = 0 \Rightarrow V_{A1} = V_{C1} = V_{L1}\ ;\ V_{A8} = V_{C2} = V_{L2}$$
$$I_{C1} = C_1\frac{dV_{C1}}{dt}\ ;\ V_{L1} = L_1\frac{dI_{L1}}{dt}\ ;\ I_{C2} = C_2\frac{dV_{C2}}{dt}$$
$$V_{L2} = L_2\frac{dI_{L2}}{dt}\ ;\ I_{C3} = C_3\frac{dV_{C3}}{dt}\ ;\ V_{L3} = L_3\frac{dI_{L3}}{dt}$$
$$I_{C4} = C_4\frac{dV_{C4}}{dt}\ ;\ V_{L4} = L_4\frac{dI_{L4}}{dt} \quad (160)$$

$$I_{C5}=C_5\frac{dV_{C5}}{dt}\ ;V_{L5}=L_5\frac{dI_{L5}}{dt}\ ;I_{C6}=C_6\frac{dV_{C6}}{dt}\\ V_{L6}=L_6\frac{dI_{L6}}{dt}\ ;I_{C7}=C_7\frac{dV_{C7}}{dt}\ ;V_{L7}=L_7\frac{dI_{L7}}{dt} \quad (161)$$

$$I_{C8}=C_8\frac{dV_{C8}}{dt}\ ;V_{L8}=L_8\frac{dI_{L8}}{dt}\ ;V_{R_P}=I_{R_P}R_P\\ V=I_{R_P}R_P+L_1\frac{dI_{L1}}{dt}=I_{R_P}R_P+V_{C1} \quad (162)$$

$$I_{C_1}=C_1\frac{dV_{C_1}}{dt}\Rightarrow V_{C_1}=\frac{1}{C_1}\int I_{C_1}dt\\ V=I_{R_P}R_P+L_1\frac{dI_{L_1}}{dt}=I_{R_P}R_P+\frac{1}{C_1}\int I_{C_1}dt \quad (163)$$

$$\frac{dV}{dt}=\frac{dI_{R_P}}{dt}R_P+\frac{1}{C_1}I_{C1}\\ I_{R_P}=C_1\frac{dV_{C1}}{dt}+I_{L1}+C_8\frac{dV_{C8}}{dt}+I_{L8}\\ V_{L1}=L_1\frac{dI_{L1}}{dt}\Rightarrow I_{L1}=\frac{1}{L_1}\int V_{L1}dt \quad (164)$$

$$V_{L8}=L_8\frac{dI_{L8}}{dt}\Rightarrow I_{L8}=\frac{1}{L_8}\int V_{L8}dt\\ I_{R_P}=C_1\frac{dV_{C1}}{dt}+\frac{1}{L_1}\int V_{L1}dt+C_8\frac{dV_{C8}}{dt}+\frac{1}{L_8}\int V_{L8}dt \quad (165)$$

$$\frac{dI_{R_P}}{dt}=C_1\frac{d^2V_{C1}}{dt^2}+\frac{1}{L_1}V_{L1}+C_8\frac{d^2V_{C8}}{dt^2}+\frac{1}{L_8}V_{L8}\\ C_8\frac{dV_{C8}}{dt}+\frac{1}{L_8}\int V_{L8}dt=C_7\frac{dV_{C7}}{dt}+\frac{1}{L_7}\int V_{L7}dt \quad (166)$$

$$V_{L8}=L_8\frac{dI_{L8}}{dt}\Rightarrow I_{L8}=\frac{1}{L_8}\int V_{L8}dt\\ V_{L7}=L_7\frac{dI_{L7}}{dt}\Rightarrow I_{L7}=\frac{1}{L_7}\int V_{L7}dt \quad (167)$$

$$C_8\frac{d^2V_{C8}}{dt^2}+\frac{1}{L_8}V_{L8}=C_7\frac{d^2V_{C7}}{dt^2}+\frac{1}{L_7}V_{L7}\\ C_7\frac{dV_{C7}}{dt}+\frac{1}{L_7}\int V_{L7}dt=C_6\frac{dV_{C6}}{dt}+\frac{1}{L_6}\int V_{L6}dt \quad (168)$$

$$V_{L6}=L_6\frac{dI_{L6}}{dt}\Rightarrow I_{L6}=\frac{1}{L_6}\int V_{L6}dt\\ C_7\frac{d^2V_{C7}}{dt^2}+\frac{1}{L_7}V_{L7}=C_6\frac{d^2V_{C6}}{dt^2}+\frac{1}{L_6}V_{L6} \quad (169)$$

$$C_6\frac{dV_{C6}}{dt}+\frac{1}{L_6}\int V_{L6}dt=\frac{1}{L_5}\int V_{L5}dt+C_5\frac{dV_{C5}}{dt}\\ V_{L5}=L_5\frac{dI_{L5}}{dt}\Rightarrow I_{L5}=\frac{1}{L_5}\int V_{L5}dt \quad (170)$$

$$C_6\frac{d^2V_{C6}}{dt^2}+\frac{1}{L_6}V_{L6}=\frac{1}{L_5}V_{L5}+C_5\frac{d^2V_{C5}}{dt^2}\\ C_5\frac{dV_{C5}}{dt}+\frac{1}{L_5}\int V_{L5}dt=C_4\frac{dV_{C4}}{dt}+\frac{1}{L_4}\int V_{L4}dt \quad (171)$$

$$V_{L4}=L_4\frac{dI_{L4}}{dt}\Rightarrow I_{L4}=\frac{1}{L_4}\int V_{L4}dt\\ C_5\frac{d^2V_{C5}}{dt^2}+\frac{1}{L_5}V_{L5}=C_4\frac{d^2V_{C4}}{dt^2}+\frac{1}{L_4}V_{L4} \quad (172)$$

$$C_4\frac{dV_{C4}}{dt}+\frac{1}{L_4}\int V_{L4}dt=C_3\frac{dV_{C3}}{dt}+\frac{1}{L_3}\int V_{L3}dt\\ V_{L3}=L_3\frac{dI_{L3}}{dt}\Rightarrow I_{L3}=\frac{1}{L_3}\int V_{L3}dt \quad (173)$$

$$C_4\cdot\frac{d^2V_{C4}}{dt^2}+\frac{1}{L_4}V_{L4}=C_3\frac{d^2V_{C3}}{dt^2}+\frac{1}{L_3}V_{L3} \quad (174)$$

$$C_3\frac{dV_{C3}}{dt}+\frac{1}{L_3}\int V_{L3}dt=C_2\frac{dV_{C2}}{dt}+\frac{1}{L_2}\int V_{L2}dt \quad (175)$$

$$V_{L2}=L_2\frac{dI_{L2}}{dt}\Rightarrow I_{L2}=\frac{1}{L_2}\int V_{L2}dt\\ C_3\frac{d^2V_{C3}}{dt^2}+\frac{1}{L_3}V_{L3}=C_2\frac{d^2V_{C2}}{dt^2}+\frac{1}{L_2}V_{L2} \quad (176)$$

We can summery our intermediate results equations:

$$C_3\frac{d^2V_{C3}}{dt^2}+\frac{1}{L_3}V_{L3}=C_2\frac{d^2V_{C2}}{dt^2}+\frac{1}{L_2}V_{L2}\\ C_4\frac{d^2V_{C4}}{dt^2}+\frac{1}{L_4}V_{L4}=C_3\frac{d^2V_{C3}}{dt^2}+\frac{1}{L_3}V_{L3} \quad (177)$$

$$C_5\frac{d^2V_{C5}}{dt^2}+\frac{1}{L_5}V_{L5}=C_4\frac{d^2V_{C4}}{dt^2}+\frac{1}{L_4}V_{L4}\\ C_6\frac{d^2V_{C6}}{dt^2}+\frac{1}{L_6}V_{L6}=\frac{1}{L_5}V_{L5}+C_5\frac{d^2V_{C5}}{dt^2} \quad (178)$$

$$C_7\frac{d^2V_{C7}}{dt^2}+\frac{1}{L_7}V_{L7}=C_6\frac{d^2V_{C6}}{dt^2}+\frac{1}{L_6}V_{L6}\\ C_8\frac{d^2V_{C8}}{dt^2}+\frac{1}{L_8}V_{L8}=C_7\frac{d^2V_{C7}}{dt^2}+\frac{1}{L_7}V_{L7} \quad (179)$$

$$\frac{dI_{R_P}}{dt}=C_1\frac{d^2V_{C1}}{dt^2}+\frac{1}{L_1}V_{L1}+C_8\frac{d^2V_{C8}}{dt^2}+\frac{1}{L_8}V_{L8}\\ \frac{dV}{dt}=\frac{dI_{R_P}}{dt}R_P+\frac{1}{C_1}I_{C1}\ ;V=I_{R_P}R_P+L_1\frac{dI_{L1}}{dt} \quad (180)$$

$$V=I_{R_P}R_P+L_1\frac{dI_{L1}}{dt}\Rightarrow L_1\frac{dI_{L1}}{dt}=V-I_{R_P}R_P\\ \Rightarrow\frac{dI_{L1}}{dt}=\frac{V}{L_1}-I_{R_P}\frac{R_P}{L_1}\ ;L_1=L \quad (181)$$

$$\frac{dI_{L1}}{dt}=\frac{V}{L_1}-I_{R_P}\frac{R_P}{L_1}\Rightarrow\frac{dI_{L1}}{dt}=\frac{V}{L}-I_{R_P}\frac{R_P}{L}\\ \frac{dI_{R_P}}{dt}=C_1\frac{d^2V_{C1}}{dt^2}+\frac{1}{L_1}V_{L1}+C_8\frac{d^2V_{C8}}{dt^2}+\frac{1}{L_8}V_{L8} \quad (182)$$

$$\frac{1}{C_1}\frac{dI_{R_P}}{dt}=\frac{d^2V_{C1}}{dt^2}+\frac{1}{L_1C_1}V_{L1}+\frac{C_8}{C_1}\frac{d^2V_{C8}}{dt^2}+\frac{1}{L_8C_1}V_{L8}\\ \mathrm{C}_1=C_2=...=C_8=C \quad (183)$$

$$\frac{1}{C}\frac{dI_{R_P}}{dt}=\frac{d^2V_{C1}}{dt^2}+\frac{1}{LC}V_{L1}+\frac{d^2V_{C8}}{dt^2}+\frac{1}{LC}V_{L8}\\ \frac{dI_{R_P}}{dt}=X\ ;L_1=L_2=...=L \quad (184)$$

We define the following new variables:

$$Y=\frac{dV_{L1}}{dt}+\frac{dV_{L8}}{dt}\\ \frac{1}{C}\frac{dI_{R_P}}{dt}=\frac{d^2V_{C1}}{dt^2}+\frac{d^2V_{C8}}{dt^2}+\frac{1}{LC}(V_{L8}+V_{L1})\\ V_{Li}=V_{Ci}\ \forall i=1,..,8 \quad (185)$$

$$\frac{1}{C}\frac{dI_{R_P}}{dt}=\frac{d^2V_{C1}}{dt^2}+\frac{d^2V_{C8}}{dt^2}+\frac{1}{LC}(V_{C8}+V_{C1})\\ \frac{1}{C}X=\frac{d^2V_{C1}}{dt^2}+\frac{d^2V_{C8}}{dt^2}+\frac{1}{LC}(V_{C8}+V_{C1}) \quad (186)$$

$$\frac{1}{C}X=\frac{dY}{dt}+\frac{1}{LC}(V_{C8}+V_{C1})\Rightarrow\frac{1}{C}X=\frac{dY}{dt}+\frac{1}{LC}Y_1\\ Y_1=V_{C8}+V_{C1}\ ;Y=\frac{dY_1}{dt} \quad (187)$$

$$\frac{1}{C}X=\frac{dY}{dt}+\frac{1}{LC}Y_1\Rightarrow\frac{dY}{dt}=\frac{1}{C}X-\frac{1}{LC}Y_1 \quad (188)$$

$$C_8\frac{d^2V_{C8}}{dt^2}+\frac{1}{L_8}V_{L8}=C_7\frac{d^2V_{C7}}{dt^2}+\frac{1}{L_7}V_{L7}\Rightarrow\\ C_8\frac{d^2V_{C8}}{dt^2}-C_7\frac{d^2V_{C7}}{dt^2}=\frac{1}{L_7}V_{L7}-\frac{1}{L_8}V_{L8} \quad (189)$$

$$Y_2=\frac{dV_{C8}}{dt}-\frac{dV_{C7}}{dt}\ ;\\ \frac{d^2V_{C8}}{dt^2}-\frac{d^2V_{C7}}{dt^2}=\frac{1}{LC}V_{L7}-\frac{1}{LC}V_{L8} \quad (190)$$

$$\frac{dY_2}{dt}=\frac{1}{LC}(V_{L7}-V_{L8})\ ;Y_3=V_{L7}-V_{L8}\Rightarrow\\ \frac{dY_2}{dt}=\frac{1}{LC}Y_3\ ;\frac{dY_3}{dt}=-Y_2 \quad (191)$$

$$C_7\frac{d^2V_{C7}}{dt^2}+\frac{1}{L_7}V_{L7}=C_6\frac{d^2V_{C6}}{dt^2}+\frac{1}{L_6}V_{L6}\Rightarrow \\ C_7\frac{d^2V_{C7}}{dt^2}-C_6\frac{d^2V_{C6}}{dt^2}=\frac{1}{L_6}V_{L6}-\frac{1}{L_7}V_{L7} \quad (192)$$

$$\frac{d^2V_{C7}}{dt^2}-\frac{d^2V_{C6}}{dt^2}=\frac{1}{LC}(V_{L6}-V_{L7})\ ;\ Y_4=\frac{dV_{C7}}{dt}-\frac{dV_{C6}}{dt} \\ Y_5=V_{L6}-V_{L7}\ ;\ \frac{dY_4}{dt}=\frac{1}{LC}Y_5 \quad (193)$$

$$Y_4=-\frac{dY_5}{dt}\ ;\ C_6\frac{d^2V_{C6}}{dt^2}+\frac{1}{L_6}V_{L6}=\frac{1}{L_5}V_{L5}+C_5\frac{d^2V_{C5}}{dt^2} \quad (194)$$

$$\Rightarrow C_6\frac{d^2V_{C6}}{dt^2}-C_5\frac{d^2V_{C5}}{dt^2}=\frac{1}{L_5}V_{L5}-\frac{1}{L_6}V_{L6} \quad (195)$$

$$\frac{d^2V_{C6}}{dt^2}-\frac{d^2V_{C5}}{dt^2}=\frac{1}{LC}V_{L5}-\frac{1}{LC}V_{L6}\ ;\ Y_6=\frac{dV_{C6}}{dt}-\frac{dV_{C5}}{dt} \\ \frac{dY_6}{dt}=\frac{1}{LC}(V_{L5}-V_{L6}) \quad (196)$$

We define $Y_7=V_{L5}-V_{L6}\ ;\ \frac{dY_6}{dt}=\frac{1}{LC}Y_7\ ;\ \frac{dY_7}{dt}=-Y_6$

$$C_5\frac{d^2V_{C5}}{dt^2}+\frac{1}{L_5}V_{L5}=C_4\frac{d^2V_{C4}}{dt^2}+\frac{1}{L_4}V_{L4}\Rightarrow \\ C_5\frac{d^2V_{C5}}{dt^2}-C_4\frac{d^2V_{C4}}{dt^2}=\frac{1}{L_4}V_{L4}-\frac{1}{L_5}V_{L5} \quad (197)$$

$$C_5\frac{d^2V_{C5}}{dt^2}-C_4\frac{d^2V_{C4}}{dt^2}=\frac{1}{L_4}V_{L4}-\frac{1}{L_5}V_{L5}\Rightarrow \\ \frac{d^2V_{C6}}{dt^2}-\frac{d^2V_{C4}}{dt^2}=\frac{1}{LC}(V_{L4}-V_{L5}) \quad (198)$$

$$Y_8=\frac{dV_{C5}}{dt}-\frac{dV_{C4}}{dt}\ ;\ \frac{dY_8}{dt}=\frac{1}{LC}(V_{L4}-V_{L5}) \quad (199)$$

We define $Y_9=V_{L4}-V_{L5}\ ;\ \frac{dY_8}{dt}=\frac{1}{LC}Y_9$

$$\frac{dY_9}{dt}=-Y_8\ ;\ C_4\frac{d^2V_{C4}}{dt^2}+\frac{1}{L_4}V_{L4}=C_3\frac{d^2V_{C3}}{dt^2}+\frac{1}{L_3}V_{L3} \\ \Rightarrow C_4\frac{d^2V_{C4}}{dt^2}-C_3\frac{d^2V_{C3}}{dt^2}=\frac{1}{L_3}V_{L3}-\frac{1}{L_4}V_{L4} \quad (200)$$

$$\frac{d^2V_{C4}}{dt^2}-\frac{d^2V_{C3}}{dt^2}=\frac{1}{LC}(V_{L3}-V_{L4})\ ;\ Y_{10}=\frac{dV_{C4}}{dt}-\frac{dV_{C3}}{dt} \\ \frac{dY_{10}}{dt}=\frac{1}{LC}(V_{L3}-V_{L4}) \quad (201)$$

We define $Y_{11}=V_{L3}-V_{L4}\ ;\ \frac{dY_{10}}{dt}=\frac{1}{LC}Y_{11}\ ;\ \frac{dY_{11}}{dt}=-Y_{10}$

$$C_3\frac{d^2V_{C3}}{dt^2}+\frac{1}{L_3}V_{L3}=C_2\frac{d^2V_{C2}}{dt^2}+\frac{1}{L_2}V_{L2}\Rightarrow \\ C_3\frac{d^2V_{C3}}{dt^2}-C_2\frac{d^2V_{C2}}{dt^2}=\frac{1}{L_2}V_{L2}-\frac{1}{L_3}V_{L3} \quad (202)$$

$$\frac{d^2V_{C3}}{dt^2}-\frac{d^2V_{C2}}{dt^2}=\frac{1}{LC}(V_{L2}-V_{L3})\ ;\ Y_{12}=\frac{dV_{C3}}{dt}-\frac{dV_{C2}}{dt} \\ \frac{dY_{12}}{dt}=\frac{1}{LC}(V_{L2}-V_{L3}) \quad (203)$$

We define $Y_{13}=V_{L2}-V_{L3}\ ;\ \frac{dY_{12}}{dt}=\frac{1}{LC}Y_{13}\ ;\ \frac{dY_{13}}{dt}=-Y_{12}$

We can summery our system differential equations:

$$\frac{dI_{R_P}}{dt}=X\ ;\ \frac{dY_1}{dt}=Y\ ;\ \frac{dY}{dt}=\frac{1}{C}X-\frac{1}{LC}Y_1 \\ \frac{dI_{L1}}{dt}=\frac{V}{L}-I_{R_P}\frac{R_P}{L}\ ;\ \frac{dY_2}{dt}=\frac{1}{LC}Y_3\ ;\ \frac{dY_2}{dt}=-Y_2 \quad (204)$$

$$\frac{dY_4}{dt}=\frac{1}{LC}Y_5\ ;\ \frac{dY_5}{dt}=-Y_4\ ;\ \frac{dY_6}{dt}=\frac{1}{LC}Y_7 \\ \frac{dY_7}{dt}=-Y_6\ ;\ \frac{dY_8}{dt}=\frac{1}{LC}Y_9\ ;\ \frac{dY_9}{dt}=-Y_8 \quad (205)$$

$$\frac{dY_{10}}{dt}=\frac{1}{LC}Y_{11}\ ;\ \frac{dY_{11}}{dt}=-Y_{10}\ ;\ \frac{dY_{12}}{dt}=\frac{1}{LC}Y_{13} \\ \frac{dY_{13}}{dt}=-Y_{12} \quad (206)$$

We can summery our system variables:
$C_1=C_2=...=C_8=C\ ;\ L_1=L_2=...=L_8=L$

New Variable	System variable	New Variable	System variable
I_{R_P}	I_{R_P}	Y_6	$\frac{dV_{C6}}{dt}-\frac{dV_{C5}}{dt}$
X	$\frac{dI_{R_P}}{dt}$	Y_7	$V_{L5}-V_{L6}$
Y	$\frac{dV_{L1}}{dt}+\frac{dV_{L8}}{dt}$	Y_8	$\frac{dV_{C5}}{dt}-\frac{dV_{C4}}{dt}$
Y_1	$V_{C8}+V_{C1}$	Y_9	$V_{L4}-V_{L5}$
I_{L1}	I_{L1}	Y_{10}	$\frac{dV_{C4}}{dt}-\frac{dV_{C3}}{dt}$
Y_2	$\frac{dV_{C8}}{dt}-\frac{dV_{C7}}{dt}$	Y_{11}	$V_{L3}-V_{L4}$
Y_3	$V_{L7}-V_{L8}$	Y_{12}	$\frac{dV_{C3}}{dt}-\frac{dV_{C2}}{dt}$
Y_4	$\frac{dV_{C7}}{dt}-\frac{dV_{C6}}{dt}$	Y_{13}	$V_{L2}-V_{L3}$
Y_5	$V_{L6}-V_{L7}$	$V_{Li}=V_{Ci}\ \forall i=1,..,8$	

Table 2. Magnetron eight cavity new variables.

We already got the expression $V=\frac{\pi}{n\lambda_0}(r_a^2-r_c^2)(B-\frac{2\pi mc}{en\lambda_0}r_a^2)$ volts

$$\frac{dI_{L1}}{dt}=\frac{V}{L}-I_{R_P}\frac{R_P}{L}\Rightarrow \\ \frac{dI_{L1}}{dt}=\frac{1}{L}\frac{\pi}{n\lambda_0}(r_a^2-r_c^2)(B-\frac{2\pi mc}{en\lambda_0}r_a^2)-I_{R_P}\frac{R_P}{L} \quad (207)$$

$$\lambda_0=\frac{c}{f}\Rightarrow \\ \frac{I_{L1}}{dt}=\frac{1}{L}\frac{\pi f}{nc}(r_a^2-r_c^2)(B-\frac{2\pi mf}{en}r_a^2)-I_{R_P}\frac{R_P}{L} \quad (208)$$

Remark: we consider for simplicity, all resonators are the same (identical, L and C parallel) [3] [4]. We consider

$$\frac{\pi}{n\lambda_0}=\frac{300\pi}{n_0}\Rightarrow\frac{1}{n\lambda_0}=\frac{300}{n_0}\ ;\ \frac{2\pi mc}{en\lambda_0}r_a^2=\frac{10.6}{n_0} \quad (209)$$

Then $V[\text{volt}]=\frac{300\pi}{n_0}(r_a^2-r_c^2)(B-\frac{10.6}{n_0})$ by Posthumus (reduce equation). The voltage V is a linear function of B. The voltage V is known as the Hartree voltage. This voltage is that at which oscillations should start provided at the same time that B is sufficiently large so that the undistorted space charge does not extend to the anode. According to Hartree there is a functional graph of voltage [kV] vs magnetic field in tesla [T]. If we take the maximum magnetic field, the table as follow: $n=4$ ($B=0.24$ T, $V=25$ kV), $n=3$ ($B=0.24$ T, $V=41$ kV), $n=2$ ($B=0.24\ T$, $V=60\ kV$).

Analysis: The analysis is done for two set of differential equations:

First set: $\frac{dI_{R_P}}{dt}=X\ ;\ \frac{dY_1}{dt}=Y\ ;\ \frac{dY}{dt}=\frac{1}{C}X-\frac{1}{LC}Y\ \frac{dI_{L1}}{dt}=\frac{V}{L}-I_{R_P}\frac{R_P}{L}$

We have five variables: $I_{R_P}, X, Y_1, Y, I_{L1}$ and four differential equations.

Second set: $\frac{dY_k}{dt}=\frac{1}{LC}Y_{k+1}\ ;\ \frac{dY_{k+1}}{dt}=-Y_k$; k is varied from 2 to 12 according to the magnetron resonator segment. The variables are $Y_{k+1}, Y_k\ \forall\ k\in 2,...,12$

$n=4$,$n_0=120, B=0.24\ T, f=3\ GHz.\ \lambda_0=\frac{c}{f}=\frac{3\cdot10^8[m/s]}{3\cdot10^9[1/s]}=0.1\ m=9.1\times10^{-31}$ kg, $e=1.6\times10^{-19}$ C

$$\frac{2\pi mc}{en\lambda_0}r_a^2=\frac{10.6}{n_0}\Rightarrow r_a^2=3.285\Rightarrow r_a=1.81 \quad (210)$$

$r_a > r_c$. We consider magnetron cathode radius (r_c) is constant and scaling down the dimension of magnetron is done by reducing the value of magnetron anode radius (r_a). We run our MATLAB script for different values of $r_a^2-r_c^2$expression [18].

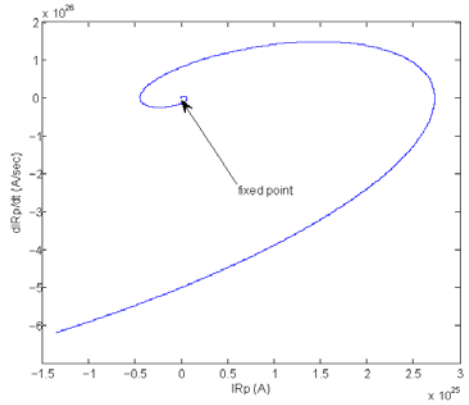

Fig. 17. Magnetron 2D function. Magnetron eight cavity $\frac{dI_{R_P}}{dt}$ A/s as a function of magnetron I_{R_P} A phase space for one cavity parameter values ($C = 1$ mF, $L = 10$ mH), magnetron filament voltage source parasitic resistance r_p is equal to 10 Ω. There is one stable spiral fixed point at $I_{R_P} = 0$, $\frac{dI_{R_P}}{dt} = 0$

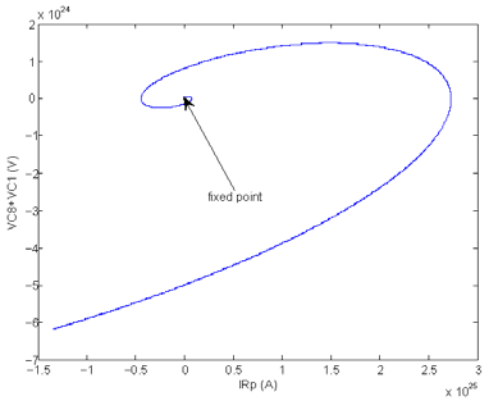

Fig. 18. Magnetron 2D function. Magnetron eight cavity $V_{C_8} + V_{C_1}$ V as a function of magnetron I_{R_P} A phase space for one cavity parameter values ($C = 1$ mF, $L = 10$ mH), magnetron filament voltage source parasitic resistance r_p is equal to 10 Ω. There is one stable spiral fixed point at $V_{C_8} + V_{C_1} = 0$, $I_{R_P} = 0$

$r_a^2 - r_c^2$	$V = \frac{300\pi}{n_0}(r_a^2 - r_c^2)(B - \frac{10.6}{n_0})$volts $n_0 = 300 \cdot 4 \cdot \frac{3 \cdot 10^8 \text{m/s}}{3 \cdot 10^9 [1/s]} = 120$ $B = 0.24$ T
10	188.4 kV
5	94.2 kV
1	18.84 kV
0.1	1.884 kV
0.01	0.188 kV

Table 3. Magnetron eight cavity V vs $r_a^2 - r_c^2$

MATLAB script for first set of differential equations: $r_p = 10$ Ω; $C = 1$ μF; $L = 1$ mH. At equilibrium points (fixed points): $\frac{dI_{R_P}}{dt} = 0$; $\frac{dY_1}{dt} = 0$; $\frac{dY}{dt} = 0$; $\frac{dI_{L1}}{dt} = 0$ then $X^* = 0$; $Y^* = 0$; $Y_1^* = 0$; $\frac{V}{L} - I_{R_P}^*$; $\frac{R_P}{L} = 0 \Rightarrow I_{R_P}^* = \frac{V}{R_P}$. If we define our system fixed points as E^* then $C = 1$ mF, $L = 10$ mH, $R_p = 10$ Ω, $IR_{p0} = 10$ A, $X_0 = 2$, $Y1_0 = 3$, $Y_0 = 4$, $IL1_0 = 5$ A. First we analyze the case $r_a^2 - r_c^2 = 10 \Rightarrow V = 188.4$ kV

where * indicates a fixed point in the phase space.

Magnetron 2D functions eight cavity phase space for different variables as can be seen in figures Figs. 17–22 for $V = 188.4$ kV.

Magnetron 2D function. Magnetron eight cavity $I_{R_P}(t), ..., I_{L_1}(t)$ as a function of time $t[sec]$ as can be seen in figure Fig. 23 for $V = 188.4$ kV.

MATLAB scripts: $r_a^2 - r_c^2 = 0.01 \Rightarrow$ V=188 V

Magnetron 2D functions eight cavity phase space for different variables as can be seen in figures Figs. 24–29 for $V = 188$ V.

Magnetron 2D function. Magnetron eight cavity $I_{R_P}(t), ..., I_{L_1}(t)$ as a function of time $t[sec]$ as can be seen in figure Fig. 30 for $V = 188$ V.

Second set: $\frac{dY_k}{dt} = \frac{1}{LC}Y_{k+1}$; $\frac{dY_{k+1}}{dt} = -Y_k$; k is varied from 2 to 12 according to the magnetron resonator segment. The variables are $Y_{k+1}, Y_k \; \forall \; k \in 2, ..., 12$. We choose k=2 then $\frac{dY_2}{dt} = \frac{1}{LC}Y_3$; $\frac{dY_2}{dt} = -Y_2$and we plot MATLAB graph for Y_3 vs Y_2, and Y_3(t), Y_2(t). MATLAB variables: $Y_2 \rightarrow x$; $Y_3 \rightarrow x$; $\frac{dY_2}{dt} \rightarrow g$; $\frac{dY_3}{dt} \rightarrow g$. $Y_2 = \frac{dV_{C8}}{dt} - \frac{dV_{C7}}{dt}$; $Y_3 = V_{L7} - V_{L8}$; $V_{C8} = V_{L8}$; $V_{C7} = V_{L7}$

We call the function: magnetronn1 (0.001,0.001,3,5).
$C = 1$ mF, $L = 1$ mH, $Y20 = 3$, $Y30 = 5$.

Magnetron eight cavity $Y_3 = V_{L_7} - V_{L_8}$[V] as a function of $Y_2 = \frac{dV_{C_8}}{dt} - \frac{dV_{C_7}}{dt}$ [V/s] magnetron phase space as can be seen in figure Fig. 31

The graph is the same for all magnetron eight cavities. Magnetron eight cavity $Y_2(t), Y_3(t)$ as a function of time t[sec] as can be seen in figure Fig. 32

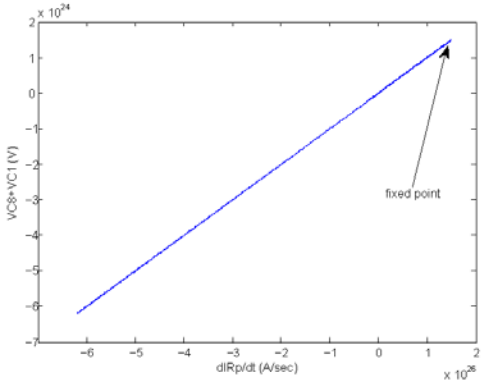

Fig. 19. Magnetron 2D function. Magnetron eight cavity $V_{C_8} + V_{C_1}$ V as a function of magnetron $\frac{dI_{R_P}}{dt}$ A/s phase space for one cavity parameter values ($C = 1$ mF, $L = 10$ mH), magnetron filament voltage source parasitic resistance r_p is equal to 10 Ω. There is one stable node fixed point at $V_{C_8} + V_{C_1} = 0$, $\frac{dI_{R_P}}{dt} = 0$

IX. Magnetron Eight Strapped Cavity Anode Equivalent Circuit Stability Analysis

Magnetron eight strapped cavity anode equivalent circuit is describe in figures Figs. 33–34. We analyse the case of magnetron eight strapped cavities anode behavior and stability under parameters variation. The below figure is a schematic of eight strapped cavities, when alternate Cavities strapped together with solid copper rings. This ensures that oscillations in cavities are in phase.

$$I_{C1} = C_1 \frac{d}{dt}(V_B - V_A) \; ; V_{L1} = V_B - V_A = L_1 \frac{dI_{L1}}{dt}$$
$$I_{C2} = C_2 \frac{d}{dt}(V_B - V_A) \; ; V_{L2} = V_B - V_A = L_2 \frac{dI_{L2}}{dt} \quad (211)$$

$$I_{C3} = C_3 \frac{d}{dt}(V_B - V_A) \; ; V_{L3} = V_B - V_A = L_3 \frac{dI_{L3}}{dt}$$
$$I_{C4} = C_4 \frac{d}{dt}(V_B - V_A) \; ; V_{L4} = V_B - V_A = L_4 \frac{dI_{L4}}{dt} \quad (212)$$

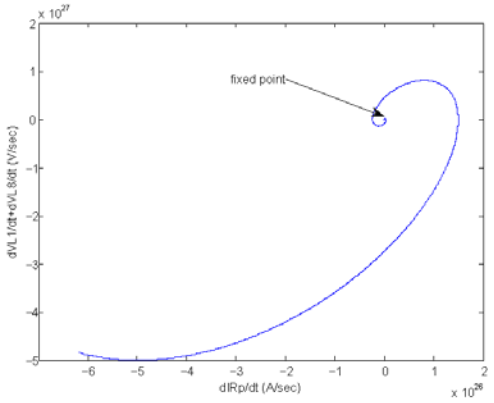

Fig. 20. Magnetron 2D function. Magnetron eight cavity $\frac{dV_{L_1}}{dt}+\frac{dV_{L_8}}{dt}$ V/s as a function of magnetron $\frac{dI_{R_P}}{dt}$ A/s phase space for one cavity parameter values ($C=1$ mF, $L=10$ mH), magnetron filament voltage source parasitic resistance r_p is equal to 10 Ω. There is one stable spiral fixed point at $\frac{dV_{L_1}}{dt}+\frac{dV_{L_8}}{dt}=0, \frac{dI_{R_P}}{dt}=0$

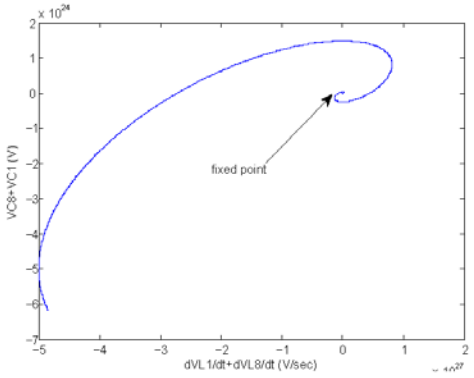

Fig. 22. Magnetron 2D function. Magnetron eight cavity $V_{C_8}+V_{C_1}$ V as a function of magnetron $\frac{dV_{L_1}}{dt}+\frac{dV_{L_8}}{dt}$ V/s phase space for one cavity parameter values ($C=1$ mF, $L=10$ mH), magnetron filament voltage source parasitic resistance r_p is equal to 10 Ω. There is one stable spiral fixed point at $V_{C_8}+V_{C_1}=0, \frac{dV_{L_1}}{dt}+\frac{dV_{L_8}}{dt}[V/s]=0$

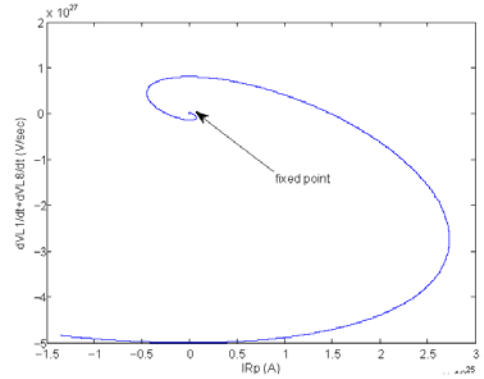

Fig. 21. Magnetron 2D function. Magnetron eight cavity $\frac{dV_{L_1}}{dt}+\frac{dV_{L_8}}{dt}$ V/s as a function of magnetron I_{R_P} A phase space for one cavity parameter values ($C=1$ mF, $L=10$ mH), magnetron filament voltage source parasitic resistance r_p is equal to 10 Ω. There is one stable spiral fixed point at $\frac{dV_{L_1}}{dt}+\frac{dV_{L_8}}{dt}=0, I_{R_P}=0$

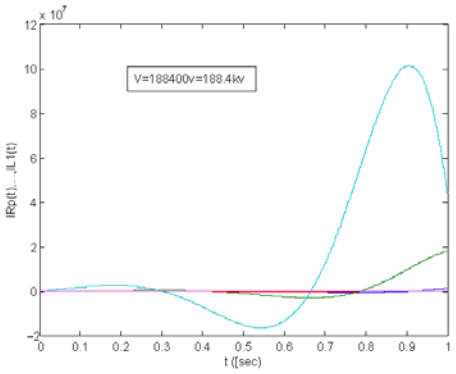

Fig. 23. Magnetron 2D function. Magnetron eight cavity $I_{R_P}(t),...,I_{L_1}(t)$ as a function of time t sec magnetron time domain for one cavity parameter values ($C=1$ mF, $L=10$ mH), magnetron filament voltage source parasitic resistance r_p is equal to 10 Ω. Magnetron variables oscillate in time and decay toward to fixed point

$$I_{C_5}=C_5\frac{d}{dt}(V_B-V_A)\,;V_{L5}=V_B-V_A=L_5\frac{dI_{L5}}{dt}$$
$$I_{C_6}=C_6\frac{d}{dt}(V_B-V_A)\,;V_{L6}=V_B-V_A=L_6\frac{dI_{L6}}{dt} \quad (213)$$

$$I_{C_7}=C_7\frac{d}{dt}(V_B-V_A)\,;V_{L7}=V_B-V_A=L_7\frac{dI_{L7}}{dt} \quad (214)$$

$$I_{C_8}=C_8\frac{d}{dt}(V_B-V_A)\,;V_{L8}=V_B-V_A=L_8\frac{dI_{L8}}{dt} \quad (215)$$

$$V=I_{R_P}R_p+V_{L1}=I_{R_P}R_p+V_{C1}\,;V_B-V_A=V_{L1}=V_{C1}$$
$$V=I_{R_P}R_p+V_B-V_A\,;I_{Ck}=C_k\frac{d}{dt}(V_B-V_A) \quad (216)$$

$$V_{Lk}=V_B-V_A=L_k\frac{dI_{Lk}}{dt}\;\forall\,k=1,...,8 \quad (217)$$

KCL @ B:

$$I_{R_P}=\sum_{k=1}^{8}I_{Lk}+\sum_{k=1}^{8}I_{Ck}\,;L_1\parallel L_2\parallel...\parallel L_8$$
$$L_1=L_2=...=L_8=L\,;\frac{1}{L_T}=\sum_{i=1}^{8}\frac{1}{L_i}|_{L_i=L}=\frac{8}{L} \quad (218)$$
$$\Rightarrow L_T=\frac{L}{8}$$

$$C_1\parallel C_2\parallel...\parallel C_8\,;C_1=C_2=...=C_8=C$$
$$C_T=\sum_{i=1}^{8}C_i|_{C_i=C}=8C \quad (219)$$

The equivalent circuit for our eight strapped cavities circuit: C_T=C_{total} ; L_T=L_{total}.

$$V=I_{R_P}R_P+V_{C_T}=I_{R_P}R_P+V_{L_T}\,;I_{R_P}=I_{C_T}+I_{L_T}$$
$$I_{C_T}=\sum_{k=1}^{8}I_{Ck}=[\sum_{k=1}^{8}C_k]\frac{dV_{BA}}{dt}\,;V_{BA}=V_B-V_A \quad (220)$$

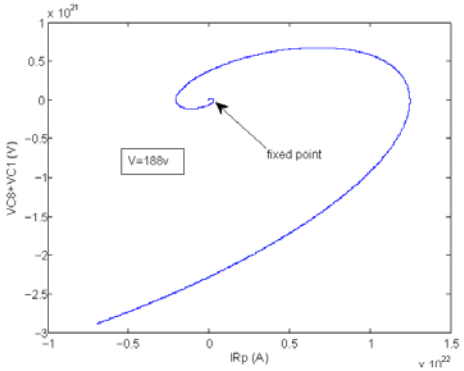

Fig. 24. Magnetron 2D function. Magnetron eight cavity $V_{C_8} + V_{C_1}$ V as a function of magnetron I_{R_P} A phase space for one cavity parameter values ($C = 1\ mF, L = 10\ mH$), magnetron filament voltage source parasitic resistance r_p is equal to 10 Ω, magnetron filament voltage is equal to $V =$ 188 V. There is one stable spiral fixed point at $V_{C_8} + V_{C_1} = 0, I_{R_P} = 0$

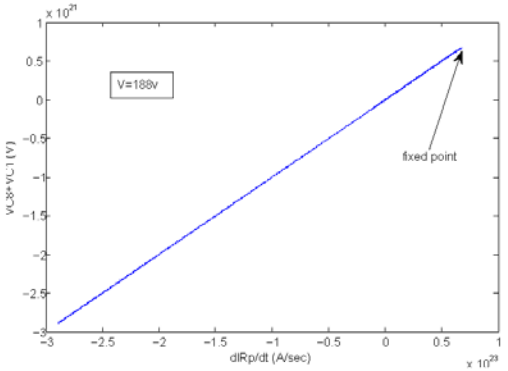

Fig. 26. Magnetron 2D function. Magnetron eight cavity $V_{C_8} + V_{C_1}$ V as a function of magnetron $\frac{dI_{R_P}}{dt}$ A/s phase space for one cavity parameter values ($C = 1$ mF, $L = 10$ mH), magnetron filament voltage source parasitic resistance r_p is equal to 10 Ω, magnetron filament voltage is equal to $V =$ 188 V. There is one stable node fixed point at $V_{C_8} + V_{C_1} = 0, \frac{dI_{R_P}}{dt} = 0$

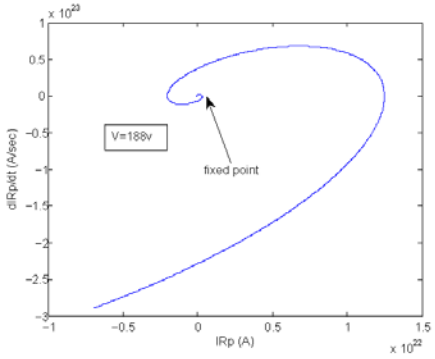

Fig. 25. Magnetron 2D function. Magnetron eight cavity $\frac{dI_{R_P}}{dt}$ A/s as a function of magnetron I_{R_P} A phase space for one cavity parameter values ($C = 1$ mF, $L = 10$ mH), magnetron filament voltage source parasitic resistance r_p is equal to 10 Ω, magnetron filament voltage is equal to $V =$ 188 V. There is one stable spiral fixed point at $I_{R_P} = 0, \frac{dI_{R_P}}{dt} = 0$

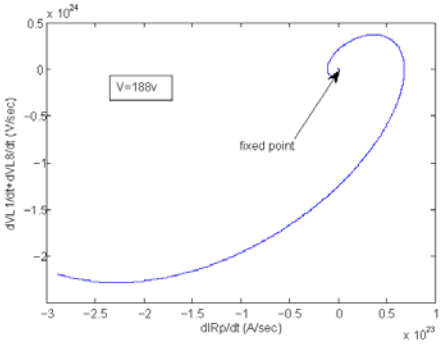

Fig. 27. Magnetron 2D function. Magnetron eight cavity $\frac{dV_{L1}}{dt} + \frac{dV_{L8}}{dt}$ V/s as a function of magnetron $\frac{dI_{R_P}}{dt}$ A/s phase space for one cavity parameter values ($C = 1$ mF, $L = 10$ mH), magnetron filament voltage source parasitic resistance r_p is equal to 10 Ω, magnetron filament voltage is equal to $V =$ 188 V. There is one stable spiral fixed point at $\frac{dV_{L1}}{dt} + \frac{dV_{L8}}{dt} = 0, \frac{dI_{R_P}}{dt} = 0$

$$V_{BA} = L_T \frac{dI_{L_T}}{dt} = L_T \frac{d[\sum_{k=1}^{8} I_{Lk}]}{dt}\ ;\ I_{L_T} = [\sum_{k=1}^{8} I_{Lk}] \qquad (221)$$
$$I_{L_T} = \frac{1}{L_T}\int V_{BA}dt\ ;\ [\sum_{k=1}^{8} I_{Lk}] = \frac{1}{L_T}\int V_{BA}dt$$

$$V = I_{R_P}R_P + V_{BA} \Rightarrow I_{R_P} = \frac{V - V_{BA}}{R_P}\ ;\ I_{R_P} = I_{C_T} + I_{L_T} \qquad (222)$$
$$\Rightarrow \frac{V - V_{BA}}{R_P} = [\sum_{k=1}^{8} C_k]\frac{dV_{BA}}{dt} + [\sum_{k=1}^{8} I_{Lk}]$$

$$\frac{V - V_{BA}}{R_P} = 8C\frac{dV_{BA}}{dt} + \frac{8}{L}\int V_{BA}dt \qquad (223)$$
$$\frac{d}{dt}\{\frac{V - V_{BA}}{R_P} = 8C\frac{dV_{BA}}{dt} + \frac{8}{L}\int V_{BA}dt\}$$

$$\frac{1}{R_P}\frac{dV}{dt} - \frac{1}{R_P}\frac{dV_{BA}}{dt} = 8C\frac{d^2V_{BA}}{dt^2} + \frac{8}{L}V_{BA} \qquad (224)$$
$$\frac{dV}{dt} = 0 \Rightarrow -\frac{1}{R_P}\frac{dV_{BA}}{dt} = 8C\frac{d^2V_{BA}}{dt^2} + \frac{8}{L}V_{BA}$$

$$X = \frac{dV_{BA}}{dt}\ ;\ \frac{dX}{dt} = \frac{d^2V_{BA}}{dt^2}\ ;\ Y = V_{BA} \qquad (225)$$

$$-\frac{1}{R_P}X = 8C\frac{dX}{dt} + \frac{8}{L}Y \Rightarrow 8C\frac{dX}{dt} = -\frac{1}{R_P}X - \frac{8}{L}Y \qquad (226)$$

$$\frac{dX}{dt} = -\frac{1}{8CR_P}X - \frac{1}{CL}Y\ ;\ \frac{dY}{dt} = X \qquad (227)$$

We can represent our system as matrix 2x2 differential set.

$$\begin{pmatrix} \frac{dX}{dt} \\ \frac{dY}{dt} \end{pmatrix} = \begin{pmatrix} -\frac{1}{8CR_P} & -\frac{1}{CL} \\ 1 & 0 \end{pmatrix}\begin{pmatrix} X \\ Y \end{pmatrix} \qquad (228)$$

To find system fixed points: $\frac{dX}{dt} = 0\ ;\ \frac{dY}{dt} = 0$

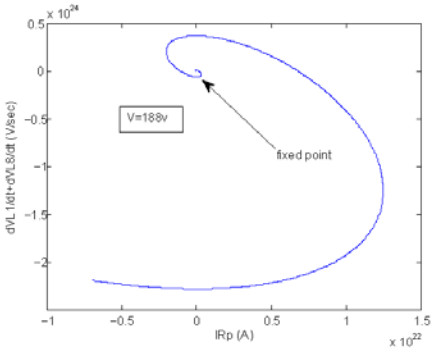

Fig. 28. Magnetron 2D function. Magnetron eight cavity $\frac{dV_{L_1}}{dt} + \frac{dV_{L_8}}{dt}$ V/s as a function of magnetron I_{R_P} A phase space for one cavity parameter values ($C = 1$ mF, $L = 10$ mH), magnetron filament voltage source parasitic resistance r_p is equal to 10 Ω, magnetron filament voltage source parasitic resistance r_p is equal to 10 Ω, magnetron filament voltage is equal to $V = 188$ V. There is one stable spiral fixed point at $\frac{dV_{L_1}}{dt} + \frac{dV_{L_8}}{dt} = 0, I_{R_P} = 0$

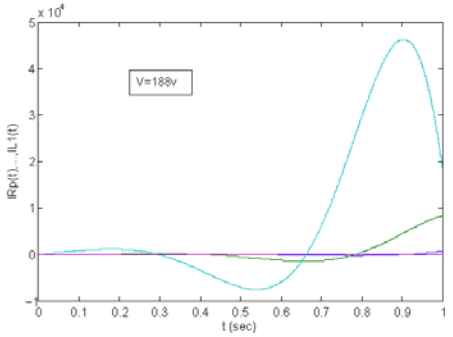

Fig. 30. Magnetron 2D function. Magnetron eight cavity $I_{R_P}(t), ..., I_{L_1}(t)$ as a function of time t sec magnetron time domain for one cavity parameter values ($C = 1$ mF, $L = 10$ mH), magnetron filament voltage source parasitic resistance r_p is equal to 10 Ω, magnetron filament voltage is equal to $V = 188$ V. Magnetron variables oscillate in time and decay toward to fixed point

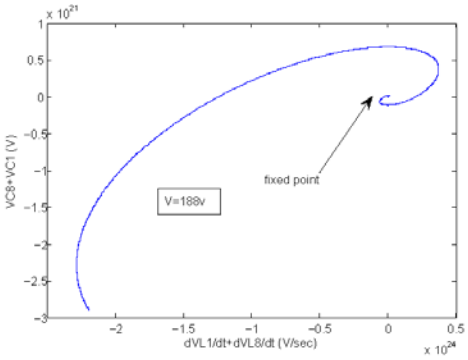

Fig. 29. Magnetron 2D function. Magnetron eight cavity $V_{C_8} + V_{C_1}$ V as a function of magnetron $\frac{dV_{L_1}}{dt} + \frac{dV_{L_8}}{dt}$ V/s phase space for one cavity parameter values ($C = 1$ mF, $L = 10$ mH), magnetron filament voltage source parasitic resistance r_p is equal to 10 Ω, magnetron filament voltage is equal to $V = 188$ V. There is one stable spiral fixed point at $V_{C_8} + V_{C_1} = 0, \frac{dV_{L_1}}{dt} + \frac{dV_{L_8}}{dt}[V/s] = 0$

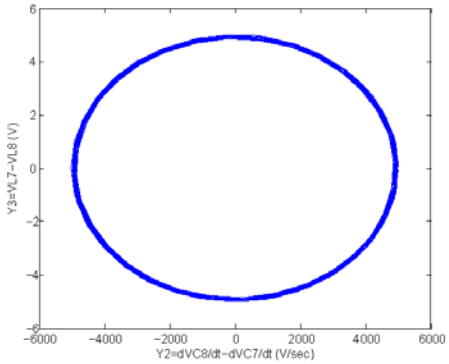

Fig. 31. Magnetron 2D function. Magnetron eight cavity $Y_3 = V_{L_7} - V_{L_8}$ V as a function of $Y_2 = \frac{dV_{C_8}}{dt} - \frac{dV_{C_7}}{dt}$ V/s magnetron phase space for one cavity parameter values ($C = 1$ mF, $L = 10$ mH), magnetron new variables initial values ($Y_{2_0} = 3, Y_{3_0} = 5$), magnetron filament voltage V and parasitic resistance r_p do not effect our phase space behavior. We see a clear phase space circle which explain the oscillation of our magnetron

$$\frac{dY}{dt} = 0 \Rightarrow X^* = 0 \; ; \frac{dX}{dt} = 0 \Rightarrow -\frac{1}{8CR_P}X^* - \frac{1}{CL}Y^* = 0 \Rightarrow Y^* = 0 \; ; E^*(X^*, Y^*) = (0,0) \tag{229}$$

$$A = \begin{pmatrix} -\frac{1}{8CR_P} & -\frac{1}{CL} \\ 1 & 0 \end{pmatrix} \; ; A - \lambda I = \begin{pmatrix} -\frac{1}{8CR_P} - \lambda & -\frac{1}{CL} \\ 1 & -\lambda \end{pmatrix} \tag{230}$$

$$\det|A - \lambda I| = 0 \Rightarrow (\tfrac{1}{8CR_P} + \lambda)\lambda + \tfrac{1}{CL} = 0 \Rightarrow \lambda^2 + \lambda\tfrac{1}{8CR_P} + \tfrac{1}{CL} = 0 \tag{231}$$

$$\lambda_{1,2} = \frac{-\frac{1}{8CR_P} \pm \sqrt{\frac{1}{64C^2R_P^2} - \frac{4}{CL}}}{2} \tag{232}$$

$$\lambda_1 = -\frac{1}{16CR_P} + \frac{1}{2}\sqrt{\frac{1}{64C^2R_P^2} - \frac{4}{CL}} \tag{233}$$

$$\lambda_2 = -\frac{1}{16CR_P} - \frac{1}{2}\sqrt{\frac{1}{64C^2R_P^2} - \frac{4}{CL}} \tag{234}$$

Stability analysis: we need to classify our system fixed point. Analysis of eigenvalues helps as to classify our system behavior.

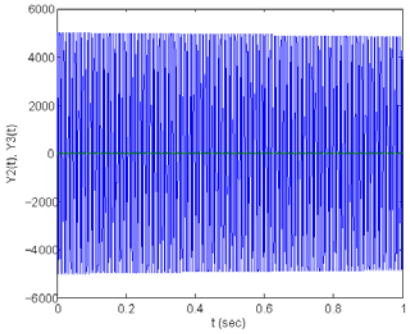

Fig. 32. Magnetron 2D function. Magnetron eight cavity $Y_2(t), Y_3(t)$ as a function of time t sec magnetron time domain for one cavity parameter values ($C = 1$ mF, $L = 10$ mH), magnetron new variables initial values ($Y_{2_0} = 3, Y_{3_0} = 5$), magnetron filament voltage V and parasitic resistance r_p do not effect our time domain graph behavior. We see a clear oscillation in time of our magnetron new variables $Y_2(t), Y_3(t)$

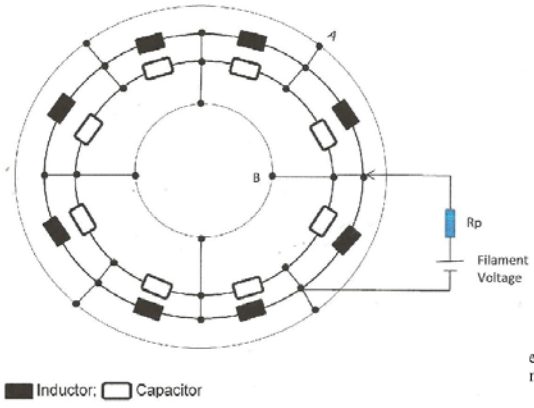

Fig. 33. Schematic of magnetron eight strapped cavity anode equivalent circuit. One cavity equivalent circuit is represented as a parallel capacitor and inductor resonant circuit. We have eight magnetron strapped cavities in loop series and one magnetron filament voltage source which is connected in parallel to one magnetron cavity element. Magnetron filament voltage source has parasitic resistance r_p.

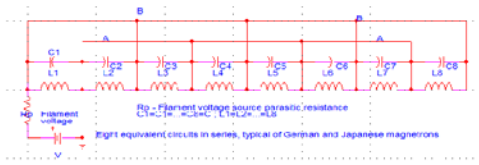

Fig. 34. Schematic of magnetron eight strapped cavity anode equivalent circuit. One cavity equivalent circuit is represented as a parallel capacitor and inductor resonant circuit. We have eight magnetron strapped cavities in loop series and one magnetron filament voltage source which is connected in parallel to one magnetron cavity element. It is typical German and Japanese magnetron. Magnetron filament voltage source has parasitic resistance r_p.

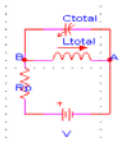

Fig. 35. Schematic of magnetron eight strapped cavity anode equivalent circuit. The equivalent circuit is represented as a parallel capacitor C_total and inductor L_total resonant circuit. We have eight magnetron strapped cavities in loop series and one magnetron filament voltage source which is connected in parallel to one magnetron cavity element. It is typical German and Japanese magnetron. Magnetron filament voltage source has parasitic resistance r_p.

Eigen values	Fixed point classification	condition
$\lambda_1<0$ & $\lambda_2>0$ Or $\lambda_1>0$ & $\lambda_2<0$ $\lambda_1\lambda_2<0$	Saddle point	$\frac{1}{[16CR_P]^2} - \frac{1}{4}[\frac{1}{64C^2R_P^2} - \frac{4}{CL}] < 0$ $\frac{1}{CL} < 0$ can't exist
$\lambda_1<0$ & $\lambda_2<0$	Stable node	$\frac{1}{64C^2R_P^2} - \frac{4}{CL} > 0$ $\Rightarrow \frac{1}{64CR_P^2} > \frac{4}{L}$ $-\frac{1}{16CR_P} \pm \frac{1}{2}\sqrt{\frac{1}{64C^2R_P^2} - \frac{4}{CL}} < 0$
$\lambda_1>0$ & $\lambda_2>0$	Unstable node	$\frac{1}{64C^2R_P^2} - \frac{4}{CL} > 0$ $\Rightarrow \frac{1}{64CR_P^2} > \frac{4}{L}$ $-\frac{1}{16CR_P} \pm \frac{1}{2}\sqrt{\frac{1}{64C^2R_P^2} - \frac{4}{CL}} > 0$
$\lambda_{1,2}=\alpha\pm j\beta$ $\alpha<0$	Stable spiral	$\frac{1}{64C^2R_P^2} - \frac{4}{CL} < 0$ $\Rightarrow \frac{1}{64CR_P^2} < \frac{4}{L}$ $\alpha = -\frac{1}{16CR_P}$ $\beta = \frac{1}{2}\sqrt{\lvert\frac{1}{64C^2R_P^2} - \frac{4}{CL}\rvert}$

Table 4. Magnetron eight strapped cavities stability analysis.

The eigenvalues of a system matrix A are given by the characteristic equation$\det(A - \lambda I) = 0$; Where I is the identity matrix. For a 2x2 system matrix:

$$A = \begin{pmatrix} -\frac{1}{8CR_P} & -\frac{1}{CL} \\ 1 & 0 \end{pmatrix} \tag{235}$$

And the characteristic equation becomes

$$\det\begin{pmatrix} -\frac{1}{8CR_P} - \lambda & -\frac{1}{CL} \\ 1 & -\lambda \end{pmatrix} = 0 \tag{236}$$

Expanding the determinant yields $\lambda^2 - \tau\lambda + \Delta = 0$ where $\tau = trace(A) = -\frac{1}{8CR_P}$; $\Delta = \det(A) = \frac{1}{CL}$

then $\lambda_1 = \frac{\tau+\sqrt{\tau^2-4\Delta}}{2}$; $\lambda_1 = \frac{\tau-\sqrt{\tau^2-4\Delta}}{2}$

are solutions of the quadratic equation $\lambda^2 - \tau\lambda + \Delta = 0$. The eigenvalue depend only on the trace and determinant of the matrix A. We can show the type and stability of all the different fixed points.

$$\lambda_{1,2} = \frac{\tau \pm \sqrt{\tau^2 - 4\Delta}}{2} \; ; \Delta = \lambda_1\lambda_1 \; ; \tau = \lambda_1 + \lambda_1 \tag{237}$$

If $\Delta<0$, the eigenvalues are real and have opposite sign; hence the fixed point is a saddle point (not exist since $\Delta = \det(A) = \frac{1}{CL} > 0$. If $\Delta = \det(A) = \frac{1}{CL} > 0$ (our case), the eigenvalues are either real with the same sign (nodes), or complex conjugate (spiral and center). Nodes satisfy $\tau^2 - 4\Delta > 0 \Rightarrow \frac{1}{64C^2R_P^2} - \frac{4}{CL} > 0$ and spiral satisfy $\tau^2 - 4\Delta < 0 \Rightarrow \frac{1}{64C^2R_P^2} - \frac{4}{CL} < 0$.

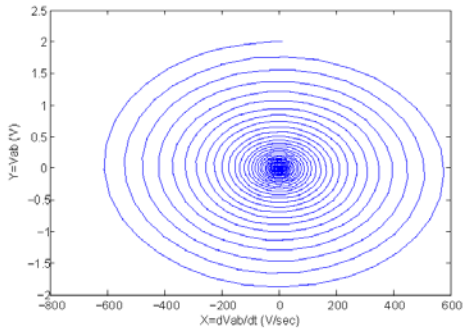

Fig. 36. Magnetron 2D function. Magnetron eight strapped cavity $Y = V_ab$ V as a function of $X = \frac{dV_ab}{dt}$ V/s magnetron phase space for one cavity parameter values ($C = 1$ mF, $L = 10$ mH) and magnetron filament parasitic resistance $r_p = 10\ \Omega$), magnetron new variables initial values ($Y_0 = 2, X_0 = 10$). We see a clear phase space spiral which explain the decay oscillation of our magnetron.

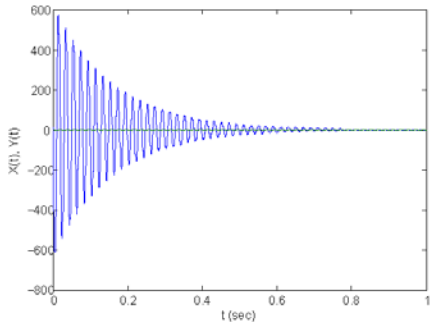

Fig. 37. Magnetron 2D function. Magnetron eight strapped cavity $X(t), Y(t)$ as a function of time t sec magnetron time domain for one cavity parameter values ($C = 1$ mF, $L = 10$ mH) and magnetron filament parasitic resistance $r_p = 10\ \Omega$), magnetron new variables initial values ($Y_0 = 2, X_0 = 10$). We see a clear decay oscillation in time of our magnetron new variables $X(t), Y(t)$.

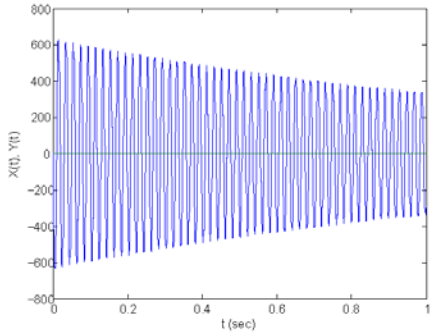

Fig. 38. Magnetron 2D function. Magnetron eight strapped cavity $X(t), Y(t)$ as a function of time t sec magnetron time domain for one cavity parameter values ($C = 1$ mF, $L = 10$ mH) and magnetron filament parasitic resistance $r_p = 100\ \Omega$), magnetron new variables initial values ($Y_0 = 2, X_0 = 10$). We see a clear oscillation in time of our magnetron new variables $X(t), Y(t)$.

The parabola $\tau^2 - 4\Delta = 0 \Rightarrow \frac{1}{64C^2R_p^2} - \frac{4}{CL} = 0$ is the borderline between nodes and spirals; star nodes and degenerate nodes live on this parabola. The stability of the nodes and spirals is determined by $\tau = trace(A) = -\frac{1}{8CR_p}$.

When $\tau = trace(A) = -\frac{1}{8CR_p} < 0$

(our case), both eigenvalues have negative real parts, the fixed point is stable. Unstable spiral and nodes have$\tau = trace(A) > 0$, not in our case. Neutrally stable centers live on the borderline$\tau = trace(A) = 0$, where the eigenvalues are purely imaginary. If $\Delta = \det(A) = 0$, at least one of the eigenvalues is zero. Then the origin is not an isolated fixed point. There is a whole line of fixed points. We run MATLAB scripts to analyze the behavior of our system. We choose the following circuit parameters values: $C = 0.001$F$= 1$mF, $L = 0.01$H$= 10$mH, $R_p = 10\ \Omega$ (case I), $R_p = 100\ \Omega$ (case II), and $R_p = 1000\ \Omega$ (case III). We choose the following initial values for our system variables X, Y.

$X(t = 0) = 10$, $Y(t = 0) = 2$. $X = \frac{dV_{BA}}{dt}$; $\frac{dX}{dt} = \frac{d^2V_{BA}}{dt^2}$; $Y = V_{BA}$

Magnetron eight strapped cavity $Y = V_ab$[V] as a function of $X = \frac{dV_ab}{dt}$[V/s] magnetron phase space as can be seen in figure Fig. 36 for $r_p = 10\ \Omega$.

Magnetron eight strapped cavity $X(t), Y(t)$ as a function of time t[sec] as can be seen in figure Fig. 37 for $r_p = 10\ \Omega$.

Magnetron eight strapped cavity $X(t), Y(t)$ as a function of time t[sec] as can be seen in figure Fig. 38 for $r_p = 100\ \Omega$.

Magnetron eight strapped cavity $Y = V_ab$[V] as a function of $X = \frac{dV_ab}{dt}$[V/s] magnetron phase space as can be seen in figure Fig. 39 for $r_p = 100\ \Omega$.

Magnetron eight strapped cavity $Y = V_ab$[V] as a function of $X = \frac{dV_ab}{dt}$[V/s] magnetron phase space as can be seen in figure Fig. 40 for $r_p = 1000\ \Omega$.

Magnetron eight strapped cavity $X(t), Y(t)$ as a function of time t[sec] as can be seen in figure Fig. 41 for $r_p = 1000\ \Omega$.

X. Magnetron Eight Cavity Hull Cutoff and Hartree Voltages

In the last discussion we inspect magnetron eight cavity behavior for applied voltage which is equal to Hartree voltage. It is the voltage which oscillations should start. We desire our magnetron Hole-Slot-Type cavity related to magnetron filament voltage. We enhance our analysis regarding the applied voltage at which oscillations start and the interval limits of that voltage. Magnetron potential difference between the anode and cathode blocks (V) should be in an interval with limits determined by the Hartree voltage V_t and Hull cutoff voltage V_0 (V_t<V<V_0). We define voltage V as the magnetron applied voltage. Hartree voltage value is bigger than Hull cutoff voltage. The interval determines the magneyron operation region. We define our enhance magnetron design parameters: the magnetron length h, the radius of the cathode (r_c), voltage between the anode and cathode blocks (V), distance between the cathode and anode blocks (r_{an_ir}-r_c), applied magnetic field orthogonal to electric field (B), inner and outer radii of the magnetron anode (r_{an_ir}, r_{an_or}), length of the magnetron slot (l_{slot}), width of the magnetron slot (w_{slot}), number of resonators (N), and magnetron hole radius slot (r_{hole}), L is the distance between cavity. V_{out} is the magnetron output DC voltage (operating DC voltage) is equal to the peak RF synchronous voltage and is related to the electron phase velocity. The magnetron output DC voltage (V_{out}) can be different from the voltage between the anode and cathode blocks (V). The magnetron required voltage (V) can be defined an applied voltage V_{app}. The magnetron mode number (n) is equal to magnetron number of resonators (N) divided by 2 ($n = N/2$). V_p is the electron phase velocity and is equal to the below equation [7].

$$v_p = \frac{\omega}{\beta}; \beta = \frac{\pi}{L}; v_p = \frac{\omega L}{\pi} \tag{238}$$

η is the efficiency. ω_0, Ω angular velocity of electron.

$$L = \frac{2\pi r_{an\_ir}}{2n}; v_p = \frac{\omega r_{an\_ir}}{n}$$
$$V_{out} = \frac{v_p^2}{2\eta}; V_{out} = \frac{\omega^2 r_{an\_ir}^2}{2\eta n^2} \tag{239}$$

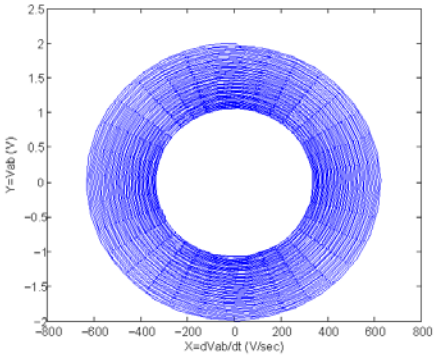

Fig. 39. Magnetron 2D function. Magnetron eight strapped cavity $Y = V_ab$ V as a function of $X = \frac{dV_ab}{dt}$ V/s magnetron phase space for one cavity parameter values ($C = 1$ mF, $L = 10$ mH) and magnetron filament parasitic resistance $r_p = 100\ \Omega$), magnetron new variables initial values ($Y_0 = 2, X_0 = 10$). We see a clear phase space circle which explain the oscillation of our magnetron.

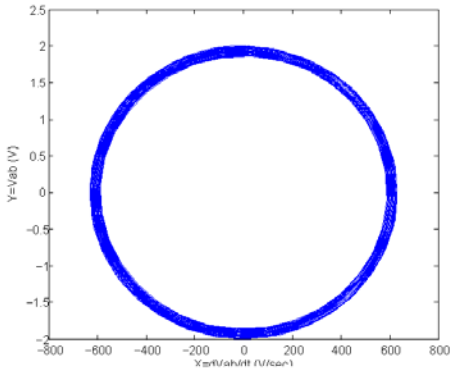

Fig. 40. Magnetron 2D function. Magnetron eight strapped cavity $Y = V_ab$ V as a function of $X = \frac{dV_ab}{dt}$ V/s magnetron phase space for one cavity parameter values ($C = 1$ mF, $L = 10$ mH) and magnetron filament parasitic resistance $r_p = 1000\ \Omega$), magnetron new variables initial values ($Y_0 = 2, X_0 = 10$). We see a clear phase space circle which explain the oscillation of our magnetron.

$$r^2_{an\_ir} = \frac{2\eta n^2 V_{out}}{\omega^2}$$
$$r_{an\_ir} = \frac{n}{\omega}\sqrt{2\eta V_{out}}; r_{an\_ir} = \frac{nv_p}{\omega} \tag{240}$$

$$\Omega = \frac{\omega}{n} = \frac{2\pi f}{n}; \omega = \omega_0 n$$
$$\Omega = \omega_0 = \frac{\omega_c}{2}(1 - \frac{r_c^2}{r^2_{an\_ir}}) \tag{241}$$

ω_c is cyclotron angular frequency. B_0 is the cutoff static magnetic field. $\omega_c = \frac{e}{m}B_0; B_{app} = B$.

$$\Omega = \omega_0 = \frac{e}{2m}B_0(1 - \frac{r_c^2}{r^2_{an\_ir}}); B_0 = \frac{2\Omega m}{e(1 - \frac{r_c^2}{r^2_{an\_ir}})} \tag{242}$$

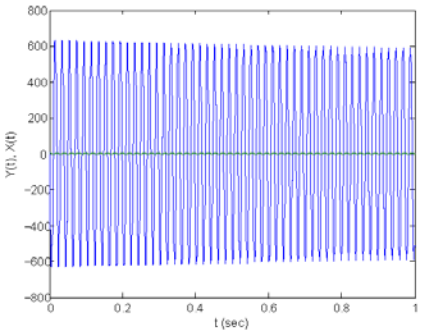

Fig. 41. Magnetron 2D function. Magnetron eight strapped cavity $X(t), Y(t)$ as a function of time t sec magnetron time domain for one cavity parameter values ($C = 1$ mF, $L = 10$ mH) and magnetron filament parasitic resistance $r_p = 1000\ \Omega$), magnetron new variables initial values ($Y_0 = 2, X_0 = 10$). We see a clear oscillation in time of our magnetron new variables $X(t), Y(t)$.

$$B_0 = \frac{2\omega_0 m}{e(1 - \frac{r_c^2}{r^2_{an\_ir}})} = \frac{2\omega m}{ne(1 - \frac{r_c^2}{r^2_{an\_ir}})}$$
$$B_0 = \frac{4\pi^2 fm}{ne(1 - \frac{r_c^2}{r^2_{an\_ir}})} \tag{243}$$

B_0 define as the cutoff static magnetic field. There are two important voltages related to magnetron operation region. The first lower limit is the Hartree voltage (V_t) and the second upper limit is Hull cutoff voltage (V_o). The expressions for these voltages are as follow:

$$V_t = \frac{r^2_{an\_ir}}{2}(1 - \frac{r_c^2}{r^2_{an\_ir}})\frac{\omega}{n}B_{app} - \frac{mr^2_{an\_ir}}{2e}(\frac{\omega}{n})^2 \tag{244}$$

$$V_0 = \frac{er^2_{an\_ir}}{8m}(1 - \frac{r_c^2}{r^2_{an\_ir}})B_0^2$$
$$V_0 > V_t; V_t < V < V_0 \tag{245}$$

$$V_0 = r^2_{an\_ir}\frac{2\pi^2 mf^2}{n^2 e(1 - \frac{r_c^2}{r^2_{an\_ir}})} \tag{246}$$

We choose our applied magnetron voltage $V = V_{app}$ to be in the middle of this limit values $V = \overline{V} = \frac{V_0 + V_t}{2}; V_0 > V_t$.
We define the gap between magnetron applied voltage upper limit and lower limit as $V_{gap} = V_0 - V_t$.

$$V_{gap} = V_0 - V_t = r^2_{an\_ir}\frac{2\pi^2 mf^2}{n^2 e(1 - \frac{r_c^2}{r^2_{an\_ir}})}$$
$$-\frac{r^2_{an\_ir}}{2}(1 - \frac{r_c^2}{r^2_{an\_ir}})\frac{\omega}{n}B_{app} + \frac{r^2_{an\_ir}m}{2e}(\frac{\omega}{n})^2 \tag{247}$$

$$V_{gap} = V_0 - V_t = \frac{mr^2_{an\_ir}}{n^2 e}(\frac{2\pi^2 f^2}{(1 - \frac{r_c^2}{r^2_{an\_ir}})} + \frac{\omega^2}{2})$$
$$-\frac{r^2_{an\_ir}}{2}(1 - \frac{r_c^2}{r^2_{an\_ir}})\frac{\omega}{n}B_{app} \tag{248}$$

We define two functions: the first is average voltage $\overline{V}$ as function of electron phase velocity and other parameters $\xi_1(v_p, ...)$ and second function is the gap voltage V_{gap} as function of electron phase velocity and other parameters $\xi_2(v_p, ...)$.

$$\xi_1 = \overline{V} = \frac{v_p^2\pi^2 mf^2}{\omega^2 e(1 - \frac{r_c^2\omega^2}{n^2 v_p^2})}$$
$$+\frac{nv_p^2}{4\omega}(1 - \frac{r_c^2\omega^2}{n^2 v_p^2})B_{app} - \frac{v_p^2}{4e}m \tag{249}$$

$$\xi_2 = V_0 - V_t = \frac{mv_p^2}{\omega^2 e}\left(\frac{2\pi^2 f^2}{(1-\frac{r_s^2\omega^2}{n^2 v_p^2})} + \frac{\omega^2}{2}\right) - \frac{n^2 v_p^2}{2\omega^2}(1-\frac{r_s^2\omega^2}{n^2 v_p^2})\frac{\omega}{n}B_{app} \quad (250)$$

We need to plot the two functions for different values of electron phase velocity when other parameters are constant.

XI. Discussion

In this paper, we discuss and analyse the behaviour of magnetron eight cavity system. We already got the expression: $V[volt] = \frac{\pi}{n\lambda_0}(r_a^2 - r_c^2)(B - \frac{2\pi mc}{en\lambda_0 r_a^2})$ (Posthumus). Which reduce to $V[volt] = \frac{300\pi}{n_0}(r_a^2 - r_c^2)(B - \frac{10.6}{n_0})$ By Posthumus (reduce equation). The voltage V is a linear function of B. The voltage V is known as the Hartree voltage. This voltage is that at which oscillations should start provided at the same time that B is sufficiently large so that the undistorted space charge does not extend to the anode. According to Hartree there is a functional graph of voltage [kv] vs magnetic field in gauss. If we take the maximum magnetic field, the table as follow: $n = 4$ ($B = 0.24$T, $V = 25$kv), $n = 3$ ($B = 0.24$T, $V = 41$kv), $n = 2$ ($B = 0.24$T, $V = 60$kv). $r_a > r_c$. We consider magnetron cathode radius (r_c) is constant and scaling down the dimension of magnetron is done by reducing the value of magnetron anode radius (r_a). We run our MATLAB script for different values of $r_a^2 - r_c^2$ expression. We plot graphs for two cases:

$r_a^2 - r_c^2$	$V[volt] = \frac{300\pi}{n_0}(r_a^2 - r_c^2)(B - \frac{10.6}{n_0})$ $n_0 = 300 \cdot 4 \cdot \frac{3\cdot 10^8 m/sec}{3\cdot 10^9 [1/sec]} = 120$; B=0.24T
10	**188.4kvolt**
0.01	**0.188kvolt**

Table 4. Magnetron eight cavity V vs $r_a^2 - r_c^2$ (two cases).

As we lowering the dimension of magnetron $(r_a^2 - r_c^2) \downarrow$ the voltage V go down. We analyze our system for the biggest $\Delta = r_a^2 - r_c^2$ value Δ=10 and lowest $\Delta = r_a^2 - r_c^2$ value Δ=0.01. The dynamical behavior is the same, stable spiral fixed point $\bar{E}^* = E(I_{Rp}^*, X^*, Y_1^*, Y^*, I_{L1}^*) = E(\frac{V}{R_p}, 0, 0, 0, I_{L1}^*)$. But the different is the size of the phase space. As we lower magnetron dimension (V?) the phase space size is smaller but the fixed point classification is the same (stable spiral). All my analysis is done by the reduce V equation (Posthumus)[24].

We see in the below graph the Magnetron oscillations. Our fixed point is a center and it exist for all 8 segments. For the second set $\frac{dY_k}{dt} = \frac{1}{LC}Y_{k+1}$; $\frac{dY_{k+1}}{dt} = -Y_k$; k is varied from 2 to 12 according to the magnetron resonator segment. The variables are $Y_{k+1}, Y_k \; \forall \; k \in 2, \ldots, 12$. Our Magnetron dimension scaling down does not influence on magnetron oscillation and amplitude. It is only effect by the L and C values. Additionally we analyse the case of magnetron eight strapped cavity anode behavior and stability under parameters variation. Alternate Cavity strapped together with solid copper rings. This ensures that oscillations in cavity are in phase.

References

[1] S. Bhattacharjee, J.-H. Booske, C.-L Kory, D.-W. Weide, S. Limbach, S. Gallagher, J.-D. Welter, M. Lopez, R.-M. Gilgenbach, R.-L. Ives, M.-E. Read, R. Divan, D.-C. Mancini "Folded waveguide traveling wave tube sources for terahertz radiation," *IEEE transactions on plasma science*, vol.32, no. 3, 2004.

[2] S. Bhattacharjee, J.-H. Booske, C.-L Kory, D.-W. Weide, S. Limbach, S. Gallagher, J.-D. Welter, M. Lopez, R.-M. Gilgenbach, R.-L. Ives, M.-E. Read, R. Divan, D.-C. Mancini "Linear electron acceleration in THz waveguides," *Proceedings of IPAC2014 Dresden Germany*, 2014.

[3] A.-W Cross, H. Yin, W. He, D. Bowes, K. Ronald, A.-D.-R. Phelps, D. Li, J. Zhou, X. Chen, J. Protz, M. Verdiel, M. Reynolds, T. Schuhmann "Pseudospark sourced electron beam for terahertz radiation generation," *29th ICPIG*, 2009 Cancun, Mexico.

[4] P.-H. Siegel "Terahertz technology," *IEEE transactions on microwave theory and techniques*, vol.50, no. 3, 2002.

[5] V.-B. Bayburin, A.-A. Terentiev, V.-I. Vislov, A.-B. Levande, I.-K. Guriev, A.-A. Sysuev "Computer simulation of magnetron devices," *Applied surface science*, 215 (2003) pp. 301-309.

[6] N.-N. Esfahani, M. Tayarani, and K. Schunemann "Design and simulation of a $\pi/2$ mode spatial harmonic magnetron," *Int.J.Electron.Commun*, (AEU) 67 (2013) pp. 426-432.

[7] T. Isenlik, K. Yegin 'Tutorial on the design of Hole-Slot-Type cavity magnetron using CST particle studio," *IEEE transactions on plasma science*, vol.41, no. 2, (2013).

[8] T.-P. Fleming, M.-R. Lambrech, P.-J. Mardahl, and J.-D. Keisling "A high efficiency megawatt class nonrelativistic magnetron," *IEEE transactions on plasma science*, vol.40, no. 9, (2012).

[9] G.-B. Collins, *Microwave Magnetrons Radiation Laboratory*, series. 6, Hard cover - January 1, 1948.

[10] A.-S. Gilmour, *Klystrons Traveling Wave Tubes Magnetrons, Cross-Field Amplifiers, and Gyrotrons* (Artech House Microwave library) - January, 2011.

[11] A.-S. Gilmour, *Microwave Tubes* (Artech House Microwave Library), Hardcover (December 1,1986).

[12] T.-E. Sheridan, M.-J, Goeckner, J. Goree, "Model of energetic electron transport in magnetron discharge," *J. Vac. Sci. Technol. A*, vol.8,no. 1, 1990.

[13] S.-M. Sze and K.-K. Ng, *Physics of Semiconductor Devices* Wiley Interscience (Hardcover - Oct 27, 2006).

[14] C.-T. Sah, *Fundamentals of Solid State Electronics* World Scientific.

[15] M. Gupta, E. Wong and W. Leong, *Microwaves and Metals* Wiley-interscience ; 1 edition (November 1, 2007).

[16] S.-C. Cripps, *RF power Amplifiers for Wireless Communication* 2006 by Artech House microwave library.

[17] C.-W. Sayre, *Complete Wireless design* McGraw-Hill companies.

[18] A.-W. Scott, *Understanding Microwaves* 2005 by John Wiley Sons Inc.

[19] J.-W. M. R.-C. Plett. Shadrivov, and I. Marsland, *Radio Frequency System Architecture and Design* Artech house 2014.

[20] D.-K. Linkhart, *Microwave Circulator Design* second edition, Artech house 2014.

[21] S. Tanaka, N. Shimomura, K. Ohtake, "Active circulators - the realization of circulators using transistors," *Proc. of the IEEE*, vol. 53, issue. 3, pp. 260-267, 1965.

[22] R. Dougherty, "Circulate signals with active devices on monolithic chips," *Microwave and RF*, pp. 85-86, 89, 1989.

[23] S. Horikoshi and N. Serpone, *Microwaves in Nanoparticle Synthesis: Fundamental and Applications*, Wiley-VCH; 1 edition (May 28, 2013).

[24] T.-H. Lee, *Planar Microwave Engineering: A practical Guide to Theory, Measurement and Circuits* (Cambridge university press: Har/Cdr edition (Agust 30, 2004).

[25] D. Czekaj, E.-K. Hollman, V.-A. Volpyas, A.-G. Zaitsev, A. Chernakova, B. Goranchev, "Ion energies distribution at the cathode of planar magnetron sputtering system," *Bulgarian Journal of Physics*, vol.18, no. , 1991.

[26] Z. Wang. and S.-A. Cohen, "Geometrical aspects of a hollow cathode planar magnetron," *Physics of plasmas*, vol.6,no. 5, 1999.

[27] N.-El. Ghazal, A. Belhaiba, M. Chraygane, B. Bahani, M. Ferfra, "New simulation method of new HV power supply for industrial Microwave generators with N=2 Magnetrons," *International Journal of Advanced Computer Science and Application*, vol.4,no. 12, 2013.

[28] M. Bassoui, M. Ferfra, M. Chraygane, M. Ould Ahmedou, N. Elghazal, and A. Belhaiba, "Optimization of a new three phase high voltage power supply for industrial Microwaves generators with N magnetrons by phase (Treated case $N = 1$)," *Internation Journal of Electrical, Electronic Science and Engineering*, vol.7,no. 11, 2013.

[29] P. Pengvanich, V.-B. Neculaes, Y.-Y. Lau, R.-M. Gilgenbach, M.-C. Jones, W.-M. White, and R.-D. Kowalczyk, "Modeling and experimental studies of magnetron injection locking," *Journal of Applied Physics*, 98, 114903, 2005.

[30] E. Lugscheider, K. Bobzin, M.-K. Lake, "Deposition of solder for micro joining on M.E.M.S components by means of magnetron sputtering," *Surface and Coatings Technology*, 142-144 (2001) 813-816.

[31] D. Desideri, A. Maschio, D. Doru, O. Ramona, M. Spolaore, "Equivalent model of a magnetron sputtering device with ferromagnetic yoke," *Przeglad Elektrotechniczny*, (Electrical Review), ISSN 0033-2097, r.88 NR 7b/2012.

[32] R. Tadjine, M. Kechouance, M. Alim, and N. Saoula, "Electrical characterization of RF magnetron sputtering," *31st ICPIG*, July 14-19, 2013, Granada Spain.

[33] A. Belhaiba, A. Bouzit, N. Elghazal, M. Ferfra, M. Bousseta, M. Chraygane, and B. Bahani, "Comparative studies of electrical functioning of magnetron power supply for one magnetron," *Journal of Engineering Sceince and technology*, Review 6 (3) (2013) 35-40.

[34] Y.-R. Yang, "A magnetron power supply with transition mode zero voltage switching inverter," *Journal of energy and power engineering*, 7 (2013) 1571-1577.

[35] H.-W. Welch, and W.-G Dow, "Analysis of synchronous conditions in the cylindrical magnetron space charge," *Journal of applied Physics*, vol.22, no. 4, 1951.
[36] H. Yamazaki, and W. Jiang, "Experimental examination of diode features in a high power magnetron with a transparent cathode," *Plasma and Fusion research: Regular articles*, vol.3, S1025 (2008).
[37] L. Brillouin, "Electronic theory of the plane magnetron," *Advanced in Electronics and Electron Physics*, vol.3, pages. 85-144, 1951.
[38] L. Brillouin, "Theory of the magnetron III," *Phys. Rev.* 63, 127, 1943.
[39] P J .S Pereira, M .L Escrivao, M R Teixeira, M J P. Maneira, and Y. Nunes, "Analytical model and measurements of the target erosion depth profile of balanced and unbalanced planar magnetron cathodes " *Plasma Sources Science and Technology*, 23, 065031, 2014.

SOCIETY FOR SCIENCE AND EDUCATION
UNITED KINGDOM

TNC TRANSACTIONS ON NETWORKS AND COMMUNICATIONS

VOLUME 4, ISSUE 2
ISSN: 2054 -7420

Topological Analysis of Network Systems for Intrusion Detections

[1]Rohitha Goonatilake and [2]Susantha Herath
[1]Texas A&M International University, TX 78041, USA
[2]St. Cloud State University, MN 56301, USA
haragr@gmail.com; harag@tamiu.edu

ABSTRACT

An understanding of how well networks will respond to ongoing attack threats is an important task in formulating strategies to protect unauthorized network activities. The study of topological properties of network architecture sheds some light in this effort. The purpose of this paper is to study several scenarios that address topological structures and related analyses of network systems to begin the appropriate discussion towards this question. Analysis of the probabilistic state finite automation and its probability distribution theory play a pivotal role in the discussion.

Keywords: Intrusion, conditional probability, network system, regression, data analysis

1 Preliminaries

There is an urgency to harden the software used in network systems as increasing incidents of network intrusions have been reported. In addition, hardening software in general is designed based on the topological construction of the network systems. Malicious incidents on the Internet as reported to CERT (Computer Emergency Response Team) provide evidence that these attacks increased exponentially from 6 incidents reported in 1988 to 314,246 incidents reported in 2011 [1 & 2]. It appears that these incidents were not widely reported for general public since then. Furthermore, from 1988 to 2003, incidents exhibited exponential growth; after that the number of incidents increased sharply even with the increased resistances due to precautionary protective measures in place, according to Figure 1 [3].

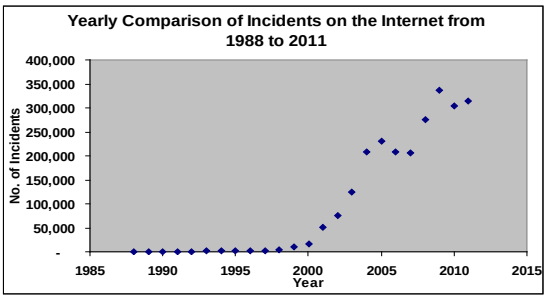

Figure 1. Exponential Growth of Malicious Incidents on the Internet

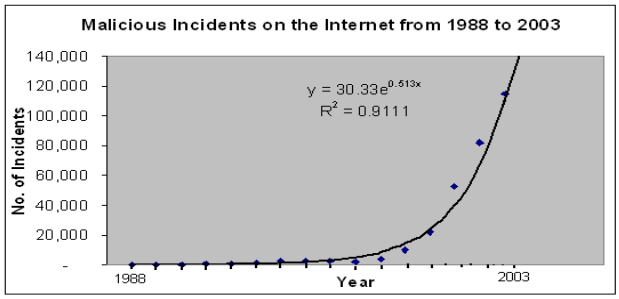

Figure 2. Exponential Growth of Malicious Incidents on the Internet

DOI: 10.14738/tnc.42.1989
Publication Date: 20th April 2016
URL: http://dx.doi.org/10.14738/tnc.42.1989

Figure 2 exhibits exponential growth of increasing malicious incidents on the Internet as plotted using the data in [4]. Moreover, in the recent past, these reported incidents grew significantly and have caused enormous disruptions for our banking and trading sectors causing unprecedented financial losses and privacy concerns.

Three aspects of the theory that are distinguished for analysis pertain to (a). the formal logic content, (b). the intuitive background, and (c). the applications. The character and applications of the structure as a whole cannot be appreciated without considering all three aspects in their relations for network traffic anomaly detections. Probability theory, on the other hand, is the mathematical theory of random (nondeterministic) phenomena. The probability distribution is derived by beginning with a statistical model, a set of assumptions about how responses are generated, and the calculations of associated probabilities. However, intrusion detection systems have widely been based on the characterization of an attack [5]. The primary focus in this effort will be the tracing of activities on the network to see if they match the known characterization. In addition, there are also a few flow-level detection schemes available [6]. Recently, intrusion detection systems based on previous known system data have appeared in the literature. In brief, the purpose is to inspect the network activities for suspicious activities that may indicate a system attack or an occurrence of misuse by unscrupulous network users [7]. An effective ISD logs actions executed by users or processes for investigation, alerts the system administrator when the activities are indicative of an attempted intrusion, and if appropriate, takes corrective measures such as expelling the intruder [8]. These vulnerabilities and bugs of information systems are often exploited by the intrusions. The extent of all possible scenarios for a network resulting from an intrusion can vary from none to an actual intrusion as depicted and appropriately color corded in Table 1. A unique obstacle eclipse effect in obstructed barriers has been observed that generates a sensor movement strategically performing definite obstructed barriers prevent intrusions [9].

Table 1. Vulnerability: Network Hardware vs. Outside Threats

Extent of intrusion	Network hardening					
		None	Mild	Reasonable	High	Very High
	None					
	Slight					
	Moderate					
	Extreme					
	Severe					

Optimal design of network topologies in multi-agent systems to facilitate effective communication on the network system is posed in the associated cost factors and the efficiency of performance [10]. This depends on the extent of network hardening software and severity of instruction in each component. The network vulnerability needs to be addressed in terms of the extent of intrusion, ranging from slight to extreme, and of network hardening which varies from mild to very high. Vulnerable devices, applications, and network software on an organization's network pose a great risk to the organization. The

determination of probability of vulnerability under these scenarios can be calculated using the conditional probabilities such as

$$\Pr(\text{Hardening} \mid \text{Volunerabilty}) = \frac{\Pr(\text{Hardening and Volunerabilty})}{\Pr(\text{Volunerabilty})} \quad \text{and}$$

$$\Pr(\text{Volunerabilty} \mid \text{Hardening}) = \frac{\Pr(\text{Volunerabilty and Hardening})}{\Pr(\text{Hardening})}.$$

These calculations determine other vulnerabilities under consideration in the areas of threat detection and vulnerability analysis. Other scenario can also be considered using Theorem of Total Probability and Bayes' Theorem, respectively. Let $\{B_1, B_2, \cdots, B_n\}$ be a set of nonempty subsets of the sample space *S* of an experiment. If the events $B_1, B_2, \cdots, B_n$ are mutually exclusive and $B_1 \cup B_2 \cup \cdots \cup B_n = S.$ For, a partition of *S*, $\{B_1, B_2, \cdots, B_n\}$: Theorem of Total Probability concludes if $B_1, B_2, \cdots$ is a partition of *S*, and *A* is any event, then $\Pr(A) = \sum_{i=1}^{\infty} \Pr(A|B_i)P(B_i)$ and that of Bayes' Theorem states if $B_1, B_2, \cdots$ is a partition of *S*, and *A* is any event, then $\Pr(B_i|A) = \frac{\Pr(B_i \cap A)}{\Pr(A)} = \frac{\Pr(B_i)\Pr(A|B_i)}{\sum_{i=1}^{\infty} \Pr(B_i)\Pr(A|B_i)}$.

The probability $\Pr(B_i)$ is called the priori probability and $\Pr(B_i \mid A)$ is called the posteriori probability. Accordingly, Bayes' Theorem determines the posteriori probability $\Pr(B_i \mid A)$ from the observation given that the event A has already occurred. This result is of many practical importances leading to Bayesian classification and Bayesian estimation.

Additionally, the attacks not only create havoc in the network system but also make the system highly congested holding the safety and the internal mechanism fails for hours and hours [11]. The characteristics of an efficient ISD that included 1) decentralized and distributed monitoring, 2) identification of coordinated attacks, and 3) passive network traffic analysis disrupting smooth automation networks [12].

2 Probabilistic State Finite Automata (PSFA)

A novelty approach that evolves around finite state automation is fascinating. A finite automaton is a mathematical model consisting of a set of states, a set of transitions between states, an input alphabet, an initial state, and a final state [13]. The following is a simple example of a transition diagram of finite automata.

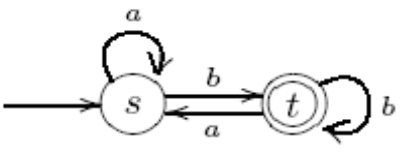

	a	b
→ s	s	t
← t	s	t

Figure 3. An Example of a Transition Diagram of Finite Automata

Components in Figure 3 specify: the set of states as $S = \{s,t\}$, the input alphabet as $A = \{a,b\}$, the initial state as s, and the set of terminal states as $\{t\}$. The transition function $\delta : S \times A \to S$ given by $\delta(s,a) = s,\ \delta(s,b) = t,\ \delta(t,a) = s,$ and $\delta(t,b) = t.$

A PSFA is an extended finite automaton in which each state has an associated probability based on a user signature. Some familiar UNIX commands such as `login, lpr, cd, vi, ls, pico, mv, mail, www`, and `exit` are used to create an example of intrusion paths with probabilities calculated in Table 2, where p_j denotes the associated probabilities for each UNIX command listed.

Table 2. Probability Distribution of Traffic Paths

Traffics	Probability
`lpr/cd/vi`	$p_1 \times p_2 \times p_3$
`ls/pico/mv`	$p_4 \times p_5 \times p_6$
`ls/mail/www`	$p_4 \times p_7 \times p_8$

For the j number of traffic paths, each path has issued k number of commands $p_{j1}, p_{j2}, p_{j3}, \ldots p_{j,k} \ldots$, then $\sum_j \sum_k p_{j,k} = 1.$ In general, computation of network reliability can often be calculated. Let $\mathcal{E}$ be the set of all nodes and links in the network and p_e be the probability that the intruder is successful at some node, $e \in \mathcal{E}.$ The subset $E_i \subseteq \mathcal{E}$ consists of these successful nodes and links. Thus, the probability that the intruder has succeeded in the network is $\Pr[E_i] = \prod_{e \in E_i} p_e \times \prod_{e \in \varepsilon \setminus E_i} (1 - p_e).$ There are 2^n possible network paths for an intruder to be successful in achieving this exponential growth of possible network avenues, where n is the number of links in $\mathcal{E}.$

The extension of time-dependent deterministic finite automation (TDFA) enables us to not only study more than just the sequence of input characters, but also to consider the time intervals between receiving input characters in recognizing behavioral patterns as normal. As a result, the uses of automata to recognize denial of service (DoS) attack signatures between arriving network packets will prove to be a reliable technique in the intrusion detection process [14]. However, TDFA uses the actual difference of arrival times between two input characters, leading to an infinite set of possible differences. This creates Boolean values resulting from the comparison of each of the differences to constants or variables defined in the automata. If we consider the problem of modeling network transition patterns, it is common to assume that rhythms occur with more frequency than those that correspond to random phonemes [15]. Hidden Markov Models (HMMs) are frequently used in many areas of pattern recognition and more specifically, in network intrusion detection. It is based on the fact that web information learning retains the ability to recognize other pattern domains, such as the Reber grammar provided in Figure 4.

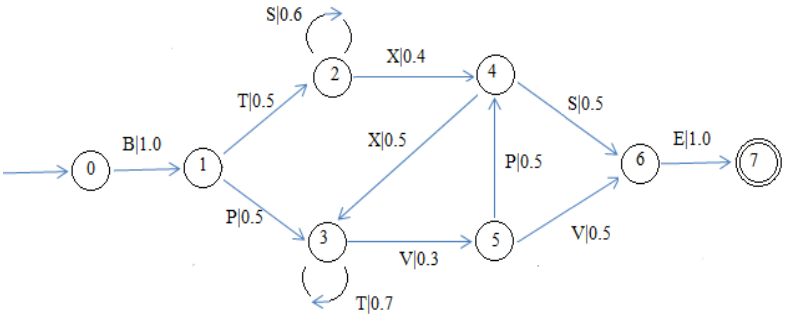

Figure 4. A SDFA Related to the Reber Grammar

A probabilistic automation defines a probability distribution over the set of strings of length η, for any particular η [16].

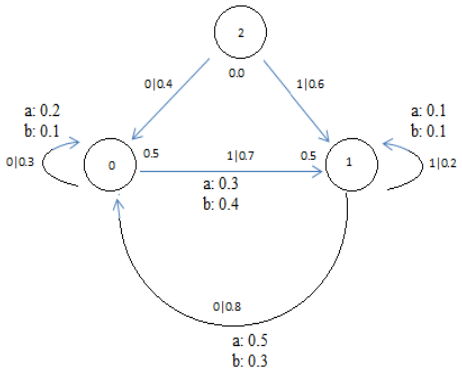

Figure 5. An Example of Probabilistic Automation

The probability assigned to this probabilistic automation in Figure 5 on the string $\omega = a \cdot a \cdot b$ is computed below:

$$P(\omega) = \pi_P(0).M_P(0,0,a).M_P(0,1,a).M_P(1,1,b) + \pi_P(0).M_P(0,1,a).M_P(1,1,a).M_P(1,0,b)$$
$$+ \pi_P(0).M_P(0,1,a).M_P(1,1,a).M_P(1,1,b)$$
$$+ \pi_P(1).M_P(1,1,a).M_P(1,1,a).M_P(1,0,b)$$
$$+ \pi_P(1).M_P(1,0,a).M_P(0,0,a).M_P(0,1,b)$$
$$+ \pi_P(1).M_P(1,1,a).M_P(1,0,a).M_P(0,0,b)$$
$$+ \pi_P(1).M_P(1,1,a).M_P(1,0,a).M_P(0,1,b)$$
$$+ \pi_P(1).M_P(1,0,a).M_P(0,0,a).M_P(0,0,b)$$

$$= 0.5 \times 0.2 \times 0.3 \times 0.1 + 0.5 \times 0.3 \times 0.1 \times 0.3 + 0.5 \times 0.3 \times 0.1 \times 0.1 + 0.5 \times 0.1 \times 0.1 \times 0.3 + 0.5 \times 0.5 \times 0.2 \times 0.4 + 0.5 \times 01 \times 0.5 \times 0.1 + 0.5 \times 01 \times 0.5 \times 0.4 + 0.5 \times 0.5 \times 0.2 \times 0.1$$

$$= 0.0480.$$

3 From Queuing Theory

Analysis of M/M/1 queue using a discrete time Markov chain (DTMC) during the times, 0, δ, 2δ, $3\delta, \cdots$, where δ is a small positive number, provides techniques for network intrusion detection. The transition

probabilities are up to an order of $o(\delta)$ terms. The transition probabilities $p_{ij} = \Pr[N_{k+1} = j \mid N_k = i]$ that are independent of k for a time-homogeneous DTMC are depicted in Figure 6.

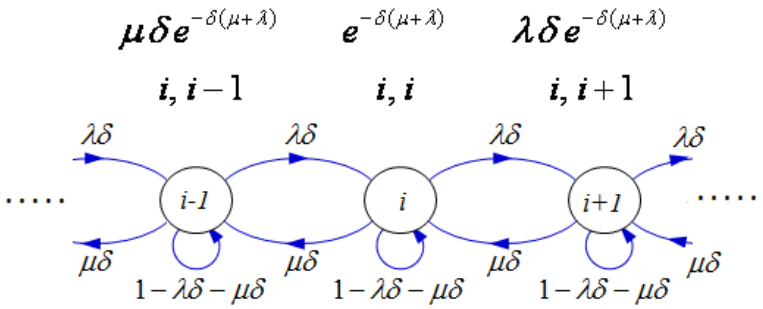

Figure 6. Transition Probabilities of DTMC for a M/M/1 queue from $i-1$ to $i+1$ States

One powerful, but simple formula in queuing theory [17], called Little's formula, has contributed to the study of intrusion detection. Little's formula of M/M/1 queues has uncovered an important phenomenon in cyber attacks. The expected number of attacks is proportional to the expected waiting time of an intruder, where the constant of proportionality is an average arrival time of attacks, $\lambda = \rho\mu$. In packet networks, the average packet delay caused by queuing is $T(c) = \dfrac{1}{\mu c - \lambda}$, where λ is the average packet arrival rate to a network link that follows a Poisson process, $\dfrac{1}{\mu}$ is the mean of average packet size that is exponentially distributed, and C is the link speed.

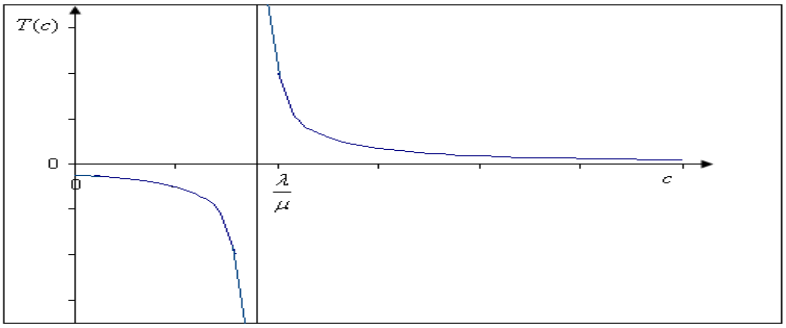

Figure 7. Average Packet Delay, $T(c)$ as a Function of Link Speed, C

Figure 7 concludes that for $c > \dfrac{\lambda}{\mu}$, average packet delay is exponentially decreasing and for $c < \dfrac{\lambda}{\mu}$, average packet delay stays negative, requiring some network justification.

Let us assume the arrival time has the geometric distribution with a parameter $(1-\rho)$ [18]. Let X be the number of unsuccessful attacks until the first successful attack has occurred. If p is the probability of successful attack then the probability that the k^{th} attack has been successful is $\Pr[X = k] = p(1-p)^k$, $k = 0, 1, 2, \cdots$ and $0 < p < 1$. This distribution has the same memory less property that has been held for Poisson distribution.

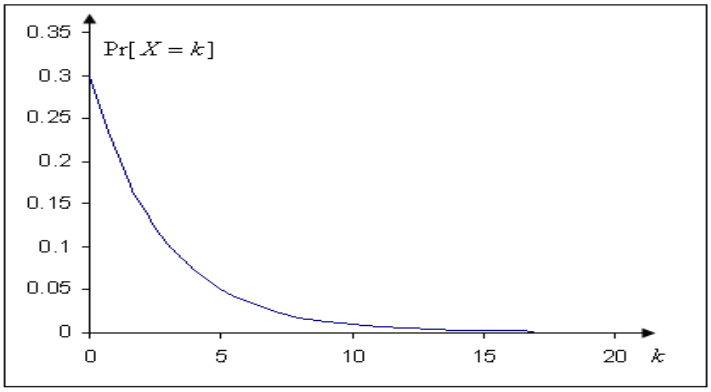

Figure 8. Probability that the k^{th} Attack has been Successful (taking $p = 0.3$)

Figure 8 exhibits the high probabilities for an attacker to be successful in his/her early attempts, as well as the diminished probability in subsequent attempts. If the attacker is selecting an address from the entire space of $N = 2^{32}$ addresses, the probability of detecting at least a single-packeted attack is $\Pr[\text{Detecting at least one - packeted attack}] = 1-(1-p)^k$, where $p = \frac{n}{N}$ is the probability of observing a single packet, assuming that the detector sensor monitors only n IP addresses [19]. As a result, the graph in Figure 6 is entirely flipped vertically, demonstrating the new probabilities. The probability of seeking j packets from the binomial distribution is $\Pr[j \text{ Packets}] = \binom{k}{j}(p)^j(1-p)^{k-j}$.

4 Profiles of Software Dynamics

Operational, functional, and module profiles have been the topics of much discussion [20]. Packet-based traffic monitoring is an application of multinomial distribution [21]. We observe certain parameters to estimate them for the population distribution. Let X be a random variable taking two values on the basis that an intrusion has occurred or otherwise. Thus, $X(\omega) = \begin{cases} 1 & if\ \omega \in A \\ 0 & if\ \omega \notin A \end{cases}$. This experiment is repeated as many as n times. Let Y be another random variable indicating the number of successes the intruder had. That is, $Y = \#\{i : X(\omega_i) = 1, \omega_i \in A\}$. Accordingly, $Y = \sum_{i=1}^{n} X(\omega_i) \rightarrow Y = B(n, p)$, where $B(n, p)$ is the binomial distribution with parameters n and p. The combined probability function of $Y_1, Y_2 \ldots, Y_n$ gives the multinomial distribution. For a given specific operation, say O_k, it will distribute its activity across the set of functionalities, $F^{(O_k)}$. At any arbitrary interval, n, during the expression of O_k, the program will be executing a functionality $f_i \in F^{(O_k)}$ with a probability, $\Pr[Y_n = i \mid X = k]$. From this conditional probability distribution for all operations, we derive the functional profile for the design specifications as a function of a user operational profile:

$$\Pr[Y = i] = \sum_j \Pr[X = j]\Pr[Y = i \mid X = j].$$

$\Pr[Y=i]=\sum_j p_j \Pr[Y=i \mid X=j]$.

$\Pr[Y=i]=\sum_j p_j \Pr[Y=i, X=j]/\Pr[X=j]$. Three possible traffic paths occur with probabilities p_i, $i=1,2,3,\ \sum_{i=1}^{3} p_i = 1$. Suppose that n independent replications of this traffic are initiated and let $X_i, i=1,2,3,$ denote the number of times outcome i appears. Now if $Y=i$ and $X=j$, then it follows that $Z=n-i-j$. However,

$\Pr[Y=i, X=j, Z=n-i-j]=\dfrac{n!}{i!\,j!(n-i-j)!}p_1^{\,i}p_2^{\,j}p_3^{\,(n-i-j)}$. This follows, since any particular sequence of n traffic paths having path 1 appearing i times, path 2 appearing j times, and path 3 appearing $(n-i-j)$ times has probability $p_1^{\,i}p_2^{\,j}p_3^{\,(n-i-j)}$ of occurring. Since there are $n!/[i!\,j!(n-i-j)!]$ such sequences, we have

$\Pr[Y=i]=\sum_j p_j \dfrac{\dfrac{n!}{i!\,j!(n-i-j)!}p_1^{\,i}p_2^{\,j}p_3^{\,(n-i-j)}}{\dfrac{n!}{j!(n-j)!}p_2^{\,j}(1-p_2)^{n-j}}$, where we have used the fact that Y has binomial distribution with parameter n and p_2. $\Pr[Y=i]=\sum_j p_j \binom{n-j}{i}\left(\dfrac{p_1}{1-p_2}\right)^i\left(1-\dfrac{p_1}{1-p_2}\right)^{n-j-i}$. For other profiles, more discussions are found in [22].

Let us now assume that an intruder attempts to attack a network system which has n components with probability p_2. The probability that he will be successful in each component is p_1. Let X_2 be the number of these components that are actually attacked. With this assumption, X_2 is then the binomial distribution with parameters x_1 and p_2, given x_1 components. The joint probability function for X_1, X_2 is the product given by

$p_{X_1,X_2}(x_1,x_2)=\binom{n}{x_1}p_1^{\,x_1}(1-p_1)^{n-x_1}\binom{x_1}{x_2}p_2^{\,x_2}(1-p_2)^{x_1-x_2}$, for $x_1=0,1,\ldots,n$ and $x_2=0,1,,\ldots,x_1$. The marginal probability function for X_2 is obtained by summing over the range of possible x_1 values for the given $x_2: x_1=x_2, x_2+1,\ldots,n$.

$$p_{X_2}(x_2)=\binom{n}{x_2}\left(\frac{p_2}{1-p_2}\right)^{x_2}\sum_{x_1=x_2}^{n}\binom{n-x_2}{x_1-x_2}\left(p_1(1-p_2)\right)^{x_1}(1-p_1)^{n-x_1}$$

$$p_{X_2}(x_2)=\binom{n}{x_2}\left(\frac{p_2}{1-p_2}\right)^{x_2}\sum_{j=0}^{n-x_2}\binom{n-x_2}{j}\left(p_1(1-p_2)\right)^{j+x_1}(1-p_1)^{n-x_1-j}$$

$$p_{X_2}(x_2) = \binom{n}{x_2}\left(\frac{p_2}{1-p_2}\right)^{x_2}\left(p_1(1-p_2)\right)^{x_2}\left(p_1(1-p_2)+(1-p_1)\right)^{n-x_2}$$

$p_{X_2}(x_2) = \binom{n}{x_2}(p_1 p_2)^{x_2}(1-p_1 p_2)^{n-x_2}$. Accordingly, X_2 has a binomial distribution with parameters n and $p_1 p_2$.

In addition, majority of assumptions in the domain of cyber security naturally meet the properties of a Poisson process, namely, the number of intrusions can be modeled by a Poisson distribution and in fact, the time between intrusions is exponentially distributed. However, the log-normal distribution significantly fits the modeling in terms of the number of detected intrusions and the time between intrusions. The Pareto distribution is an alternative to both of these distributions that analyzing whether time-to-compromise (TTC) increase for each successful intrusion of network systems [23 & 24].

5 Conclusions and Future Work

The probability distribution theory assisted us in breaking down several parts of the analysis. The hardening hardware should be done at very appropriate levels using the topological nature of these analyses. In every case beginning with the identification of operating systems, network strengths, weaknesses, opportunities, and threats should be analyzed in a logical fashion. Assessing present strategies is done only when we are fully aware and conversant with the detective analysis of the systems. Necessary changes, improvements, and recommendations for any system will inevitably benefit the analysis and its mere purpose for preventing intrusion. Stating explicitly how to identify strengths of the methods to exploit the intrusion, rectifying the weaknesses, and preventing intrusion's threats to thus outline precautions to safeguard the network system is in fact needed.

REFERENCES

[1] Kumar, V. Anil (2004). *Sophisticated in Distributed Denial-of-Service Attacks on the Internet*, Current Science, Vol. 87, No. 7, pp. 885-888

[2] CERT Insider Threat Center (2009). Software Engineering Institute, Carnegie Mellon University, Last updated February 12, 2009, http://www.cert.org/stats/

[3] Internet Crime Report, Internet Crime Complaint Center (2012). http://www.ic3.gov/media/annualreport/2011_ic3report.pdf

[4] Chang, H.-Y., Wu, S. F. and Jou, Y. F. (2001). *Real-Time Protocol Analysis for Detecting Link-State Routing Protocol Attacks,* ACM Trans. Inf. Sys. Sec., Vol. 1, (2001), pp. 1-36

[5] Barbará, D., Couto, J., Jajodia, S., Popyack, L., and Wu, N. (2001). *ADAM: Detecting Intrusions by Data Mining*, Proceedings of the 2001 IEEE Workshop on Information Assurance and Security United States Military Academy, West point, NY, pp. 5—6, June 2001

[6] Li, Z., Gao, Y., and Chen, Y. (2005). *Towards a High-speed Router-based Anomaly/Intrusion Detection System,* Northwestern University, http://www.sigcomm.org/sigcomm2005/poster-121.pdf

[7] Sebyala, A. A., Olukemi, T., and Sacks, L., (2002). *Active Platform Security through Intrusion Detection Using Naïve Bayesian Network for Anomaly Detection,* http://www.ee.ucl.ac.uk/lcs/papers2002/LCS116.pdf

[8] Kang, D.-K., Fuller, D., and Honavar, V. (2005). *Learning Classifiers for Misuse and Anomaly Detection Using a Bag of System Calls Representation*, Proceedings of the 2005 IEEE Workshop on Information Assurance and Security United States Military Academy, West Point, NY

[9] Yang, G., Zhou, W., and Qiao, D. (2007). Defending against barrier intrusions with mobile sensors, the Proceedings of 2007 International Conference on Wireless Algorithms, Systems and Applications, 2007, pp. 113-120

[10] Rafiee, M. and Bayen, A. M. (2010). Optimal network topology design in multi-agent systems for efficient average consensus, Decision and Control (CDC), 2010 49th IEEE Conference on, Atlanta, GA, 2010, pp. 3877-3883

[11] Barbosa, R. R. R. and Pras, A. (2010). Intrusion Detection in SCADA Networks, the Proceedings of the Conference: Mechanisms for Autonomous Management of Networks and Services, 4th International Conference on Autonomous Infrastructure, Management and Security, AIMS 2010, Zurich, Switzerland, June 23-25

[12] Schuster, F. and Paul, A. (2012). A distributed intrusion detection system for industrial automation networks," Emerging Technologies & Factory Automation (ETFA), 2012 IEEE 17th Conference on, Krakow, 2012, pp. 1-4

[13] Freeman, *S.,* Branch, J., Bivens, A., and Szymanski, *B*. (2002). *Host-Based Intrusion Detection Using User Signatures,* Proc. Research Conference, Troy, NY 12180-3590, http://www.cs.rpi.edu/~szymansk/papers/signature.pdf

[14] Petersson, K. M., Grenholm, P., and Forkstam, C. (2005). Artificial grammar learning and neural networks. In G. B. Bruna, L. Barsalou, & M. Bucciarelli (Eds.), Proceedings of the 27th Annual Conference of the Cognitive Science Society, pp. 1726-1731

[15] Kermorvant, C. and Dupont, P. (2002). Stochastic grammatical inference with multinomial tests. In 6th International Colloquium on Grammatical Inference: Algorithms and Applications (ICGI), Vol. 2484 of Lecture Notes in Computer Science, Springer, 2002, pp. 149–160

[16] Abe, N. and Warmuth, M. K. (1990). On the Computational Complexity of Approximating Distributions by Probabilistic Automata, Machine Learning, 1990, pp. 205-260

[17] Bose, K. Sanjay (2002). An Introduction to Queueing Systems Kluwer Academic/Plenum Publishers, New York, 2002

[18] Myers, J. L. and Well, A. D. (2003). *Research Design and Statistical Analysis,* second edition, 2003, Lawrence Erlbaum Associates, Inc. Publishers

[19] Wegman E. J. and Marchette, D. J. (2004). *Statistical Analysis of Network Data for Cybersecurity,* Chance, Vol. 17, No. 1 (2004), pp. 9-19

[20] Elbaum, S. and Munson, J. C. (1999). *Intrusion Detection: Through Dynamic Software Measurement*, Proceedings of the Workshop on Intrusion Detection and Network Monitoring, Santa Clara, California, USA, April 9—12, 1999, The USENIX Association, The Advanced Computing Systems Association

[21] Boodnah, J. and Scharf, E. M. (2005). *Applying Clustering to a Framework for Generating Trust,* http://www.ctr.kcl.ac.uk/iwwan2005/papers/39.pdf

[22] Munson, J. C. and Elbaum, S. (1999). Software Reliability as a Function of User Execution Patterns, Proceedings of the 32nd Hawaii International Conference on System Sciences – 1999, pp. 1-12, http://cse.unl.edu/~elbaum/papers/workshops/hawai99.pdf

[23] Van Oorschot, P. C., Robert, J.-M., and Martin, M. V. (2006). A monitoring system for detecting repeated packets with applications to computer worms Int. J. Inf. Secur. (2006) 5(3): pp. 186–199

[24] Holm, H. (2014). A large-scale study of the time required to compromise a computer system, Browse Journals & Magazines: Dependable and Secure Computing, IEEE Transactions, Vol. 11 Is. 1, 2014, pp. 2-15

SOCIETY FOR SCIENCE AND EDUCATION
UNITED KINGDOM

TNC TRANSACTIONS ON NETWORKS AND COMMUNICATIONS

VOLUME 4, ISSUE 2
ISSN: 2054 -7420

The Altitude Attainment and Inclination Alignment for the Satellite Launched from Kourou Site

Shkelzen Cakaj, Bexhet Kamo and Elson Agastra
Faculty of Information Technology, Polytechnic University of Tirana, Albania
shkelzen.cakaj@fulbrightmail.org, bkamo@fti.edu.al, eagastra@fti.edu.al

ABSTRACT

The geostationary orbit is a circular orbit 35786 kilometers above the Earth's equator and following the direction of the Earth's rotation. Communications satellites are often placed in the geostationary orbit. The rockets are used to place the satellite in geostationary orbit. The main goal of the launching process is to enable the satellite to acquire the desired geostationary orbit space parameters. There are two methods applied for putting satellites in the geostationary orbit, the first one is when a rocket takes the spacecraft to a low Earth circular orbit and then towards geostationary transfer orbit, and by the second method, the low circular orbit is skipped and the satellite goes straight to geostationary transfer orbit. Because of too large distance from the Earth's surface this placement to geostationary transfer orbit is not done at once. The location of Kourou at French Guiana is the launching site of France and also shared with ESA (European Space Agency). The launch process from Kourou site firstly places the satellite at geostationary transfer elliptical orbit, and then the orbit geostationarity is achieved through two phases, the first phase is the altitude attainment at 35786km and the second is the inclination to be aligned with equatorial plane. During the whole process, the needed satellite's propellant mass must be minimized. Three thrusts apogee and nodal thrust method applied for the altitude attainment and then the inclination alignment for the satellite to be consolidated in geostationary orbit, which is launched from Kourou site, is simulated and analyzed within this paper.

Keywords: GEO; satellite; orbit; inclination

1 Introduction

Usually, to attain the geosynchronous or geostationary Earth orbit, the propellant makes up about half of a satellites mass, what directly impacts the launching process and satellite's lifetime. When launching and then consolidating the satellite on its own high circular orbit (ex. geosynchronous), the needed satellite's propellant mass must be minimized.

The Hohmann transfer is well known for the minimum of propellant mass used for satellite transfer into high orbits. The Hohmann transfer orbit is based on two instantaneous velocity changes. The transfer consists of a velocity impulse on an initial circular orbit, in the direction of motion and collinear with velocity vector, which propels the space vehicle into an elliptical transfer orbit. The second velocity impulse also in the direction of motion is applied at apogee of the transfer orbit which propels the space vehicle into a final circular orbit at the final altitude [1].

DOI: 10.14738/tnc.42.1985
Publication Date: 21th April 2016
URL: http://dx.doi.org/10.14738/tnc.42.1985

After too long efforts and experiments, in January 2013, the Robotic Refueling Mission (RRM) performed its first test on board the ISS (International Space station), demonstrating that remotely controlled robots successfully transfer fuel in space. Lofting a satellite with only a portion of the fuel it would need to complete its mission, with the ability to inject more propellant in the future, creates two advantages: the lower launching cost and more room for instruments to be packed aboard. Robotically refueling satellites in orbits in the near future, will allow satellite service providers to dramatically extend their services and the satellites' lifetime [2].

This paper considers the concept of satellite acquirement of space orbit parameters, followed by main characteristics of launching vehicles and launching methods towards geosynchronous (geostationary) orbits. The launching process toward geostationary orbit from the site in Kourou is analyzed, associated with maneuvers and thrust to be applied in order the geostationary orbit to be attained and consolidated. Maneuvers and applied thrusts are directly correlated with propellant consumption/saving, what is among main goals on future scientific research related to satellite systems.

2 Acquiring Space Orbit Parameters

The main goal of the launching process is to enable the satellite acquire the desired space orbit parameters. The position of the orbital plane in space is specified by means of two parameters - the *inclination i* and the *right ascension of the ascending node* (Ω). Inclination *i* represents the angle of the orbital plane with respect to the Earth's equator. The right ascension of the ascending node Ω defines the location of the ascending and descending orbital crossing nodes (these two nodes make a *line of nodes*) with respect to a fixed direction in space, known as Vernal equinox. Vernal equinox is direction of line joining the Earth's center and the Sun on the first day of spring [3]-[5].

In order the orbit plane to attain the exact desired position in space it is too important that correct conditions are established at the satellite injection point. Further, to keep the desired orbit position in order to enable the appropriate satellite mission, the various in orbit operations such as orbit stabilization, orbit correction and stations keeping are mandatory.

The angle defining the right ascension of the ascending node Ω, is basically the difference between two angles, α and β, where α is the angle made by the longitude of the injection point at the time of launch with the direction of vernal equinox and β is the angle made by the longitude of the injection point at the time of launch with the line of nodes, as shown in Fig. 1 [3] and given as (1):

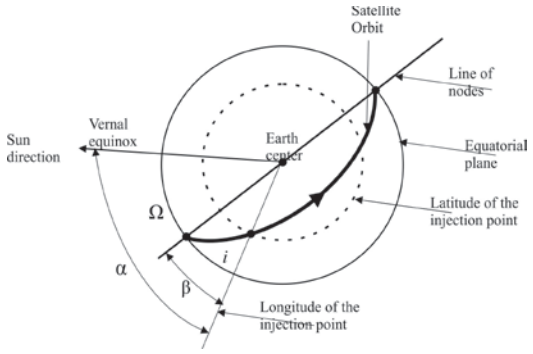

Figure. 1 Two Space orbit parameters.

$$\Omega = \alpha - \beta \quad (1)$$

Considering Fig.1, it is obvious that to ensure the satellite orbits within a given plane, the satellite must be injected at a certain specific time, depending upon the longitude of the injection point, at which the line of nodes makes the required angle with the direction of the vernal equinox. Thus, for a known angle of inclination and the longitude of injection point (launching site) the launching time must be exactly determined in order to acquire the desired right ascension of the ascending node *Ω* [3]-[4].

The angle of inclination *i* of the orbital plane can be determined from the known values of the azimuth angle (A_Z)and the latitude (*l*) of the injection point, expressed as [3]:

$$cosi = sinA_Z cosl \quad (2)$$

The azimuth angle (A_Z) at a given point in a satellite orbit is the angle made by the projection on the local horizon of the satellite vector velocity at that point with the north.

From Eqn. (2), for the angle of inclination to be zero, the right hand side of (2) should be one, what could happen only if the launching site is at Equator plane, thus the latitude *l=0* and $A_Z = 1$. For launching sites above the Equatorial plane it is $l > 0$ and$sinA_Z < 1$, what will decrease $cosi$ and consequently increase inclination angle *i*, mathematically expressed as [3]:

$$i > l \quad (3)$$

Thus, it can be concluded that the satellite will tend to orbit in a plane which will be inclined to the equatorial plane at the angle equal to or greater than the latitude of the injection point.

3 Launching Methods

Metadata information in the Web Pages and Expansio used to launch a satellite is known as a launch vehicle. There are two types of launch vehicles: expendable rockets such as Ariane of the European Space Agency and Atlas Centaur of the United States which are destroyed while completing their mission, and the other that is employed by a re-usable launch vehicle such as the Space Shuttle of the United States and the Buran of Russia [6].

In order for a satellite to be launched successfully, the launch rocket must be placed in a vertical position initially. This allows the rocket to penetrate the densest layer of the Earth's atmosphere quickly, which helps reduce fuel consumption. The concept of the launch vehicle is given in Fig. 2 [6].

Expendable rockets for communication satellites have three stages. The first stage raises the satellite at about 50 miles (80 km), and then the second stage raises the satellite to 100 miles above the Earth's surface, and when the launch vehicle is out of the Earth's atmosphere, the satellite separates from the upper stage and places it into the transfer orbit.

The upper stage of the launch vehicle is connected to the satellite itself, which is enclosed in a metal shield, called a "fairing." The fairing protects the satellite while it is being launched and makes it easier for the launch vehicle to travel through the resistance of the Earth's atmosphere. Once the rocket reaches an altitude near the satellite's orbit height, the satellite is ejected from the rocket's nose cone and the rocket falls back to Earth, burning up upon reentering our atmosphere. The rockets of the upper stage fire after the satellite is in space and put the satellite in the exact spot where it is needed. The fairing splits apart once the satellite is above the Earth's atmosphere and burns up in the Earth's atmosphere. Once the satellite reaches its desired orbital height, it unfurls its solar panels and communication antennas, which

had been stored away during the flight. The satellite then takes its place in orbit with other satellites and is ready to provide services. After the satellite is placed in its transfer orbit, the rocket's mission is complete, and its remnants fall to Earth. When the satellite is already placed in the orbit, then there are mandatory activities in order to consolidate the desired in advance determined orbit space parameters, what is the further subject of this paper [7].

To attain the geostationary orbit, firstly we need to get to the appropriate high altitude and the secondly is needed to change the inclination (most launch pads are not located at the equator) to zero angle. There are two methods applied for putting satellites in the geostationary orbit. One of methods is when rocket takes the spacecraft to a circular orbit at an altitude of 200-300km and then towards geostationary transfer orbit. By the second method, further discussed, the circular orbit is skipped and the satellite goes straight to geostationary transfer orbit. Transfer orbits are often used to test vehicle systems before committing to further action [3]-[4].

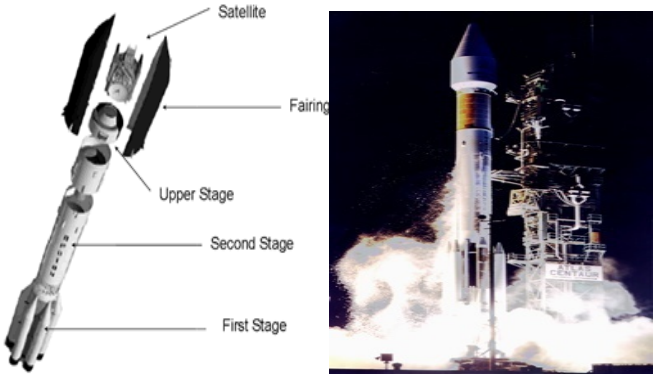

Figure 2. The launch vehicle concept (left) and Atlas expendable satellite launch vehicle (right) [6].

The Geostationary Transfer Orbit (GTO) is elliptical in shape with its perigee at an altitude between 180 km and 200 km and its apogee at the geostationary altitude. The spacecraft has an engine that is called the Apogee Kick Motor (AKM). That motor is fired on while the satellite is at the apogee of its elliptical transfer orbit aiming to circularize the orbit. But it usually is not all done at once. Usually the AKM is used three times respectively by three burns. Further is discussed the satellite launch process from the launch site Kourou in French Guiana toward final geostationary orbit.

4 Kourou launching site

The location of Kourou at French Guiana was selected in 1964 to become the spaceport of France and it is operational since 1968. In 1975, France offered to share Kourou with ESA (European Space Agency) [8].

The satellite launch site at Kourou in French Guyana is located at coordinates of 5° 9′ 34.92″ N, 52° 39′ 1.08″ W and it is particularly suitable as a location for a spaceport as it fulfills the two major geographical requirements of such a site: it is quite close to the equator, and it has uninhabited territory, so that lower stages of rockets and debris from launch failures cannot fall on human habitations.

The structure of Kourou center is presented in Fig. 4, where it is obvious that the control center is located around 12km far from the launching zone because of safety reasons [6].

5 Launching Process and Parameters Acquisition

The entire satellite launching process by Ariane vehicle toward geostationary orbit, launched from Kourou site at French Guiana is further described by activity steps.

The orbit circularization and the geostationarity are achieved through two phases, the first one is the altitude attainment at 35786km (geosynchronous orbit altitude) and the second is the inclination alignment (zero inclination) with Earth's equatorial plane.

5.1 Circularization and Altitude Attainment

The launch vehicle takes the satellite to a point that is intended to be the perigee of the transfer orbit, at a height of about 200km above the Earth's surface. At this point the satellite is ejected from the rocket's nose cone (see Fig. 2); respectively it is injected in the transfer orbit. The satellite along with its apogee boost motor is injected before the launch vehicle crosses the equatorial plane.

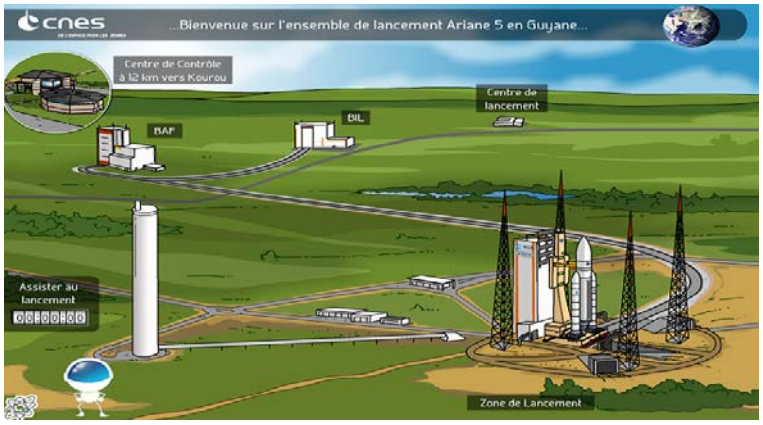

Figure 4. Satellite launch site at Kourou [6]

The injection velocity at perigee v_p expressed as

$$v_p = \sqrt{\left(\frac{2\mu}{r_p}\right) - \left(\frac{2\mu}{r_a + r_p}\right)} \tag{4}$$

is such that the injected satellite attains an eccentric elliptical orbit with an apogee altitude at about 35786km where the velocity is v_a expressed by:

$$v_a = \sqrt{\left(\frac{2\mu}{r_a}\right) - \left(\frac{2\mu}{r_a + r_p}\right)} \tag{5}$$

r_p and r_a are respectively perigee and apogee distances (from the Earth's center), $\mu = m \cdot G = 3.986 \cdot 10^5 \, km^3 / s^2$, G is the Earth's gravitational constant and m Earth's mass. The correlations in between apogee (r_a), perigee (r_p) distances with respective attitudes at apogee (h_a) and at perigee (h_p) is:

$$r_{a,p} = R_E + h_{a,p} \tag{6}$$

For launching conditions from the site at Kourou toward geostationary orbit, and considering Earth's radius R_E= 6371km, stem out that the perigee and apogee distances, respectively are r_p=6571km and $r_a = 42159$km [1]. Applying these parameters in (4) and (5), yields out that the velocity at the injection point (perigee) in order to create a geostationary transfer orbit, is:

$$v_p = 10.248 \text{ [km/s]} \quad (7)$$

and the velocity at apogee of the geostationary transfer orbit is

$$v_a = 1.589 \text{ [km/s]} \quad (8)$$

The main goal is to circularize the orbit, but usually it is not all done at once. For this purpose, usually the Apogee Kick Motor (AKM) is used three times respectively by three burns, generating three velocity thrusts as presented in Fig. 5.

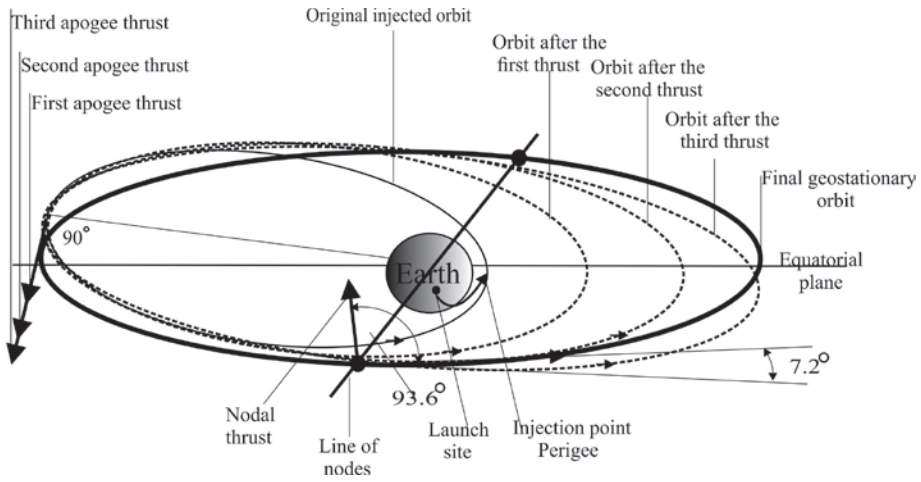

Figure 5. Three thrust at apogee and nodal thrust.

Considering that the initial altitude at the injection point is at 200km, then attempting by the first burn (thrust) to attain an altitude of about 12000km, by the second one an altitude of about 24000km, and finally the geostationary altitude of 35786km by the third thrust, further applying (4), (5), and (6) the respective velocities and altitudes attained up to the final orbit circularization are given in Table 1.

Table 1. Velocities and respective altitudes

	Velocity at perigee (v_p) [km/s]	**Altitude at perigee (h_p)** [km]	**Velocity at apogee (v_a)** [km/s]	**Altitude at apogee (h_a)** [km]
Injection phase	10.248	200	1.589	35786
Under thrust 1	5.501	12000	2.383	35786
Under thrust 2	3.910	24000	2.801	35786
Under thrust 3 (Final stage)	3.067	35786	3.067	35786

Table1 confirms that under the third thrust at apogee point it is attained the geostationary altitude and the orbit is already circularized. The variation of velocities after each thrust is presented in Fig, x, where it is obvious the convergence of both velocities, at apogee and perigee after the third thrust, when the orbit is circularized and consequently the satellite has constant velocity at each point of the orbit.

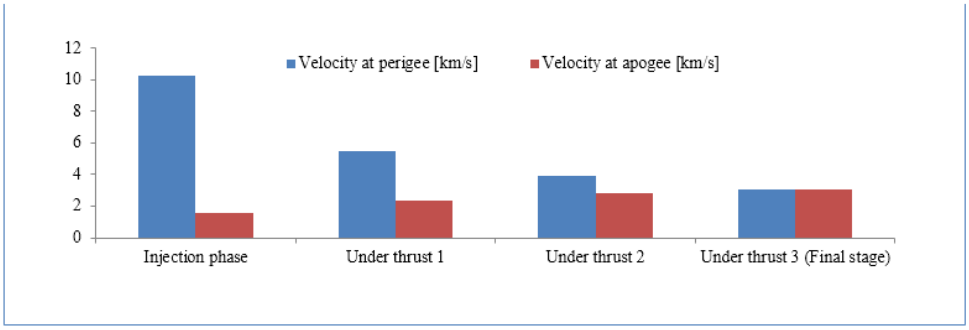

Figure 6. Velocities variation.

Under the consideration of only the orbit circularization respectively altitude attainment, the applied thrust velocity vectors at apogee point in order to increase the perigee distances are coplanar at each burn (thrust) and having the same direction of the satellite's motion. Each velocity vector is tangential at apogee point of the orbit (see Fig. 5).

The satellite is always in move with an actual velocity at apogee, thus in order to increase the perigee, the increment on apogee velocity vector by the apogee thrust has to be applied, expressed as:

$$\Delta v_{a(i)} = v_{a(i)} - v_{a(i-1)} \tag{9}$$

where i indicates burning-thrust step, and $i - 1 = 0$ indicates injection phase. Finally, based on Table 1 and (9) the intensities of coplanar thrust vectors applied three times at apogee for orbit circularization are:

$$\Delta v_{a1} = 794[\text{m/s}] \quad \Delta v_{a2} = 418[\text{m/s}] \quad \Delta v_{a3} = 266[\text{m/s}] \tag{10}$$

This orbit circularization is achieved by three appropriate thrust maneuvers without affecting any change to the inclination. For the attained circularization and attitude of 35786km the satellite velocity in the circularized orbit is

$$v_a = 3.067\ [\text{km/s}] \tag{11}$$

5.2 Inclination Alignment

The projection of the injection velocity vector in the local horizon plane at launching site of Kourou makes an azimuth angle of 85°. The latitude of the launch site is 5° 9′ 34.92″. The inclination angle attained by the geostationary transfer orbit is calculated from (2), and it is:

$$i = 7.2° \tag{12}$$

Next action is another thrust to be applied in order to bring the orbit inclination to 0◦, respectively the already circularized orbit to be aligned with equatorial plane, and finally the geostatinarization to be completed.

The change in inclination Δican be externally affected by applying a thrust velocity vector Δv_i at angle of $(90° + \Delta i/2)$ at one of nodes as illustrated in Fig. 5. The thrust is given by [3]:

$$\Delta v_i = 2v sin\left(\frac{\Delta i}{2}\right) \tag{13}$$

where *v* is the satellite's velocity at circularized orbit, at (11) and Δi is the inclination range that should be corrected. Since, the already circularized orbit has inclination of $7.2°$ which should be brought at 0°,

then $\Delta i/2$ is $3.6°$. Finally the velocity thrust to be applied for orbit alignment with equatorial plane, and making the orbit as fully geostationary one, is:

$$\Delta v_i = 385.15[\text{m/s}] \quad (14)$$

This thrust is applied at either of the two nodes (ascending or descending), as in Fig. 5. The last step is fine tuning to attain the exact inclination, attitude and longitude of the satellite.

6 Conclusion

The satellite launching process from the Kourou site is given. It is confirmed that the geostationarity is achieved by three thrusts applied at apogee and a single thrust applied at the nodal point. By three apogee thrusts it is attained the geostationary orbit altitude and circularity, then by the nodal thrust the satellite orbit is aligned with Earth's equatorial plane. Apogee thrust vectors are tangential with orbit and the nodal vector is normal with orbit plane. Mathematical thrust velocity vectors calculation is also given.

REFERENCES

[1] S. Cakaj, at.al. "The Velocity Increment for Hohmann Coplanar Transfer from Different Low Earth Orbits" *Journal – Frontiers in Aerospace Engineering*, Vol. 4, No. 1, 2015, pp. 35-41.

[2] http://ssco.gsfc.nasa.gov/rrm_refueling_task.html [2016, February].

[3] A. K. Maini and V. Agrawall, *Satellite Technology*, Wiley, UK, 1998.

[4] D. Roddy, *Satellite communications*, Mc.Hill, New York, 2006.

[5] S. Cakaj, B. Kamo, K. Malaric, "The Nodal Regression Simulation for Sun Synchronized Orbits", IEEE ConTEL , 12th International Conference in Telecommunications, Croatia, 2013, pp. 59-63.

[6] www.google.com/?gws_rd=ssl#q=KOUROU, [2016, February].

[7] J.Pocha, *An Introduction to Mission Design for Geostationary Satellites*, 1987.

[8] www.esa.int/Our_Activities/Launchers/Europe_s_Spaceport/Europe_s_Spaceport2, [2016, February].